Is string theory falsifiable?

Martim Martins da Costa Dams Carvalho
Mestrado em Física
Departamento de Física e Astronomia
2023

Orientador
Carlos José Amaro Parente Martins
Investigador Principal FCT,
Centro de Astrofísica da Universidade do Porto

Centro de Astrofísica
da Universidade do Porto

U. PORTO

FACULDADE DE CIÊNCIAS
UNIVERSIDADE DO PORTO

MSc

" I'm not gonna say it's all done, 'cause it ain't ever all done "

"Dimebag" Darrell Lance Abbott

Acknowledgements

First, I would like to thank to my supervisor, Prof. Carlos Martins, for all the help and opportunities provided. It has been a wonderful experience to work with you and I hope our collaboration goes well into the future.

To all my colleagues at and outside CAUP, it has been a pleasure getting to know you and having shared great times in and out of office. Special thanks to Léo, João and Nils! I have learned a great deal from the three of you and I am very thankful for all the conversations, support and inclusion.

To my family and friends, who have always stood by my side and motivated me to achieve my goals, I have a ton of appreciation for you and would never take any of you for granted.

Finally, to the three most important women in my life – my mother, my sister and my love – I could not have pulled through the past few years without your love and dedication. I hope to someday be able to give back all that you have given me. Thank you, Luísa, Madalena and Inês!

UNIVERSIDADE DO PORTO

Abstract

Faculdade de Ciências da Universidade do Porto
Departamento de Física e Astronomia

MSc. Physics

Is string theory falsifiable?

by Martim Carvalho

String theory is the best candidate framework for building theories of quantum gravity. The string Landscape of consistent theories of quantum gravity is surrounded by a Swampland of seemingly consistent effective field theories, which lack ultra-violet completion. The Swampland conjectures are a set of conditions which help identify whether a theory belongs to the Landscape or the Swampland. This thesis studies the late-time cosmological predictions of three string theory inspired models – quintessence, the runaway dilaton scenario and an extended Bekenstein-type model – mainly focusing on the expected dark energy equation of state and variations of the fine-structure constant. In all models, we consider the single field case, where the dilaton, ϕ, which arises as part of the superstring spectrum, is the only scalar in the effective theory and is subject to some potential, $V(\phi)$. Specifically, we look at the simplest cases of potentials which agree with the two formulations of the de Sitter conjecture of the Swampland program, $V(\phi) \propto \exp(-\lambda\phi)$ and $V(\phi) \propto \cos(c\phi)$. We find that constraints from varying-α can be more stringent than other cosmological data, depending on the model, making them a viable test for questions in fundamental physics.

Contents

List of Figures

Notation and Conventions

Units

Throughout this work we use natural units as follows:

- Planck constant and speed of light: $\hbar = c = 1$
- Planck mass and Newton's constant: $M_{\rm Pl} = \frac{1}{\sqrt{8\pi G}} = 1$, such that $G = \frac{1}{8\pi}$

Although in certain equations we leave the dependence on $M_{\rm Pl}$ explicit, we always set it to $M_{\rm Pl} = 1$ when performing calculations.

Acronyms

For figure captions in Chapter 5, we have developed a convention to facilitate the connection between text and figure. At the beginning of each caption we include "[**model**, **potential**]", with **model** $\in \{\mathbf{Q}, \mathbf{RaDS}, \mathbf{BSBM}\}$ and **potential** $\in \{\mathbf{exp}, \mathbf{cos}\}$, where:

- **Q** = Quintessence
- **RaDS** = Runaway Dilaton Scenario
- **BSBM** = Bekenstein-Sandvik-Barrow-Magueijo extension
- **exp** = exponential
- **cos** = cosine

Other

Unless explicitly stated otherwise, we shall:

- use a subscript '0' to denote the present day value of a given quantity,
- use $a(t)$ to denote the scale factor of the FLRW metric,

- use N to denote the number of e-folds of expansion relative to the present, i.e. $N(t) = \ln\left(\frac{a(t)}{a_0}\right)$,
- use dots, e.g. $\dot{f}$, to represent derivatives with respect to cosmic time, t,
- use primes, e.g. f', to represent derivatives with respect to N.

To my dogs, Stitch, Zeca, Feijão e Facho...

Chapter 1

Introduction

Physics is incomplete. As it is currently formulated, there are incompatibilities between the quantum description of the small components of the universe, such as particles and quantum fields, and general relativity (GR), which describes large scale structure. These incompatibilities are particularly clear in very high energy and spatially confined phenomena, such as the singularities at the centers of black holes and the Big Bang singularity. At the heart of the problem, seems to be our inability to quantize gravity into a renormalizable quantum field theory (QFT). There are theoretical frameworks which may be able to achieve this, perhaps the most relevant of which is *string theory*.

From an effective field theory (EFT) perspective, there is a vast number of effective Lagrangians, $\mathcal{L}_{\text{eff}}$, which can be built using strings and which correspond to different constructions, resulting from different compactification schemes. These Lagragians yield seemingly consistent, anomaly-free QFTs. In reality, though, only a few of them can be made consistent with a quantum theory of gravity and we say these theories belong to the string *Landscape*. The rest, which are not consistent with quantum gravity, form the *Swampland*. Over the past two decades, a set of conditions which allow to distinguish between the Landscape and the Swampland has been developed and studied. They are referred to as the Swampland conjectures [1, 2].

Independently of the underlying physical theory (if there is one) which eventually supersedes current ones (GR and the QFTs describing particle interactions), experimental exploration will continue, either to discover new phenomena or to more accurately constrain the parameter spaces of physical theories. Thus, in a more general study of deviations from our best and currently accepted models of physics, the Standard Model of Particle Physics (SM) and Hot Big Bang Cosmology (ΛCDM), one should try to find violations of physical laws and variations of the fundamental constants of nature, as they may point to new physics, explain phenomena not under the current umbrella of physical knowledge and possibly help in the unification of the fundamental forces of nature in a grand unified theory (GUT).

In the context of fundamental physics, the most easily detectable deviations from theoretically "understood" physical behaviour are violations of the Equivalence Principle (EP) and spacetime variations of the fundamental coupling constants, such as the fine-structure constant $\alpha \propto e^2$, where e is the modulus of the electron charge. Both of these effects have been widely studied and searched for, using solar system and earth-bound experiments and astronomical observations.

1.1 Violations of the equivalence principle

The EP has 3 main forms: the Weak EP (WEP), the Einstein EP (EEP) and the Strong EP (SEP), each containing the previous one. The WEP postulates the universality of free-fall, due to the apparent equivalence of inertial and gravitational mass. The EEP adds to the WEP the postulates of special relativity: local Lorentz and position invariance of experimental results. General Relativity is built on the EEP, so any physical phenomenon which violates it is evidence that the theory might be wrong or at best incomplete.

An extensive review on tests of GR can be found in [3], where modelling of deviations from GR using the parameterized post-Newtonian (PPN) formalism is explained and contemporary experimental results are reported. In short, the PPN formalism provides a consistent way of quantifying violations of Lorentz invariance, total momentum conservation, EP, etc., which are inherent to beyond SM theories, modified theories of gravity, quantum gravity and other non-standard theories. The PPN parameters are relatable to different experimental setups and subject to constraints imposed by experiment, thus allowing us to rule out theories based on whether or not they belong to the constrained parameter space.

One particularly relevant experimental observable is the Eötvös parameter:

$$\eta \equiv 2\frac{a_A - a_B}{a_A + a_B} \ , \tag{1.1}$$

which compares the accelerations of two test bodies, A and B, due to gravity. It is used to quantify violations of the WEP and is typically tested in torsion balance, lunar laser ranging and orbital experiments. Most recently, the MICROSCOPE mission, which is a satellite experiment, set the most stringent bound on η to date, $|\eta| \lesssim 10^{-14}$ [4]. In our context, the Eötvös parameter is important, because it is related the coupling constants appearing in quintessence, runaway dilaton and Bekenstein-type models (see Chap. 3).

1.2 Varying fundamental constants

The SM is without a doubt a huge success. Its predictive power is unmatched by any other model physicists have ever come up with. But, despite its achievements, it contains 19 free parameters (particle masses, charges, mixing-angles, etc.) which must be pinned down by experiments and whose values seem highly tuned to produce the universe we observe today, which is capable of harbouring life. The mystery of how those values arose from a seemingly infinite distribution of possibilities is generally referred to as the *fine-tuning problem* [5].

Among other explanations, one possibility is that the values of the SM parameters are actually natural. This is one of the expectations of string theory, which only has one fundamental parameter, the string tension T. In the perturbative limit, where the string action is broken down into a spectrum of particle species which interact with one another, the parameters governing this "string derived SM" are all related to the dilaton and the various moduli fields (see Sec. 2.1), whose dynamics are determined by the tension of the string. Hence, varying fundamental constants are naturally expected if string theory is to be the underlying theory of everything.

Even in more general phenomenological models of cosmology, it is somewhat restrictive to assume the couplings between the several components of the universe to be constant. One particular example is the inclusion of a single scalar degree of freedom, ϕ, which can be coupled to the $U(1)$ sector of the EFT via a change of the form:

$$\mathcal{L}_F = -\frac{1}{4}F_{\mu\nu}F^{\mu\nu} \quad \longrightarrow \quad -\frac{1}{4}B_F(\phi)F_{\mu\nu}F^{\mu\nu} \quad , \tag{1.2}$$

where $B_F(\phi)$ is some general function which we call the gauge coupling function. This new term will be responsible for variations of the fine-structure constant, that may be detected through space and/or time. Its present value must of course be $B_F(\phi_0) = 1$, in order to maintain the validity of our description of $U(1)$ gauge fields in the present.

For instance, an effect of these variations is that the relative wavelength separation of pairs of spectral lines, due to the same pairs of transitions, may differ throughout spacetime. Spectroscopic analyses (such as [6, 7]) can and have been used to test whether or not this happens. Other quantifiable variations of fundamental constants and tests thereof exist, although, experiments seem to be most sensitive to varying-α. An in-depth review of the literature on varying coupling constants – including a meta-analysis of experimental evidence up until 2017 and descriptions of theoretical and phenomenological models – can be found in [8].

1.3 Motivation and organization

Fortunately for the Swampland program and string theory in general, studies have not yet found any incurable tension between observation and the Swampland conjectures. This does not, however, mean that these conditions are bulletproof.

An interesting perspective on the Swampland and its scientific basis can be found in [2]. With the push of string theorists and cosmologists to accurately understand and quantify the conjectures, some are on more solid theoretical footing than others. The most valuable evidence for the validity of a given conjecture is that it is satisfied by all string-*derived* models, i.e. models which are built from the ground up on elementary principles of string theory or quantum gravity. These differ from string-*inspired* models, which can be interpreted as QFTs merged with mathematical structures which are known to arise in string theory.

For our purposes, the most important of these structures is, of course, the dilaton, which is ubiquitous to *all* known string theories and, being a scalar field, can be used to model dark energy and other cosmological phenomena.

In this work, we intend to study the behaviour of several string-inspired models, with a focus on their predictions for the dark energy equation of state, $w_{\rm DE} = p_{\rm DE}/\rho_{\rm DE}$, and for variations of the fine-structure constant, $\Delta\alpha/\alpha$. Our goal is to see whether these observables can be used to test the models against the Swampland conjectures, whether tensions between models and conjectures arise and, if so, whether they are model-dependent.

There will be several lenses one can adopt to interpret the results. First, one can assume the Swampland conjectures to be correct and use them to falsify models based on their agreement with the conjectures. On the other hand, we can assume the models to be correct and use the results to constrain the parameter space of the conjectures. Lastly and most humbly, we can simply compare the tension between each model and the Swmapland conjectures, maintaining the possibility that both are wrong.

The models we are particularly interested in are: quintessence, the runaway dilaton scenario and an extension of Bekenstein's model for varying-α. Part of the work on quintessence has been included in [9]*, of which I am a co-author. In [9], we have explored a larger range of potentials and done a robust statistical analysis. Here, we intend to focus on a qualitative comparison of the three models to find out whether there could be detectable differences.

In Chap. 2, we give a short review of string theory, cosmology and the relevance of the Swampland conjectures to cosmology. We introduce the models in some detail in Chap. 3. The numerical implementation and all the relevant caveats are discussed in Chap. 4. In Chap. 5, we present and discuss our results and conclude in Chap. 6.

*Submitted and accepted for publication at the Journal of Cosmology and Astroparticle Physics (JCAP).

Chapter 2

Strings and the Universe

2.1 String theory

The study of string theory began in the late 60s as an attempt to explain the strong interaction of the SM. It ended up not being adopted by the particle physics community, as the quark model and its formulation through gauge theory proved very accurate in modelling the strong force. However, the interest in string theory did not die down throughout the following decades. Part of it was due to the natural emergence of a spin-2 particle in the string spectrum, a *graviton* candidate. Consistency requirements on bosonic string theory, the initially studied form, imply it to be defined on a 26-dimensional manifold. The inclusion of fermionic degrees of freedom, which resolve a multitude of technical issues, shed light on a (at the time) new symmetry, *supersymmetry*, that implies the existence of a bosonic/fermionic partner to every fermion/boson. The theory was consequently dubbed *superstring theory* and consistency requires it to be a 10-dimensional theory, a much closer number to our familiar 4-dimensional low-energy reality. Superstring theory can be realized by five symmetry groups, related to each other via dualities*, highlighting the deeper mathematical framework underpinning string theory. Additionally, dualities relate some superstring theories to 11-dimensional M-theory. In the classical limit, superstring- and M-theory correspond to 10- and 11-dimensional supergravities, respectively. For a review of string theory see [10].

Although superpartners to most of the SM's particles have never been observed, e.g. as was hoped for CERN – meaning that supersymmetry has never been directly detected – there are reasons to believe the energy scale or mass of these particles is way beyond

*Dualities, in particular T-duality, are important in understanding the distance conjecture.

current experimental capabilities. Many string theorists have, thus, moved on to work on the problem of the 6 (or 7) unseen dimensions.

The most generally adopted technique to dealing with said problem is called compactification, where the extra dimensions are assumed to have some closed geometry with a tiny spatial extent compared to our 3-dimensional space. This would solve the question of why we cannot see those extra directions. As it turns out, there is a huge number of ways that string theory can be compactified. Each compactification scheme typically leaves an imprint of massless scalar fields, called *moduli*, related to the geometric properties of the compactification, on the resulting EFT. This plague of massless scalars strongly contradicts observations, because it would lead to strong deviations from GR (strong WEP violations, etc.) [11], so these fields usually have to be stabilized via some mechanism, yielding a fixed value at low energies. The existence of an extremely large number of *vacua*, the metastable points in theory space, is how the idea of a string theory Landscape came to be. For more on compactification see [12].

2.1.1 The Landscape and the Swampland

In the midst of this abundance of possible vacua to represent our universe, there are certain criteria which need be satisfied. These stem from the fact that not all string vacuum constructions are consistent theories of quantum gravity. This has led to the idea of a *Landscape* of vacua which yield consistent QFTs and a likely bigger *Swampland* of seemingly consistent QFTs which cannot be ultraviolet complete, i.e. they cannot represent quantum gravity when brought to the Planck scale. The Swampland program has been a theoretical effort in trying to map the edges separating the Landscape from the Swampland. As of now, all the requirements for vacua to be in the Landscape have taken the form of conjectures, typically placing rough bounds on certain values related to the moduli fields described above. A comprehensive review of this now decades-long venture can be found in [2].

Three conjectures were first formally proposed in [1], where finiteness criteria for (i) the volumes of moduli spaces of scalar fields and (ii) the number of matter fields present in a resulting EFT, as well as (iii) restrictions on the ranks of gauge fields are discussed. Other conditions have since been conjectured and recent work on their cosmological consequences has leaned on two of them: the *de Sitter* (dS) and *distance* conjectures. In what follows, we adopt the notation of [13] which is different from that of [14, 15].

One ubiquitous prediction of string theory based models of gravity is the existence of a scalar particle called the *dilaton* – which also appears as an excitation on the string spectrum and is associated with the spin-2 graviton. The behaviour of the dilaton field, ϕ, and its potential are supposed to satisfy the Swampland conjectures for a given model to be consistent, in other words, for the string theory construction to be in the landscape.

2.1.1.1 Distance conjecture

As was first pointed out in [16], when the scalar fields in an EFT traverse an infinite distance in moduli space, the appearance of a tower of massless states seems unavoidable. Further, it is conjectured that the particles appear even at finite displacements, $\Delta\phi$, and that these must be roughly $\mathcal{O}(1)$ in Planck units. In that case, the states are not massless, but have exponentially decaying masses with growing field displacement, consistent with the massless limit at infinite displacement. A worked example of this behaviour in Kaluza-Klein theory can be found in [2]. There, it is clear that the towers emerge even when the theory is transformed under T-duality. Evidence for such behaviour can be found in a large number of string theory setups (see for example Sec. 6 of [17]) and it is deeply connected to T-duality.

One of the consequences of this conjecture is that the effective Lagrangian is fundamentally changed once the finite limit is crossed. Hence, one can also conjecture a limit on the field excursion over cosmological history to some distance in field space of order $M_{\rm Pl}$:

$$\frac{\Delta\phi}{M_{\rm Pl}} \lesssim d \sim \mathcal{O}(1) \quad , \tag{2.1}$$

arguing that we do not see the exponentially decaying massive particles.

2.1.1.2 De Sitter conjecture

It is extremely difficult to construct stable, and even metastable, de Sitter vacua in string theory, i.e. compactifications producing the effect of a positive cosmological constant. However, some contribution to the energy density resembling a cosmological constant could arise as a nowadays slow, but dynamical, degree of freedom, which could have had a wildly different behaviour in the past. This is seen, for instance, in certain quintessence models, discussed in Sec. 3. The dS conjecture – first proposed in [18] – reflects this apparent impossibility of dS vacua arising in string theory, which can be translated into a lower bound on the logarithmic slope of the potentials that the scalar fields (moduli and dilaton) in the low-energy EFTs are subject to:

$$M_{\rm Pl}\frac{|\nabla_\phi V|}{V} \gtrsim \lambda \sim \mathcal{O}(1) \tag{2.2}$$

where ∇_ϕ represents the gradient in field space. This form of the conjecture forbids extrema in the potential and is thus in tension with the known physics of the Higgs boson [19].

The dS conjecture has since been refined [20] by combining the distance conjecture with Bousso's covariant entropy bound [21]. The refinement results in an alternative bound on the eigenvalues of the Hessian operator. For simplicity, we only state the conjecture in the single field case:

$$M_{\rm Pl}\frac{|V'|}{V} \gtrsim \lambda \sim \mathcal{O}(1) \quad \textbf{or} \quad -M_{\rm Pl}^2\frac{V''}{V} \gtrsim c^2 \sim \mathcal{O}(1) \quad , \tag{2.3}$$

where the primes denote derivatives with respect to ϕ. In models where these parameters are constant, the potentials resulting from the first and second inequalities of Eq. 2.3 take exponential and sinusoidal forms, respectively. Even this refined formulation the dS conjecture implies that de Sitter spacetime is in the Swampland [13, 14, 18].

2.2 Cosmology

Cosmology is the study of the universe as a whole. The current standard model of cosmology, called ΛCDM, is one of the greatest successes of twentieth century physics. It is completely based on Einstein's General Theory of Relativity, with a Friedmann-Lemaître-Robertson-Walker (FLRW) metric describing the geometric background over which everything evolves. The ΛCDM model very accurately describes the evolution, dynamics and thermal history of the universe from the emission of the Cosmic Microwave Background (CMB) until the present. The inclusion of the cosmological constant, Λ, has enabled us to model the recent accelerated expansion of the universe, detected in the 1990's (see for example [22, 23]). It is not without its problems, though.

One of the most striking requirements – one which incidentally gives it its name – for ΛCDM to explain the gravitational behaviour of the universe we observe is that roughly 95% of it is not composed of regular matter. Dark energy (DE) and dark matter (DM), whose nature is still an unsolved mystery, respectively account for around 68% and 27% of the energy content in our observable universe [24]. Dark energy is thought to be responsible for the accelerated expansion we observe and for preventing gravitational collapse of the universe. Dark matter is required to explain many gravitational phenomena through the lens of GR, e.g. galaxy rotation curves, gravitational lensing, etc. In the ΛCDM model, DE = Λ and DM = CDM, where 'C' refers to "cold" or non-relativistic. Many efforts in theoretical cosmology over recent decades have been in trying to characterize this dark sector of the universe. So far, attempts at finding an explanation for the observed Λ in particle physics have proved fruitless. For instance, the sum of zero-point energies of a massive scalar field up to a Planck scale cutoff yields an energy density, $\rho_{\rm QFT}$ [25]:

$$\frac{\rho_{\rm QFT}}{\rho_\Lambda} \gtrsim 10^{118} \quad . \tag{2.4}$$

This is known as the *cosmological constant problem* and the solution might be related to quantum gravity. This is yet another reason to study models beyond ΛCDM and the SM.

The so called Hubble tension (or H_0 tension) is the problem that the Hubble constant inferred from late-time cosmological data, such as type-Ia supernovae (SNeIa), differs from that inferred from early-time features of the universe, such as CMB and Baryon Acoustic Oscillations (BAO) measurements, at a $\sim 4.4\sigma$ level. Many of the proposed solutions, i.e. extensions of or modifications to the standard ΛCDM paradigm, hinge on the existence of scalar fields. For an extensive review, see [26].

Moreover, inflation, first studied by Guth [27] and Linde [28, 29], is a field of cosmology which attempts to address several shortcomings of ΛCDM when it comes to describing the early universe – before the release of the CMB radiation. These include the *horizon problem*, the *flatness problem*, the *magnetic monopole problem*, etc. (see [30]). The main ingredient to inflationary model building is one or more scalar fields, whose quantum fluctuations explain the anisotropies in the CMB and matter clustering. Before the recombination epoch (the formation of neutral hydrogen atoms) and the subsequent photon decoupling (emission of the CMB), these anisotropies cause gravitational clumping of the primordial plasma, planting the seeds for large-scale structure formation.

As we have seen, scalar fields find a natural home in string theory – recall that the dilaton is an inherent part of the string spectrum. Hence, it might very well be that some of our current puzzles are deeply connected to the nature of quantum gravity, and that the answer might be lurking somewhere in the string Landscape. Each model has a signature of cosmological observables, such as energy densities of different components of the universe, ρ_i, Hubble expansion rate, $H(z)$, amplitudes of matter clustering and CMB power spectra, σ_8 and A_s, spectral tilt, n_s, ratio of tensor-to-scalar perturbations produced by inflation, r, etc. Thus, we arrive at the possibility of using astronomical and cosmological data to falsify said string-inspired models and constrain the Swampland.

2.3 Cosmological implications of string theory

We now turn to and summarize some recent studies which have looked at the connection between cosmology and the Swampland conjectures. The field of string-cosmology seems to be gaining attention over the past few years, as testable predictions of string theory seem to require a cosmic laboratory. A recent extensive review of the topic can be found in [31].

Agrawal *et al.* (2018)

Ref. [14] studied the validity of different cosmological models when the Swampland conjectures expressed as in Eq. 2.1 and Eq. 2.2 are taken into account. The paper first looks at consequences of the Swampland conjectures for the early universe, then for the present epoch and finally a prediction for the future evolution is made.

Both "chaotic" and "plateau" inflationary models are shown to be in tension with these Swampland criteria. Chaotic (with power-law or exponential potentials) models are ruled out, because observational constraints on the tensor-to-scalar ratio, r, set $(M_{\rm Pl}|V'|/V)^2 \simeq 2\epsilon < 0.0044$,* such that $\lambda \lesssim 0.07$ is smaller than the $\mathcal{O}(1)$ lower bound by at least one order of magnitude. This bound also prohibits the existence of extrema in the potential, since they are defined by $V'(\phi) = 0$. Plateau models also have minima, which provide a mechanism to end inflation, thus being excluded by the same argument. Since almost all inflationary scenarios have some combination of these qualities, both simple and complex models, e.g. multi-field inflation†, have trouble satisfying the Swampland conditions.

It is argued that, because they do not behave like a cosmological constant, certain quintessence models can satisfy the de Sitter conjecture (Eq. 2.2). Thus, the paper studies the consequences of single-field quintessence with an exponential potential, $V(\phi) \propto e^{\lambda\phi}$, for the distance and de Sitter conjectures. The 2σ constraints of [33] (with SNeIa, CMB and BAO datasets) on the Chevallier-Polarski-Linder (CPL) [34, 35] parameterization of the dark energy equation of state:

$$w_{\rm DE}(z) = w_0 + w_a \frac{z}{1+z} \tag{2.5}$$

*The slow-roll parameter ϵ tends to zero towards the end of inflation, which occurs at a minimum of 60 e-folds of expansion.

†We highlight that more involved studies, such as [32], have arrived at the opposite conclusion, that multi-field inflation is actually preferred.

are used to draw an upper bound $\lambda \lesssim 0.6$, valid below a redshift $z = 1$.

The authors suggest further bounds can be placed on λ through improved measurements of the dark energy equation of state, w_ϕ. Also, further constraints on r could make the discrepancy between inflationary models and the string landscape more evident.

Ref. [14] also draws an interesting connection between the cosmological constant problem (recall the discussion around Eq. 2.4) and the distance conjecture in a quintessence type scenario, showing the relation between the expected cosmological constant and the GUT scale.

In a subsequent paper, Agrawal *et al.* (2021) [15] has explored the cosmological consequences of the so called *fading dark matter* model, where it was assumed that the tower of light states, which always emerges according to the distance conjecture, is responsible for the observed dark matter in the universe.

Raveri *et al.* (2019)

Ref. [13] looks at the implications of the refined de Sitter conjecture (Eq. 2.3) and the distance conjecture (Eq. 2.1) on late-time cosmology. As in [14], dark energy is assumed to be provided by a quintessence field. In [13], however, both an exponential, $V(\phi) \propto e^{\lambda\phi}$, and a cosine, $V(\phi) \propto \cos(c\phi)$, potential are considered, to test the refined de Sitter conjecture under the assumption of constant parameters, λ and c, respectively.

The work focuses on *thawing* models, where the field is nearly frozen by Hubble drag until Λ domination, since they easily satisfy the distance conjecture, because they tend to have lower field excursions, $\Delta\phi$. Once the field is released, it behaves like generic quintessence, slowly rolling towards an asymptotic minimum of the potential.

After the radiation and matter domination epochs, the potential, $V(\phi)$, is nearly linear and the Hubble constant is approximated by ΛCDM's. Taking the relative energy density of the cosmological constant to be $\Omega_\Lambda \simeq 0.69$, yields the following linear relation between field excursion and λ:

$$|\Delta\phi| \simeq 0.29\lambda \ , \tag{2.6}$$

after integrating the cosmological Klein-Gordon equation.

A statistical analysis, using a combination of CMB, SNe and H_0 data, finds $\lambda \leq 0.51$ and $c \leq 0.73$, at 95% C.L., which seems reasonable, if we are somewhat flexible about the meaning of "$\lambda \sim \mathcal{O}(1)$". However, the constraints at 68% C.L. are lower by about one order of magnitude, pointing to some tension between the refined de Sitter conjecture and observations, under these simple models. Through Eq. 2.6, the field excursion was found to be about $|\Delta\phi|_{z=0} < 0.15$ and $|\Delta\phi|_{z=1.5} < 0.14$ at 95% C.L., raising no tension between the distance conjecture and the models.

Chapter 3

Models

In this chapter, we give an overview of the theoretical basis and mathematics of the models we intend to compare. As a starting point, we clarify some terminology to avoid confusion. We use the words "model" and "scenario" interchangeably. Later in Chaps. 4 and 5, we will be studying each model with two distinct potentials (exponential and cosine). The descriptions found in this chapter for each model apply to both the exponential and cosine potential, i.e. they are irrespective of the potential.

To facilitate the connection between text and figures, we also include [**model, potential**] at the beginning of each caption, where **model** $\in \{\mathbf{Q}, \mathbf{RaDS}, \mathbf{BSBM}\}$ and **potential** $\in \{\mathbf{exp}, \mathbf{cos}\}$.

3.1 Quintessence

Quintessence is a canonical scalar field, minimally coupled to gravity, which is invoked to replace the cosmological constant as dark energy. Since de Sitter vacua do not seem to arise in string theory, quintessence models, where the field is eternally rolling down its potential, are the simplest candidate to modify the dark sector in string-inspired EFTs. The action for a canonical scalar field in Planck units is:

$$S = \int d^4x\sqrt{-g}\left\{\frac{R}{16\pi G} - \frac{1}{2}g^{\mu\nu}\partial_\mu\phi\partial_\nu\phi - V(\phi) - \frac{1}{4}B_F(\phi)F_{\mu\nu}F^{\mu\nu} + ...\right\} \quad , \tag{3.1}$$

where we have added the phenomenological coupling of ϕ to the electromagnetic sector, through the gauge coupling function, $B_F(\phi)$. To derive the equation of motion for the field, we may disregard the effect of this coupling, since it is expected to be subdominant.

This means that the scalar field evolves almost independently of the EM-field, while producing variations of the fine-structure constant, according to the gauge coupling function, $B_F\big(\phi(z)\big) = \alpha_0/\alpha(z)$. Varying the action with respect to ϕ, gives:

$$\begin{aligned}\delta S &= \int d^4x\sqrt{-g}\Big\{-g^{\mu\nu}\partial_\mu\phi\partial_\nu(\delta\phi) - \frac{\partial V(\phi)}{\partial\phi}\delta\phi + ...\Big\} \\ &= \int d^4x\Bigg\{-\partial_\nu\big[\sqrt{-g}g^{\mu\nu}\partial_\mu\phi\delta\phi\big] + \Bigg[\partial_\nu\big(\sqrt{-g}g^{\mu\nu}\partial_\mu\phi\big) - \sqrt{-g}\frac{\partial V(\phi)}{\partial\phi}\Bigg]\delta\phi + ...\Bigg\} \quad .\end{aligned} \tag{3.2}$$

The first term is zero by definition, because the field does not vary at the end points of its trajectory. The second term should be set to zero in order to satisfy the Principle of Least Action, resulting in the equation of motion:

$$-\frac{1}{\sqrt{-g}}\partial_\mu\big(\sqrt{-g}\partial^\mu\phi\big) + \frac{\partial V(\phi)}{\partial\phi} = 0 \quad . \tag{3.3}$$

As is most usual in cosmology, we assume a universe with homogeneous and isotropic background and, thus, use the Friedmann-Lemaître-Robertson-Walker (FLRW) metric. Since we are most interested in studying recent cosmological history, we further assume a flat FLRW background, whose metric in cartesian coordinates with $(-+++)$ convention is:

$$g_{\mu\nu} = \mathrm{diag}\Big(-1, a^2(t), a^2(t), a^2(t)\Big) \quad , \quad \sqrt{-g} = a^3(t) \quad , \tag{3.4}$$

where $a(t)$ is the scale factor, t is cosmic time and g is the determinant of the metric. Plugging this metric into Eq. 3.3 gives us:

$$\ddot{\phi} - \nabla^2\phi + 3\frac{\dot{a}}{a}\dot{\phi} + \frac{\partial V}{\partial\phi} = 0 \quad . \tag{3.5}$$

Using the familiar definition of the Hubble parameter $H = \dot{N} = \frac{\mathrm{d}}{\mathrm{d}t}\ln a = \dot{a}/a$ and assuming spatial variations to be negligible on cosmic scales, i.e. at the background level, we get:

$$\ddot{\phi} + 3H\dot{\phi} + \frac{\partial V}{\partial\phi} = 0 \quad . \tag{3.6}$$

As is sometimes convenient, the field equation can be equivalently expressed in terms of N, rather than t:

$$\phi'' + \left(3 + \frac{H'}{H}\right)\phi' + \frac{\partial_\phi V}{H^2} = 0 \quad . \tag{3.7}$$

From the action, one can also determine the Friedmann equation. The only difference from the Friedmann equation for the ΛCDM model is that the energy density attributed to the cosmological constant is now the energy density of the quintessence field. So, we have:

$$H^2 = \frac{8\pi G}{3}\rho = \frac{8\pi G}{3}\left\{\rho_{\rm m} + \frac{\dot{\phi}^2}{2} + V(\phi)\right\} \quad , \tag{3.8}$$

where $\rho_{\rm m}$ is a "matter" density which accounts for all other components of the universe. With this definition, what we call matter clearly has a time dependent equation of state:

$$w_{\rm m} = \frac{p_{\rm m}}{\rho_{\rm m}} = \frac{\sum_i p_i}{\sum_i \rho_i} = \frac{\sum_i w_i \rho_i}{\sum_i \rho_i} \ , \quad i = {\rm b}, {\rm cdm}, {\rm r}, \ldots \tag{3.9}$$

Of course, during the matter the dark energy dominated epochs $w_{\rm m} \sim 0$. For a detailed review of quintessence, see [36].

The gauge coupling function, introduced in Eq. 3.1, can be expanded as a Taylor series around ϕ_0:

$$B_F(\phi) = 1 - \zeta\frac{\phi - \phi_0}{M_{\rm Pl}} + \mathcal{O}\left(\phi^2\right) \quad , \tag{3.10}$$

where ζ and the coefficients of higher order terms become phenomenological parameters. As a reasonably good approximation, one can truncate the series at first order, because, if $B_F(\phi)$ does indeed vary, it is an extremely small effect. Variations of the fine-structure constant in quintessence models are, thus, simply given by [8]:

$$\frac{\Delta\alpha}{\alpha} = \frac{\alpha - \alpha_0}{\alpha_0} = \frac{1}{B_F(\phi)} - 1 \simeq \zeta\frac{\phi - \phi_0}{M_{\rm Pl}} \quad . \tag{3.11}$$

The ζ parameter can be shown to be related to the Eötvös parameter, η, introduced in Sec. 1.1:

$$\eta \simeq 10^{-3}\zeta^2 \quad . \tag{3.12}$$

Hence, measurements of WEP violations help break the degeneracy between ζ and $\Delta\phi$ of Eq. 3.11 and we find our first example of how data on varying-α can be used to test the distance conjecture.

3.1.1 Phase space analysis

In this subsection, we introduce a useful dimensionless parameterization as in [36], which allows us, in certain cases, to qualitatively determine the initial conditions for integrating the dilaton's equation of motion. We will call it "phase space" and define it to be the 2-dimensional space of points (x, y), such that:

$$x \equiv \frac{\dot{\phi}}{\sqrt{6}M_{\rm Pl}H} \quad , \quad y \equiv \frac{\sqrt{V(\phi)}}{\sqrt{3}M_{\rm Pl}H} \tag{3.13}$$

and in terms of which the energy densities relative to critical can be written:

$$\Omega_\phi \equiv \frac{\rho_\phi}{\rho_c} = x^2 + y^2 \quad , \quad \Omega_m = 1 - x^2 - y^2 \quad . \tag{3.14}$$

Next we want to substitute x, y and their derivatives into Eq. 3.7. To do so, notice that $H'/H = \dot{H}/H^2$ and that we can calculate this term by differentiating Eq. 3.8 with respect to time and dividing through by $2H^3$:

$$\begin{aligned} \frac{H'}{H} = \frac{\dot{H}}{H^2} &= \frac{1}{2H^3}\frac{8\pi G\dot{\rho}}{3} = -\frac{1}{2H^3}\frac{8\pi G}{3}3H(\rho+p) \\ &= -\frac{1}{2}\frac{\dot{\phi}^2 + (1+w_m)\rho_m}{M_{Pl}^2 H^2} \\ &= -3x^2 - \frac{3}{2}(1+w_m)(1-x^2-y^2) \quad , \end{aligned} \tag{3.15}$$

where we have used the thermodynamic relation $\dot{\rho} = -3H(\rho+p)$*.

If we further note that $x = \phi'/\sqrt{6}M_{Pl}$, it becomes easy to substitute the result above in the field equation:

$$x' = \sqrt{\frac{3}{2}}Ly^2 - \frac{3}{2}x\left[(1-w_m)\left(1-x^2\right) + (1+w_m)y^2\right] \quad , \tag{3.17}$$

where we have defined $L \equiv -M_{Pl}\partial_\phi V/V$ as in [9], so that in the limiting case $\lambda = |L|$. For the y variable, we can also derive a differential equation by first differentiating y^2 with respect to N:

$$\begin{aligned} \left(y^2\right)' = 2yy' = \left(\frac{V}{3M_{Pl}H^2}\right)' &= \frac{\phi'\partial_\phi V}{3M_{Pl}H^2} - 2\frac{V}{3M_{Pl}H^3}H' \\ &= y^2\left(M_{Pl}\frac{\partial_\phi V}{V}\sqrt{6}x - 2\frac{H'}{H}\right) \quad . \end{aligned} \tag{3.18}$$

Now we divide the result by $2y$ and substitute our expressions for H'/H and L to get:

$$y' = -\sqrt{\frac{3}{2}}Lxy + \frac{3}{2}y\left[(1-w_m)x^2 + (1+w_m)\left(1-y^2\right)\right] \quad . \tag{3.19}$$

So, we finally have two coupled differential equations for x and y with parameters w_m and L. It is clear that there are 3 trivial fixed points (x^*, y^*) in phase space, meaning $x'|_{x=x^*,y=y^*} = y'|_{x=x^*,y=y^*} = 0$, namely:

$$(x^*, y^*) = (0,0) \ , \ (\pm 1, 0) \quad . \tag{3.20}$$

*Using energy and entropy conservation $dU = dQ + dW$, where $U = \rho V$, $dQ = TdS = 0$, $dW = -pdV$ and $V = a^3$, we have:

$$d(\rho a^3) = TdS - pd(a^3) \quad \Leftrightarrow \quad a^3 d\rho + 3\rho a^2 da = -3pa^2 da \quad \Rightarrow \quad \frac{d\rho}{dt} = -\frac{3(\rho+p)}{a}\frac{da}{dt} \tag{3.16}$$

Besides the fixed points at $y = 0$, there are two additional ones, which require some algebra to find (see Appendix A):

$$(x^*, y^*) = \begin{cases} \left(\frac{L}{\sqrt{6}} \;,\; \sqrt{1 - \frac{L^2}{6}} \right) \;, & \text{red} \\ \left(\sqrt{\frac{3}{2}}\frac{1+w_\mathrm{m}}{L} \;,\; \sqrt{\frac{3}{2}}\frac{\sqrt{1-w_\mathrm{m}^2}}{L} \right) \;, & \text{blue} \end{cases} \tag{3.21}$$

The vector field defined by Eqs. 3.17 and 3.19 is akin to a fluid flowing between the fixed points above. The shape of the flow field is determined by the parameters w_m and L and an example is given in Fig. 3.1. One thing that should be clear is that, since at least w_m is guaranteed to be time dependent, so is the flow field. Thus, a fixed value of w_m, as is most commonly used, is only reliable to study individual cosmic epochs.

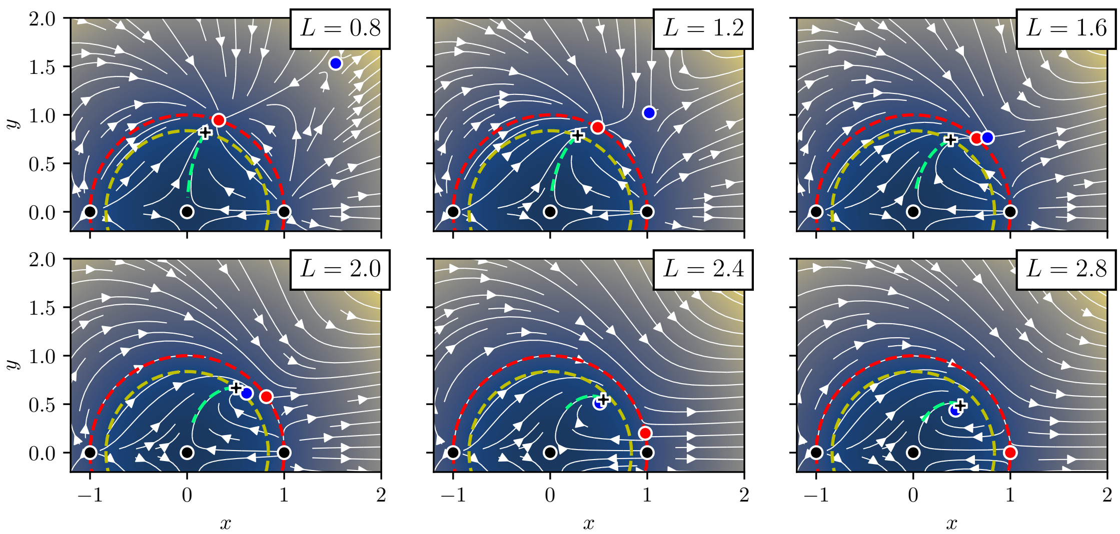

Figure 3.1: **[Q, exp]** Example phase space plot for $w_\mathrm{m} = 0$ and various constant values of L. The trivial fixed points are the black circles and the non-trivial ones are in red and blue. The red and yellow dashed circles correspond to $\Omega_\phi = 1$ and $\Omega_\phi = 0.7$, respectively. The green dashed line and black cross are the trajectory up to $z = 4$ and its initial condition, respectively. Figure also included in [9].

That being said, we can make use of the phase space parameterization to define the initial conditions for integrating the field equations. In this sense it is important to look at the stability of the fixed points, which we have summarized in Table B.1 of Appendix B. During matter- and later dark energy-domination, one can make the approximation $w_\mathrm{m} = 0$. For matter domination, one requires $\Omega_\mathrm{m} \sim 1$ and $\Omega_\phi \ll 1$. These conditions imply that only $(x^*, y^*) = (0, 0)$ and $(x^*, y^*) = \left(\sqrt{\frac{3}{2}}\frac{1+w_{\rm m}}{L}, \sqrt{\frac{3}{2}}\frac{\sqrt{1-w_{\rm m}^2}}{L}\right)$ can represent a matter-dominated past, since all other fixed points have $\Omega_\phi = 1$. For the latter to be matter-dominated, it is also required that $L \gg 1$, because in that case $\Omega_\phi = 3/L^2$. This is, however, incompatible with the requirement set by cosmic acceleration during dark energy-domination that $L^2 < 2$ (for the explicit argument see [9]). Non-domination of dark energy in the past is needed for large scale structure formation, so we can conclusively say that the fixed point $(x^*, y^*) = (0, 0)$ is the only viable matter-dominated representation of the past.

It can be seen in Table B.1 that the non-trivial fixed points switch stability at $L^2 = 3(1 + w_{\rm m})$. So, while the blue fixed point is not a suitable past, it can be a suitable present or future, as long as $\Omega_\phi = 3/L^2 \gtrsim 0.7$, i.e. $L \lesssim 2.07$. If $L > 2.07$, the blue fixed point in Fig. 3.1 lies within the yellow dashed circle and quintessence cannot fully account for the observed amount of dark energy.

Notice that x^2 and y^2 are, respectively, the kinetic and potential energy densities *relative to critical*. This means that choosing $(x^*, y^*) = (0, 0)$ as an initial condition is an assertion on the percentage of dark energy in the past, not a fine-tuning of actual initial conditions, as would be, for example, choosing $\phi_{\rm i}$ and $\phi'_{\rm i}$ or ϕ_0 and ϕ'_0. This is one of the most useful features of the phase space parameterization.

3.2 Runaway dilaton scenario

One of the main challenges of string theory at the beginning of the millennium was to address the undesirable consequence that a massless dilaton, which is naturally expected in string theory and whose VEV determines the string coupling constant, $g_s^2 = e^\phi$, induces WEP violations, as well as other effects, that strongly contradict experimental evidence [37]. The mechanism introduced in [37], dubbed *Damour-Polyakov screening*, allows for dilaton-matter decoupling, yielding almost dilaton-independent masses and coupling constants. The runaway dilaton scenario was proposed by Damour, Piazza and Veneziano in [38, 39] in an attempt to reconcile a massless dilaton with observation, by showing that the dilaton could be cosmologically attracted to some fixed point at infinity, where the coupling functions have some smooth finite limit:

$$B_i(\phi) = C_i + \mathcal{O}\left(e^{-\phi}\right) \quad , \quad i = g, \phi, F, \psi... \tag{3.22}$$

The field equation governing the motion of the dilaton in this scenario, can be written in the Einstein frame as the following [8]:

$$\frac{2}{3-\phi'^2}\phi'' + \left(1-\frac{p}{\rho}\right)\phi' = -\sum_i \alpha_i(\phi)\frac{\rho_i - 3p_i}{\rho} \quad , \tag{3.23}$$

where the index i is used to sum over all components of the universe and the dilaton's potential energy, but excluding its kinetic energy. Here, we call attention to the fact that, in this definition, the field has different units than in the definition of Sec. 3.1. The couplings $\alpha_i(\phi)$, which model the interaction of the dilaton with the fluids filling the universe, are not to be confused with the gauge coupling functions of Eq. 3.22. These coupling parameters can be expressed as the gradients of specific mass scales [38, 40]:

$$\alpha_i(\phi) = \frac{\partial \ln m_i(\phi)}{\partial \phi} \tag{3.24}$$

and, specifically for the dilaton's self-interaction through its potential, $\alpha_V = \frac{1}{4}\,\partial \ln V(\phi)/\partial\phi$, since $m_V = V^{1/4}$. We now redefine L to have the same numerical value as that of [9] and the previous section, due to the different field units commonly used to study the runaway dilaton, ϕ, and quintessence, $\tilde{\phi} = \phi/\sqrt{4\pi G}$:

$$L = -\frac{M_{\rm Pl}}{V}\frac{\partial V}{\partial \tilde{\phi}} = -\frac{1}{\sqrt{2}V}\frac{\partial V}{\partial \phi} \quad \Rightarrow \quad \alpha_V = -\frac{L}{2\sqrt{2}} \quad . \tag{3.25}$$

Note that in the matter and dark energy eras, besides the scalar field, we only consider the contributions of baryonic and cold dark matter to cosmic evolution. The coupling of the dilaton to hadrons, and consequently to baryons, is expected to be [8]:

$$\alpha_{\rm had}(\phi) \simeq \alpha_{\rm had0}e^{-(\phi-\phi_0)} \quad , \tag{3.26}$$

where the present-day coupling, $\alpha_{\rm had0}$, is constrained by solar-system gravitational lensing and WEP violation experiments encoded in the Eddington and Eötvös parameters, γ and η, respectively. A conservative estimate gives $|\alpha_{\rm had0}| \lesssim 10^{-4}$.

Following [41]*, we are going to study the runaway dilaton scenario under three simplifying assumptions for the effective coupling of the field to dark matter, $\alpha_{\rm cdm}$. This includes considering a universal coupling to matter, $\alpha_{\rm cdm} = \alpha_{\rm b}$, a universal coupling to the dark sector, $\alpha_{\rm cdm} = \alpha_V$, and a dynamical coupling to field's kinetic energy, $\alpha_{\rm cdm} = -\phi'$.

*Ref. [41] considered a constant potential for the dilaton, which clearly differs from our analysis.

In the runaway dilaton scenario, the variations of α are approximately given by [38]:

$$\frac{\Delta\alpha}{\alpha} = \frac{\alpha_{\rm had0}}{40}\left[1 - e^{-(\phi-\phi_0)}\right] \quad . \tag{3.27}$$

Defining the density and pressure of the fluid as:

$$\rho = \rho_{\rm b} + \rho_{\rm cdm} + V(\phi) \tag{3.28}$$

$$p = p_{\rm b} + p_{\rm cdm} - V(\phi) \tag{3.29}$$

and noting that $p_{\rm b} = p_{\rm cdm} = 0$, the field equation can be rewritten:

$$\begin{aligned}\phi'' &= -\frac{3-\phi'^2}{2}\left\{\left(1+\frac{V}{\rho_{\rm b}+\rho_{\rm cdm}+V}\right)\phi' + \frac{\alpha_{\rm b}\rho_{\rm b}+\alpha_{\rm cdm}\rho_{\rm cdm}+4\alpha_V V}{\rho_{\rm b}+\rho_{\rm cdm}+V}\right\} \\ &= -\frac{3}{2}\frac{1-\phi'^2/3}{\rho}\left\{(\rho_{\rm b}+\rho_{\rm cdm}+2V)\phi' + \alpha_{\rm b}\rho_{\rm b}+\alpha_{\rm cdm}\rho_{\rm cdm}+4\alpha_V V\right\} \\ &= -\frac{3}{2}\frac{1-\phi'^2/3}{\rho}\left\{(\phi'+\alpha_{\rm b})\rho_{\rm b} + (\phi'+\alpha_{\rm cdm})\rho_{\rm cdm} + 2(\phi'+2\alpha_V)V\right\} \quad .\end{aligned} \tag{3.30}$$

On the other hand, the Friedmann equation is:

$$3H^2 = 8\pi G\rho + H^2\phi'^2 \quad \Leftrightarrow \quad \frac{3H^2}{8\pi G} = \frac{\rho}{1-\phi'^2/3} \quad \Leftrightarrow \quad \frac{H^2}{H_0^2} = \frac{\rho/\rho_{\rm c0}}{1-\phi'^2/3} \quad . \tag{3.31}$$

Subsituting this back into the previous equation and using $\Omega_i \equiv \rho_i/\rho_{\rm c}$ we get:

$$\begin{aligned}\phi'' &= -\frac{3}{2\rho_{\rm c}}\left\{(\phi'+\alpha_{\rm b})\rho_{\rm b} + (\phi'+\alpha_{\rm cdm})\rho_{\rm cdm} + 2(\phi'+2\alpha_V)V\right\} \\ &= -\frac{3}{2}\left\{(\phi'+\alpha_{\rm b})\Omega_{\rm b} + (\phi'+\alpha_{\rm cdm})\Omega_{\rm cdm} + 2(\phi'+2\alpha_V)\Omega_V\right\} \quad .\end{aligned} \tag{3.32}$$

It is convenient to write:

$$\Omega_i = \frac{8\pi G}{3H^2}\rho_i = \frac{H_0^2}{H^2}\frac{8\pi G}{3H_0^2}\rho_i = \frac{H_0^2}{H^2}\frac{\rho_i}{\rho_{\rm c0}} = \frac{H_0^2}{H^2}\frac{\rho_{i0}}{\rho_{\rm c0}}\frac{\rho_i}{\rho_{i0}} = \frac{H_0^2}{H^2}\Omega_{i0}\frac{\rho_i}{\rho_{i0}} \ , \tag{3.33}$$

since we know how the fluids dilute with expansion, i.e. the last factor in this expression. The matter components redshift as $\rho_{\rm m}/\rho_{\rm m0} = a^{-3} = (1+z)^3$, where a is the scale factor. In this case, V is not a cosmological constant and evolves as $V/V_0 = \exp\left[-\sqrt{2}\int L d\phi\right]$.

3.2.1 Phase space analysis

Note that in this case, the different definition of the field $\phi' \to \sqrt{2}M_{\rm Pl}\phi'$, compared to the one we use in Sec. 3.1, leads to a slightly altered definition of the phase space variables:

$$x \equiv \frac{\phi'}{\sqrt{3}} \quad , \quad y \equiv \frac{\sqrt{V}}{\sqrt{3}M_{\rm Pl}H} \quad \Rightarrow \quad \Omega_\phi = \frac{\phi'^2}{3} + \frac{V}{\rho_{\rm c}} = x^2 + y^2 \quad . \tag{3.34}$$

As before, the second-order differential equation for the dilaton, Eq. 3.32, can be expressed as a first-order differential equation for x and, similarly to the previous section, we get an equation for y:

$$x' = \sqrt{\frac{3}{2}}Ly^2 - 3x + \frac{3}{2}x\left[\left(1 - \frac{x_{\rm fp}}{x}\right)x^2 + \left(1 + \frac{x_{\rm fp}}{x}\right)\left(1 - y^2\right)\right] , \tag{3.35}$$

$$y' = -\sqrt{\frac{3}{2}}Lxy + \frac{3}{2}y\left[\left(1 + \frac{xx_{\rm fp}}{1-x^2}\right)x^2 + \left(1 - \frac{xx_{\rm fp}}{1-x^2}\right)\left(1 - y^2\right)\right] . \tag{3.36}$$

Note that we have defined $x_{\rm fp} = -(\alpha_{\rm b}\Omega_{\rm b0} + \alpha_{\rm cdm}\Omega_{\rm cdm0})/\sqrt{3}\Omega_{\rm m0}$, with the subscript "fp" to highlight the fact that it is the x-coordinate of a non-trivial fixed point. Note also that, in the limit where the field is uncoupled to matter, $x_{\rm fp} = 0$, we get Eqs. 3.17 and 3.19 with $w_{\rm m} = 0$. An explicit derivation of both Eqs. 3.35 and 3.36 and their fixed points are left for Appendix A. The existence and stability conditions of the fixed points are summarized in Table B.2 of Appendix B. As we did in the previous subsection, Fig. 3.2 shows the phase space plots for the runaway dilaton scenario.

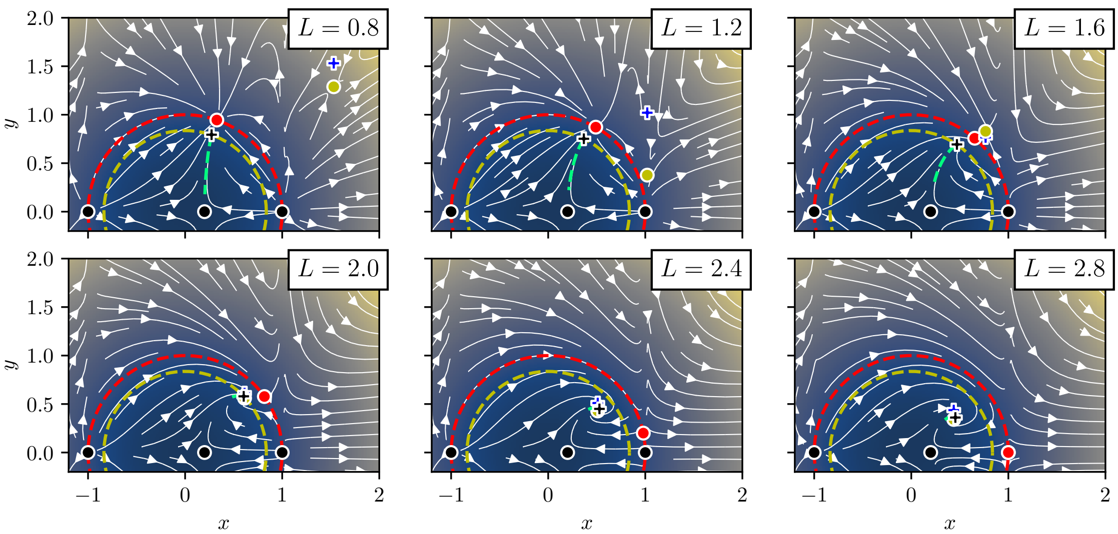

FIGURE 3.2: **[RaDS, exp]** Example phase space plot for $x_{\rm fp} = 0.2$ and various constant values of L. The trivial fixed points are the black circles and the non-trivial ones are in red and yellow ((*c*) and (*e*) of Table B.2, respectively). The black crosses mark the present day (x_0, y_0). The blue cross marks the position of the other non-trivial fixed point in the quintessence case, i.e. the blue point of Fig. 3.1 (point (*d*) in Table B.1). The red and yellow dashed circles correspond to $\Omega_\phi = 1$ and $\Omega_\phi = 0.7$, respectively.

3.3 Bekenstein-type models

In [42], Bekenstein derived a "minimalist" framework for introducing electromagnetic charge variations into the successful theory of quantum electrodynamics (QED). In his work, QED is approximated by semi-classical electromagnetism (EM), where a quantum EM-field, $F_{\mu\nu}$, interacts with classical matter, such as point charges. Maxwell's electrodynamics is then modified because of the assumed e-variations. The general spacetime dependence of e is:

$$e(x^\mu) = e_0 \epsilon(x^\mu) \ , \tag{3.37}$$

where e_0 is the present-day electron charge and ϵ is a dimensionless scalar field modulating its variation. Under several assumptions, intended to maintain the validity of GR and QED in contemporary experiments, dynamical equations for $\epsilon(x)$ were derived from an action principle and it was shown that its effects were small enough to still be compatible with experiment.

One of the key aspects of Bekenstein's model and its extensions is that they make no assumptions on the nature of dark energy. These models simply introduce the dependence of the coupling on the phenomenological scalar field. This behaviour differs from that of quintessence, where dark energy is expected to be provided by the scalar field itself. However, we will introduce this exact assumption into the Bekenstein-type model, since it is at the core of our analysis.

Extended Bekenstein-type models are a great tool to study low-energy EFTs, since they are relatively simple and their results are easily compared to experiment. The relevance of these models for our purposes is that they will allow us to test the couplings which typically arise in string-inspired EFTs from a phenomenological point of view. For simplicity, we focus on the Sandvik-Barrow-Magueijo (BSBM) extension of Bekenstein's model (see 3.3.1). It is not as general as the Olive & Pospelov (O&P) extension [43] (for recent studies see [44, 45]), which allows the dilaton to couple to many different degrees of freedom, but still provides interesting cosmological phenomenology.

3.3.1 BSBM extension

Bekenstein's model for varying-e was later extended by Sandvik, Barrow and Magueijo in [46] to include the variation's effects on gravity and cosmological evolution. The dilaton-like field $\psi \equiv \ln \epsilon$ couples to the electromagnetic sector of the Lagrangian, $\mathcal{L}_{\text{EM}} = -\frac{1}{4} f_{\mu\nu} f^{\mu\nu}$, where $f_{\mu\nu} = \epsilon F_{\mu\nu}$. The action in this model is then given by:

$$S = \int d^4x\sqrt{-g}\left\{\frac{R}{16\pi G} - \frac{\omega}{2}g^{\mu\nu}\partial_\mu\psi\partial_\nu\psi + \mathcal{L}_{\rm EM}e^{-2\psi} + ...\right\} \quad , \tag{3.38}$$

where ω is a phenomenological parameter shown to be ~ 1 and the ellipses include the matter fields, not coupled to the dilaton. The field equation resulting from this action is:

$$\ddot{\psi} + 3H\dot{\psi} = -\frac{2}{\omega}e^{-2\psi}\zeta_{\rm m}\rho_{\rm m} \quad , \tag{3.39}$$

where we have introduced the only significant phenomenological parameter of the model, $\zeta_{\rm m} = \mathcal{L}_{\rm EM}/\rho_{\rm m}$. The Friedmann equation in this case is given by:

$$H^2 = \frac{8\pi G}{3}\left\{\rho_{\rm m}\left(1 + \zeta_{\rm m}e^{-2\psi}\right) + \rho_{\rm r}e^{-2\psi} + \rho_\Lambda + \frac{\dot{\psi}^2}{2}\right\} \quad , \tag{3.40}$$

$\rho_{\rm m}$, $\rho_{\rm r}$ and ρ_Λ being the energy densities of matter, radiation and the cosmological constant, respectively. In our case however, we are interested in having a field with non-zero potential energy and no cosmological constant providing dark energy. This leads to the following field and Friedmann equations:

$$\ddot{\psi} + 3H\dot{\psi} + \frac{\partial V(\psi)}{\partial\psi} = -\frac{2}{\omega}e^{-2\psi}\zeta_{\rm m}\rho_{\rm m} \quad , \tag{3.41}$$

$$H^2 = \frac{8\pi G}{3}\left\{\rho_{\rm m}\left(1 + \zeta_{\rm m}e^{-2\psi}\right) + \rho_{\rm r}e^{-2\psi} + \frac{\dot{\psi}^2}{2} + V(\psi)\right\} \quad . \tag{3.42}$$

In either case, a non-zero field displacement $\Delta\psi$ produces fine-structure constant variations of the form:

$$\frac{\alpha(\psi)}{\alpha_0} = e^{2(\psi-\psi_0)} \quad . \tag{3.43}$$

The $\alpha(z)$ variations obtained with this model in [46] were in agreement with contemporary experimental data, including laboratory, geonuclear and astronomical experiments. As opposed to quintessence, the runaway dilaton scenario and the O&P extension of Bekenstein's model, in the BSBM extension the field value alone determines the coupling of the scalar field to the EM-sector of the Lagrangian.

Unfortunately, the BSBM model we are interested in is not as amenable to the phase space parameterization of the scalar field as quintessence and the runaway dilaton scenario have been. This is mainly due to the high prevalence of $e^{-2\psi}$ factors and, in particular, the $\rho_{\rm r}e^{-2\psi}$ term present in the Friedmann equation, which is not simply dismissible by assuming some coupling to be small. For this reason, we will not bother trying to express the BSBM equations in terms of x and y, as was done in the previous sections.

Chapter 4

Numerical implementation

Having derived the fundamental equations for each model, we are now in a position to integrate them numerically. All the differential equations were integrated using either the "RK45" method of the `solve_ivp` function provided by the `scipy` library of Python or a self-implemented 4^{th}-order Runge-Kutta method where convenient.

4.1 Exponential potential

As a simple starting point we consider the case of the exponential potential. Later, we will comment on the more nuanced cosine potential.

4.1.1 Quintessence

A quintessence-type scenario with a single exponential potential is a very simple and attractive model, since the equations of motion become independent of the initial field value, depending only on its displacement over cosmic evolution. The phase space parameterization introduced earlier (Sec. 3.1) can be used with almost no caveats or approximations*.

As discussed previously, the matter-dominated past, with $w_{\mathrm{m}} \sim 0$, can only be represented by the fixed point at $(x^*, y^*) = (0, 0)$, so we start by integrating Eqs. 3.17 and 3.19 with initial condition $(x, y) = (0, \delta_y)$. The value $\delta_y = 10^{-2} \ll 1$ is chosen as a small perturbation to allow the integration to evade the fixed point and its direction is the one which flows away from the fixed point, which is a saddle-point, as shown in Appendix B. This is called the *fast-manifold* in dynamical systems language and it is the trajectory in phase space we intend to find (see Chapter 2 of [47]). We integrate until we

*This will not be the case with the runaway dilaton scenario.

find $x_0^2 + y_0^2 = \Omega_{\phi 0} = 0.7$. The solution of this first integration is then used as the initial condition for a second integration over a targeted redshift range. Recall that, if $L > 2.07$, the fixed point in the far future has $\Omega_\phi < 0.7$. To prevent overcomplication, we add the simple condition that, if Ω_ϕ starts to grow smaller, we stop the integration and use (x_0, y_0) which yields the maximum value of Ω_ϕ. In practice, this does not seem problematic, since we have not found any cases where trajectories go back and forth radially.

As has been shown in [14], experimental values of the equation of state of dark energy, alone, exclude values of $L \gtrsim 0.6$, so we only consider values of L below 0.6. For each value of L, the variation of α is proportional to the field displacement, $\Delta\phi$, according to Eq. 3.11. The only cosmological parameters which have to be predetermined for this numerical process are $\Omega_{\phi 0}$ and L. The phenomenological parameter, ζ, which determines the proportionality between field displacement and α variations is taken to be its maximum possible value in light of the MICROSCOPE result $|\eta| \leq 10^{-14}$ [4]:

$$\zeta^2 \simeq 10^3 |\eta| \quad \Rightarrow \quad \zeta_{\max} \sim 10^{-5.5} \simeq 3.16 \times 10^{-6} \quad . \tag{4.1}$$

4.1.2 Runaway dilaton scenario

The whole numerical scheme described in the previous subsection for the canonical scalar field is almost identical to the one we apply for the runaway dilaton. The main difference is that we now have to perform the first integration starting at $(x^*, y^*) = \big(x_{\rm fp}, 0\big)$. As simple as this may sound, defining $x_{\rm fp}$ requires four additional cosmological parameters, namely: $\Omega_{\rm b0}$, $\Omega_{\rm cdm0}$, $\alpha_{\rm b}$ and $\alpha_{\rm cdm}$. The complication arises in particular in the definition of the latter two.

Recall from Eq. 3.26 that the coupling to hadrons depends on the field displacement, $\Delta\phi = \phi - \phi_0$, requiring prior knowledge of the field value at the initial point of integration (close to the fixed point), which we do not have. Because there is no way around this issue, we make the approximation that $e^{-(\phi-\phi_0)} \sim 1$, such that for the first integration $\alpha_{\rm had} \sim \alpha_{\rm had0}$. After finding the present day kinetic and potential energy densities, (x_0, y_0), we integrate back in time, but now performing the integral:

$$\phi(z) - \phi_0 = \int\limits_0^{N(z)} \sqrt{3} x dN \tag{4.2}$$

at each step, where $0 - N(z)$ is obviously the number of e-folds of expansion between the given redshift, z, and the present, hence $N(z) \leq 0$. Thus, there is an inherent inaccuracy in the phase space trajectory.

Since $|\alpha_{\rm had0}| \ll 1$, the contribution of the coupling would only significantly help drive the field evolution – and help deviate the trajectory – if $e^{\Delta\phi} \sim 10^3$. However, as we will see, for the low L values required to satisfy the constraints on w_ϕ, field displacements will be rather small, so, although real, the inaccuracy is not much of a deterrent.

Again, we use the maximal MICROSCOPE result for the Eötvös parameter, in this case to find $\alpha_{\rm had0}$:

$$\alpha^2_{\rm had0} \simeq \frac{10^5}{5.2}|\eta| \quad \Rightarrow \quad \alpha_{\rm had0,max} \sim \frac{10^{-4.5}}{\sqrt{5.2}} \simeq 1.39 \times 10^{-5} \quad . \tag{4.3}$$

We stress once more the fact that the coupling which induces variations of α in the runaway dilaton scenario is also partly responsible for the dilaton's evolution.

4.1.3 BSBM extension

For the reason described at the end of Sec. 3.3, we cannot use the phase space parameterization to find viable trajectories. The alternative is to define initial conditions, ψ_0 and ψ'_0, and directly integrate the field equation. As in the other models with exponential potentials, the equations are independent of ψ_0, so we set it to $\psi_0 = 0$.

First, we study the model over a range of L values assuming $\psi'_0 \simeq 0.007 \times 10^{-6}$, due to atomic clock bounds (see Sec. 4.3.2) and which is in accordance* with the most likely value found in [45] of $\psi'_0 \simeq (0.0071 \pm 0.0075) \times 10^{-6}$. Note that, although taking the model with a cosmological constant as fiducial might seem a little too constraining, we generically expect the dilaton's potential energy to account for most of the dark energy, so that the dark energy equation of state remains close to $w_\psi \sim -1$.

We also look at how the model behaves over a range of present day field speeds, $\psi'_0 \in [0.001, 0.01, 0.1, 1.0]$, with fixed $L = 1$.

For each case, we define the present day relative potential energy, $\Omega_{V0} = V_0/\rho_{c0}$, by balancing the budget equation:

$$\Omega_{V0} = 1 - \Omega_{\rm m0}(1 + \zeta_{\rm m}) - \Omega_{\rm r0} - \frac{\psi'^2_0}{6M^2_{\rm Pl}} \quad , \tag{4.4}$$

*Implying that atomic clocks really offer tight constraints on the present day field speed.

where the last term is the kinetic energy relative to critical. Note the $\Omega_{\rm m0}\zeta_{\rm m}$ term, which is essentially a coupling energy. This constraint was directly implemented in the phase space equations (cf. Eqs. 3.17, 3.19, 3.35 and 3.36), where we instead found $\Omega_{\rm m}$ given any point (x, y).

In the BSBM extension, the phenomenological parameter $\zeta_{\rm m}$ is also related to Eötvös parameter and we take its maximal value:

$$\zeta_{\rm m} \simeq \frac{10^9}{3}\eta \quad \Rightarrow \quad \zeta_{\rm m,max} \simeq 6.67 \times 10^{-6} \quad . \tag{4.5}$$

4.2 Cosine potential

For each model with the cosine potential we perform the same numerical operations as in the BSBM with an exponential potential with a few minor changes and one key difference. First, we note that for quintessence and the runaway dilaton, we have the following balance equations:

$$\textbf{Quintessence}: \quad \Omega_{V0} = 1 - \Omega_{\rm m0} - \Omega_{\rm r0} - \frac{\phi_0'^2}{6M_{\rm Pl}^2} \quad , \tag{4.6}$$

$$\textbf{Runaway dilaton}: \quad \Omega_{V0} = 1 - \Omega_{\rm m0} - \Omega_{\rm r0} - \frac{\phi_0'^2}{3} \quad . \tag{4.7}$$

Second, for a sensible choice of present day field speed, we again use the atomic clocks data presented below (Sec. 4.3.2), otherwise the qualitative comparison of results we wish to make would not make sense. Hence:

$$\textbf{Quintessence}: \quad \phi_0' \simeq 4.43 \times 10^{-3} \tag{4.8}$$

$$\textbf{Runaway dilaton}: \quad \phi_0' \simeq 4.038 \times 10^{-2} \tag{4.9}$$

$$\textbf{BSBM extension}: \quad \psi_0' \simeq 0.007 \times 10^{-6} \tag{4.10}$$

The third and most crucial detail to note is that the most general solution to the second statement of the refined de Sitter conjecture (cf. Eq. 2.3) with constant c, can be written:

$$V(\phi) = A\cos(c\phi + \gamma) \quad , \tag{4.11}$$

where A is some constant amplitude and γ is some constant phase. To equate the potential to its present day value, $V(\phi_0) = V_0$, we can absorb the constant phase into the definition of ϕ without changing the equations of motion*. We cannot do the same for the amplitude,

*This applies to all models.

so we find the most general form of the potential to be:

$$V_0 = A\cos(c\phi_0) \quad \Rightarrow \quad V(\phi) = \frac{V_0}{\cos(c\phi_0)}\cos(c\phi) \quad , \tag{4.12}$$

which strongly depends on the choice of ϕ_0. Note in particular that this may lead to numerical complications, because, assuming $V_0 \neq 0$, if $c\phi_0 \to \frac{\pi}{2}$, A tends towards infinity. So, when doing the computations one should steer away from $\phi_0 = \frac{n\pi}{2c}$, $n \in \mathbb{N}$.

Moreover, the balance Eqs. 4.6, 4.7 and 4.4 will always give us a value of $\Omega_{V0} \simeq 0.7 > 0$, which translates into some $V_0 > 0$. Since V_0 must be positive:

$$\text{sign}[A] = \text{sign}\big[\cos(c\phi_0)\big] \quad . \tag{4.13}$$

Obviously, the cosine function is only symmetric under phase shifts of 2π, but it is also anti-symmetric under phase shifts of π. So, a ratio between cosine functions is symmetric under phase shifts of π. Thus, to explore the dependence on ϕ_0 of our models with a cosine potential, we only need to look at cases in the range $c\phi_0 \in [0, \pi]$.

Another way to look at it is the following. Since the equations only "care" about the field displacement:

$$\begin{aligned}\frac{\cos(c\phi)}{\cos(c\phi_0)} &= \frac{\cos\big(c(\phi-\phi_0)+c\phi_0\big)}{\cos(c\phi_0)} \\ &= \frac{\cos(c\Delta\phi)\cos(c\phi_0)-\sin(c\Delta\phi)\sin(c\phi_0)}{\cos(c\phi_0)} \\ &= \cos(c\Delta\phi)-\sin(c\Delta\phi)\tan(c\phi_0) \quad ,\end{aligned} \tag{4.14}$$

and, since the tangent function has a periodicity of π, we can cover the whole spectrum of behaviours by analysing the range $c\phi_0 \in [0, \pi]$. Of course, any shift in field value does not affect its displacement.

Having cleared this up, for simplicity, we will consider values of $c\phi_0 \in \,]-\frac{\pi}{2}, \frac{\pi}{2}[$, where the outward facing brackets denote open limits on the interval.

4.3 Data

We now move on to presenting the data which we have used to derive some rough contraints and to choose the present day field speeds when required.

4.3.1 Dark energy equation of state

As we have seen, [14] has used data provided by [33] on the CPL parameterization. The procedure for reproducing the bounds obtained by [14] from Fig. 21 of [33] has been detailed in [48] and we have tried to reproduce it ourselves. In the first panel of Fig. 4.1, we show a screenshot of part of Fig. 21 of [33], where the yellow contours encompass the w_0 and w_a values in the 2σ range according to CMB, SNeIa, BAO and H_0 data.

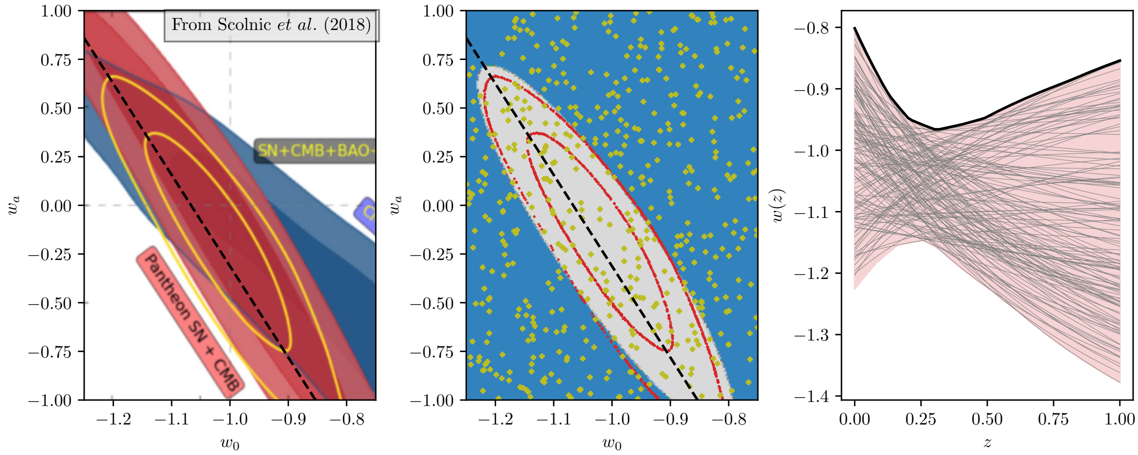

FIGURE 4.1: Process of reproducing the $w_{\mathrm{DE}}(z)$ data used in [14]. Note: not all the sample points and $w(z)$ curves are represented, but the upper bound (black line in the right panel) corresponds to the upper bound on all generated curves.

Since we want to find the points corresponding to the yellow contours, we choose some pixels on the contour, register their RGB colour profile and then search the image for pixels exibiting the same colour. This gives us the red contours in the middle panel. Then, we arbitrarily model the contours with an elliptical shape and roughly find it by adjusting the parameters of the ellipse by hand, resulting in the gray ellipse seen on the background of the middle panel. Finally, we sample this space (green points) and plot the resulting $w(z)$ for each point on the right panel. At each redshift value we have some maximum allowed by the 2σ constraints on w_{CPL}, represented by the black line, which is very similar to the one seen in Fig. 1(a) of [14].

4.3.2 Drift rate of α

The drift rate of the fine-structure constant refers to its relative variation in time, $\frac{1}{\alpha}\frac{\mathrm{d}\alpha}{\mathrm{d}t}$. Recently, atomic clock experiments [49] have placed stringent, model-independent bounds on the current drift rate of α :

$$\left.\frac{\dot{\alpha}}{\alpha}\right|_{z=0} = (1.0 \pm 1.1) \times 10^{-18}\ \mathrm{year}^{-1} \quad . \tag{4.15}$$

Noting that $\frac{\mathrm{d}}{\mathrm{d}t} = \frac{\mathrm{d}N}{\mathrm{d}t}\frac{\mathrm{d}}{\mathrm{d}N} = H\frac{\mathrm{d}}{\mathrm{d}N}$, we can conveniently express the drift rate in terms of $N = \ln a$:

$$\left.\frac{\alpha'}{\alpha}\right|_{z=0} = \left[\frac{1}{H}\frac{\dot{\alpha}}{\alpha}\right]_{z=0} \simeq (0.014 \pm 0.015) \times 10^{-6} \quad , \tag{4.16}$$

where we have introduced a model-dependent assumption of $H_0 = 70$ km/s/Mpc. In each model, the drift rate can be associated with the present day field speed, depending on the particular $U(1)$ gauge coupling function:

$$\left.\frac{\alpha'}{\alpha}\right|_{z=0} = \left[-\frac{\phi'\partial_\phi B_F(\phi)}{B_F^2(\phi_0)}\right]_{z=0} = \begin{cases} \zeta\phi_0' \ , & \text{quintessence} \\ \frac{\alpha_{\mathrm{had0}}}{40}\phi_0' \ , & \text{runaway dilaton} \\ 2\psi_0' \ , & \text{BSBM} \end{cases} \quad . \tag{4.17}$$

4.3.3 Variations of α

As a simple, but still interesting, comparison of our models to observations, we will use the two $\Delta\alpha/\alpha$ datasets used in [50] to plot an effective measurement of fine-structure constant variations. The effective value is calculated as a weighted mean with weights, x, given by each measurement's variance as $x_i = 1/\sigma_i^2$. An effective redshift, z_{eff}, is calculated by making the weighted mean of the redshifts at which each measurement was made. So:

$$\left.\frac{\Delta\alpha}{\alpha}\right|_{\mathrm{eff}} = \frac{\sum\limits_i \left[\frac{\Delta\alpha}{\alpha}\right]_i \sigma_i^{-2}}{\sum\limits_i \sigma_i^{-2}} \quad , \quad z_{\mathrm{eff}} = \frac{\sum\limits_i z_i\sigma_i^{-2}}{\sum\limits_i \sigma_i^{-2}} \quad . \tag{4.18}$$

One of the two datasets corresponds to archival data, which had been taken for other studies, but was later repurposed for measuring spacetime variations of α by [51]. The result is:

$$\left.\frac{\Delta\alpha}{\alpha}\right|_{\mathrm{eff}} = -2.16 \pm 0.85\ \mathrm{ppm} \quad \textbf{at} \quad z_{\mathrm{eff}} = 1.5 \quad . \tag{4.19}$$

Although this data shows a preference for non-zero variations at more than 2σ, there are many problems with it such as difficulties in modelling systematic errors, calibration issues in the measurements and other challenges which are clearly exposed in [8] and references therein. For this reason, we give the caveat that any constraints obtained with the archival dataset, must not be taken too seriously.

The other dataset consists of a compilation of dedicated measurements of variations of α from [7] and other works (for details, see [50]), which do not suffer from the same fatalities as the archival data. The effective variation of α from the dedicated measurements is:

$$\left.\frac{\Delta\alpha}{\alpha}\right|_{\text{eff}} = -0.23 \pm 0.56 \text{ ppm} \quad \textbf{at} \quad z_{\text{eff}} = 1.29 \;\;, \tag{4.20}$$

which is consistent with a null result at 1σ.

Since we are interested in studying these effects in late-time cosmology, we will not use high redshift observations, such as data coming from the CMB or Big Bang Nucleosynthesis (BBN). It would, however, be interesting to see their effect in constraining the models considered here, but that is left for future work.

Chapter 5

Results and discussion

In the present chapter, we will look at the results obtained by the methods presented in Chap. 4. It is worth mentioning, once again, the fact that all of the following results assume the phenomenological couplings of the three models to be single-handedly determined by the Eötvös parameter at the maximum value allowed by current MICROSCOPE constraints, i.e. $\eta \sim 10^{-14}$ [4].

All plotted results of $w_{\rm DE}(z)$ and $\Delta\alpha/\alpha$ presented in this section have the three following elements:

- Solid black line in $w(z)$ plots for $z \in [0, 1]$: upper bound on $w_{\rm CPL}$ derived from Scolnic *et al.* (2018) [33] data (see Sec. 4.3.1);
- Red point with error bars in $\Delta\alpha/\alpha$ plots: weighted mean of archival data (see Sec. 4.3.3, Eq. 4.19);
- Blue point with error bars in $\Delta\alpha/\alpha$ plots: weighted mean of dedicated data (see Sec. 4.3.3, Eq. 4.20).

To facilitate the connection between text and figures, we also include **[model, potential]** at the beginning of each caption, where **model** $\in \{\mathbf{Q}, \mathbf{RaDS}, \mathbf{BSBM}\}$ and **potential** $\in \{\mathbf{exp}, \mathbf{cos}\}$.

5.1 Exponential potential

For quintessence and the runaway dilaton scenario with an exponential potential, we used the phase space parameterization introduced in Chap. 3. For demonstrative purposes, in each of these models, we present the phase space plots and the resulting dark energy equations state, w_ϕ, and variations of α for high and low L regimes. The high L plots serve to showcase the critical behaviour of the fixed points, while the low L cases are observationally preferred.

5.1.1 Quintessence

5.1.1.1 High L

The phase space equations for a range of $L \gtrsim \mathcal{O}(1)$, result in the phase space plots presented as examples in Fig. 3.1. Integrating the resulting x from the present until $z = 4$ yields the variations of fine-structure constant of Fig. 5.1.

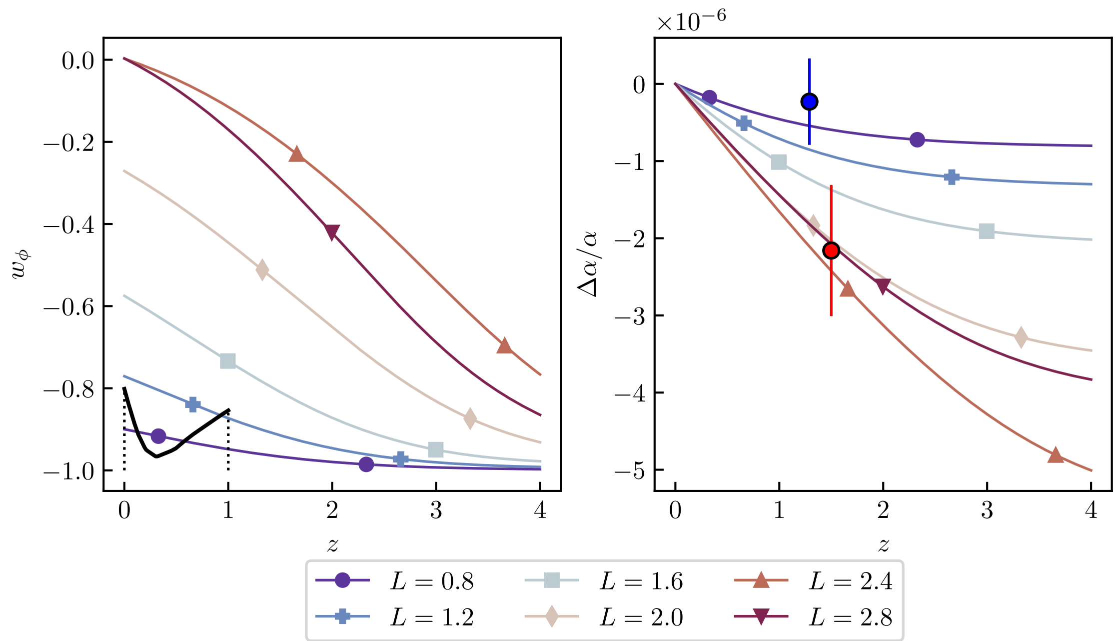

FIGURE 5.1: **[Q, exp]** Dark energy equation of state, w_ϕ, and variations of fine-structure constant, $\Delta\alpha/\alpha$, in high L regime. For the corresponding phase space plots, see Fig. 3.1.

Note that constraints on the dark energy equation of state cannot be satisfied by any of these values. It is still interesting to point out how the behaviour starts to change once we go beyond $L = \sqrt{3} \simeq 1.73$ and the attractor solution becomes the blue point of Fig. 3.1.

The fact that $w_\phi(z = 0) \simeq 0$ for both $L = 2.4$ and $L = 2.8$ means the present day (x_0, y_0) (black cross of Fig. 3.1) are very close to the scaling solution (blue fixed point of Fig. 3.1), because at that point $x = y$, so $w_\phi \propto x^2 - y^2 = 0$. The strange behaviour of the $L = 2.8$ solution is a consequence of the flow field starting to curve and swirl around the scaling solution.

The variation of α is only in line with current bounds (dedicated dataset), which set it at the ppm level [8, 52], for the lowest value of $L = 0.8$. Although many individual data points from studies such as [6, 7] have non-zero $\Delta\alpha/\alpha$, the statistical and systematic errors are big enough to encompass a zero result. Values of $L \gtrsim 1.6$ are preferred by the archival dataset.

We note that, while the w_ϕ data seems to be more constraining than the α data, there are two things to take into account. First, there are no direct measurements of the dark energy equation of state, such that estimates are all based on proxy measurements (e.g. supernova light-curves), whereas varying-α estimates are directly obtained from spectroscopy.

Second, one of the reasons we are predicting such low values for $\Delta\alpha/\alpha$ is that we have chosen to constrain the couplings through the Eötvös parameter, which acts as a sort of prior. If we had used solely α data to constrain the degenerate product $\zeta\Delta\phi$, we would not be able to discard the possibility of lower values of $\Delta\phi$, beyond the bounds established by w_ϕ data. In other words, if ζ was allowed to vary, the tightest constraints on $\Delta\phi$ and consequently on L would probably come from $\Delta\alpha/\alpha$ data.

5.1.1.2 Low L

In the low L case, which has the same upper limit as the one found in [14], we get the phase space plots of Fig. 5.2. The corresponding w_ϕ and α-variations are plotted in Fig. 5.3.

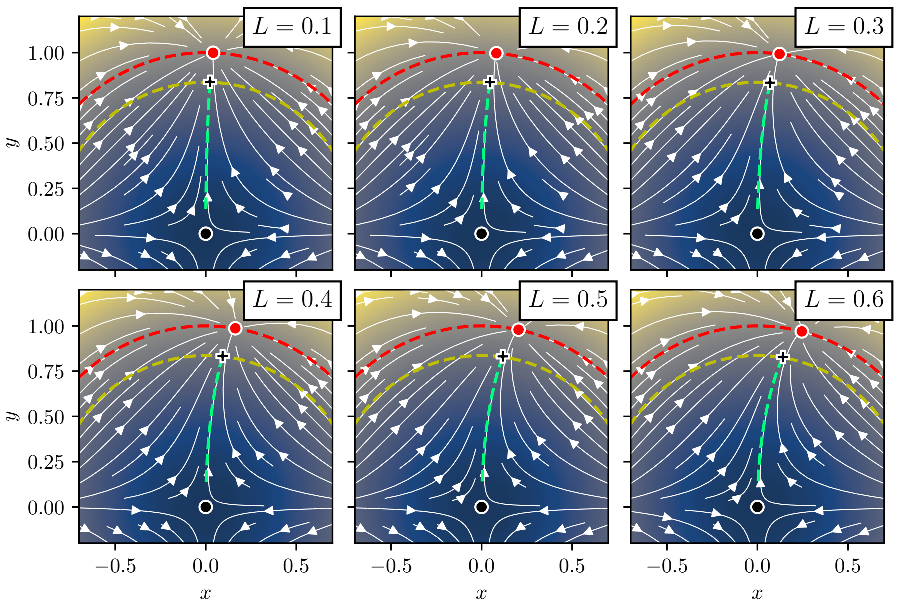

Figure 5.2: **[Q, exp]** Phase space plots in the low L regime.

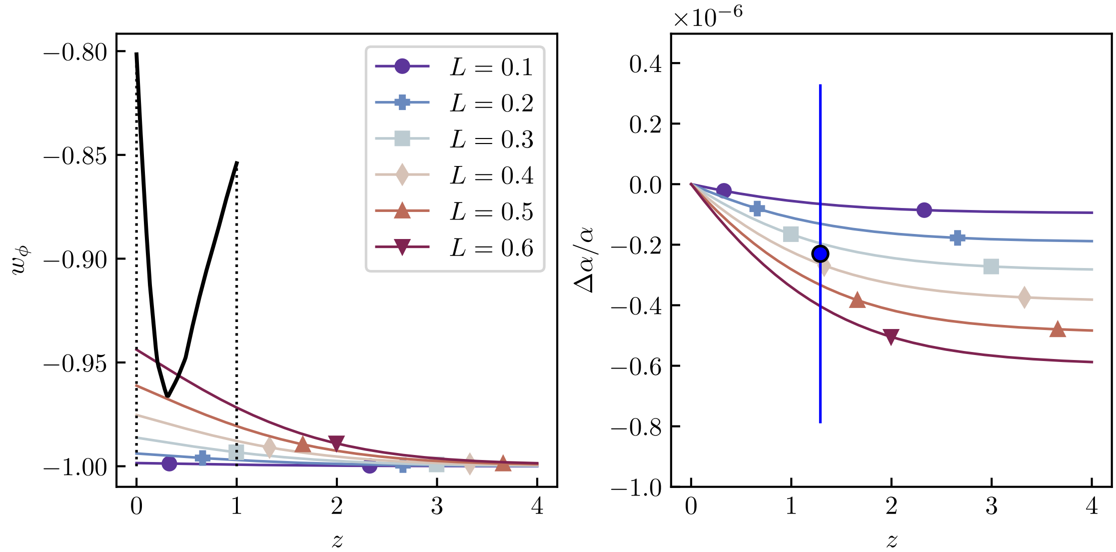

FIGURE 5.3: **[Q, exp]** Dark energy equation of state, w_ϕ, and variations of fine-structure constant, $\Delta\alpha/\alpha$, in low L regime. For the corresponding phase space plots, see Fig. 5.2.

At redshift $z \sim 1$, we have a maximum value of $|\Delta\alpha/\alpha| \simeq 3 \times 10^{-7}$, i.e. about a third of a ppm level variation. This means that, using the MICROSCOPE [4] bound (recall the discussion in the last paragraph of the previous subsection), measurements of the dark energy equation of state place more stringent constraints on L, leading to more tension between the quintessence with an exponential potential and the Swampland conjectures.

We see that all values of L satisfy the 1σ bounds of the effective α variations from the dedicated dataset.

The upper bound on L given by the $w_{\rm DE}$ data is roughly $L \leq 0.5$. Notice the slight difference in comparison to Agrawal *et al.* [14], which had found $L \leq 0.6$. This is an indication of undersampling in our analysis described in Sec. 4.3.1. Some specific regions in (w_0, w_a)-space probably allow for higher values of $w_{\rm CPL}$, which explains the minor discrepancy. Since it is beyond the point, we will continue with our results (if nothing else, for the sake of originality).

5.1.2 Runaway dilaton

5.1.2.1 High L

The runaway dilaton scenario exhibits very distinct behaviour under the three different assumptions we have considered for the coupling to cold dark matter, as evidenced by the phase space plots of Fig. 5.4. The dark energy equation of state and variation of α can be seen in Fig. 5.5.

We draw attention to the similarity between the phase space plots of quintessence (Fig. 3.1) and the matter coupling of the runaway dilaton (Fig. 5.4a). This is expected because, in that case, $x_{\rm fp} \ll 1$, so the phase space equations are very similar. Of course, the evolution of the dark energy equation of state is also similar, since it only depends on the phase space trajectory. The variations of α are different due to their distinct nature in the two models (see Eqs. 3.11 and 3.27).

In dark and field coupling cases, Figs. 5.4b and 5.4c respectively, we see the discontinuities at $x = \pm 1$. Since we are considering a flat universe, such that $\Omega_\phi + \Omega_{\rm m} = 1$ at low redshifts, the relative dark energy density is always smaller than 1. Thus, we have $x^2 + y^2 \leq 1$, so $-1 \leq x \leq 1$ and the discontinuity is only reached in extreme cases and from a single side. The dark energy equation of state has a totally different behaviour and even takes on positive values for the higher L cases. This can be understood by looking at the position of the yellow fixed point, which is the attractor in the $L = 2,\ 2.4,\ 2.8$ cases, in Fig. 5.4b; in Fig. 5.4c we could not represent the actual fixed point, due to the complexity of its mathematical expression (see Appendix A), but it lies somewhere close to the black cross, which is the present day (x_0, y_0) that we found. As the fixed points get closer to $y = 0$ with finite x, we get bigger values of w_ϕ.

In all coupling scenarios, the variations of the fine-structure constant $\left|\Delta\alpha/\alpha\right| \sim \mathcal{O}\left(10^{-6}\right)$ are covered by the dedicated data. We reach the opposite conclusion with w_ϕ data, which excludes all of the represented values.

5.1.2.2 Low L

The low L phase space, w_ϕ and $\Delta\alpha/\alpha$ plots can be seen in Figs. 5.6 and 5.7. Although the matter and dark coupling phase space plots look fairly similar, their equation of state and fine-structure constant evolve quite differently. A non-zero value of $x_{\rm fp}$ means that, as we get close to the fixed point at $(x, y) = (x_{\rm fp}, 0)$, the equation of state rises to $w_\phi \to 1$. Higher values of $x_{\rm fp}$ give higher overall values of w_ϕ and seem to raise w_ϕ sooner, as evidenced in the center panel of Fig. 5.7, which has the highest $x_{\rm fp}$ of all three cases.

The three scenarios are in accordance with dedicated observations of $\Delta\alpha/\alpha$. The bound from w_ϕ data excludes $L \gtrsim 0.5$ for a matter coupling, $L \gtrsim 0.3$ for a dark sector coupling and $L \gtrsim 0.4$ for a field coupling scenario.

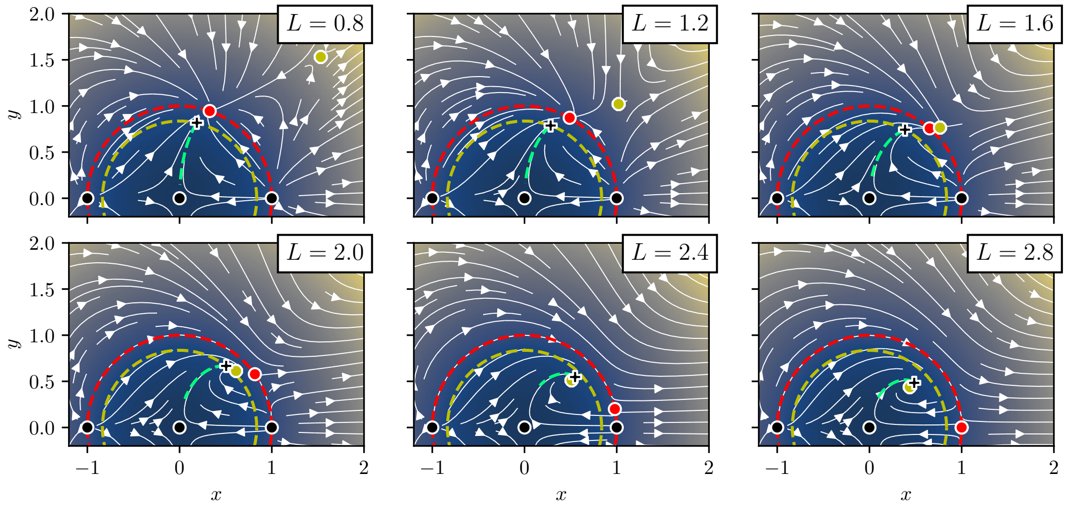

(A) Matter coupling: $\alpha_{\rm cdm} = \alpha_{\rm b}$

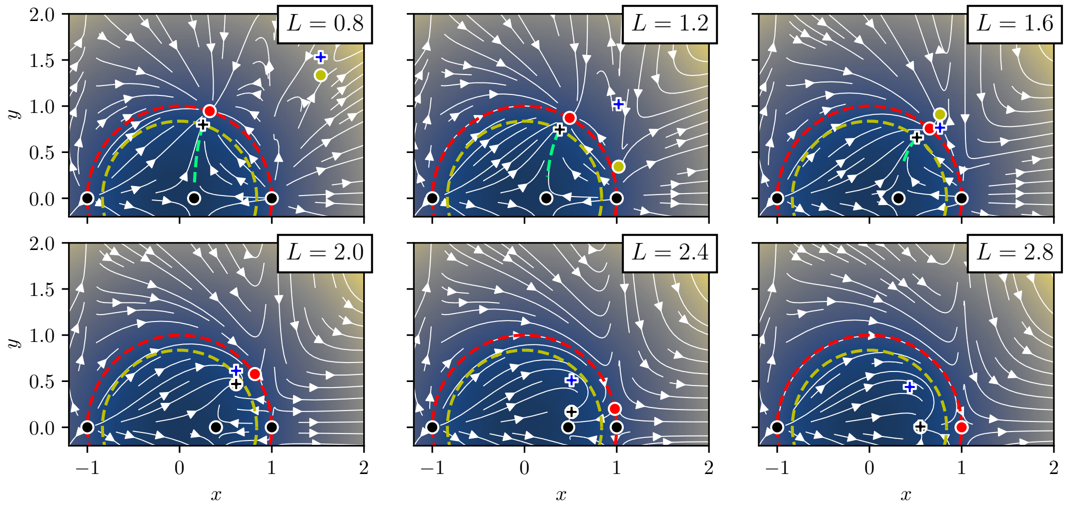

(B) Dark coupling: $\alpha_{\rm cdm} = \alpha_V$

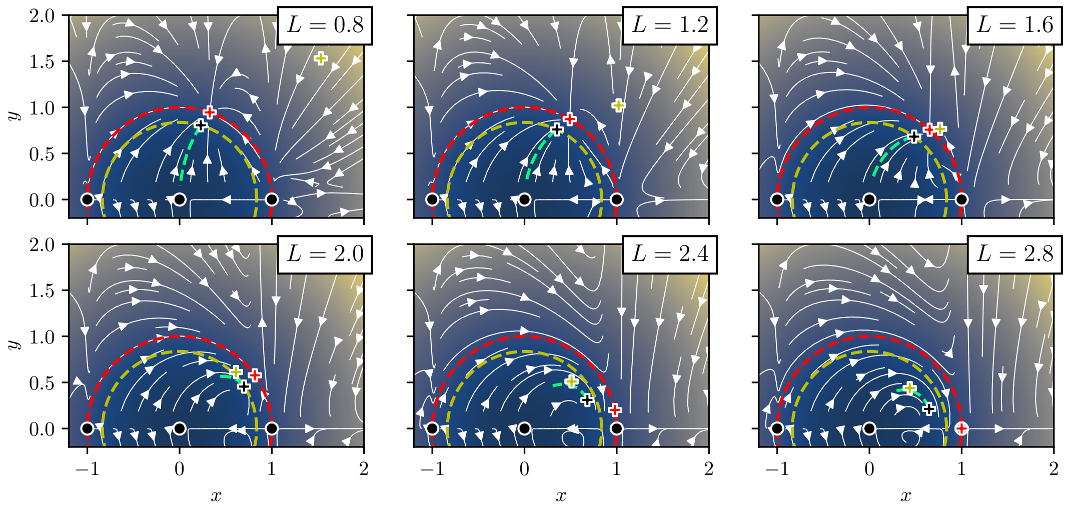

(C) Field coupling: $\alpha_{\rm cdm} = -\phi'$

FIGURE 5.4: **[RaDS, exp]** Phase space plots in high L regime.

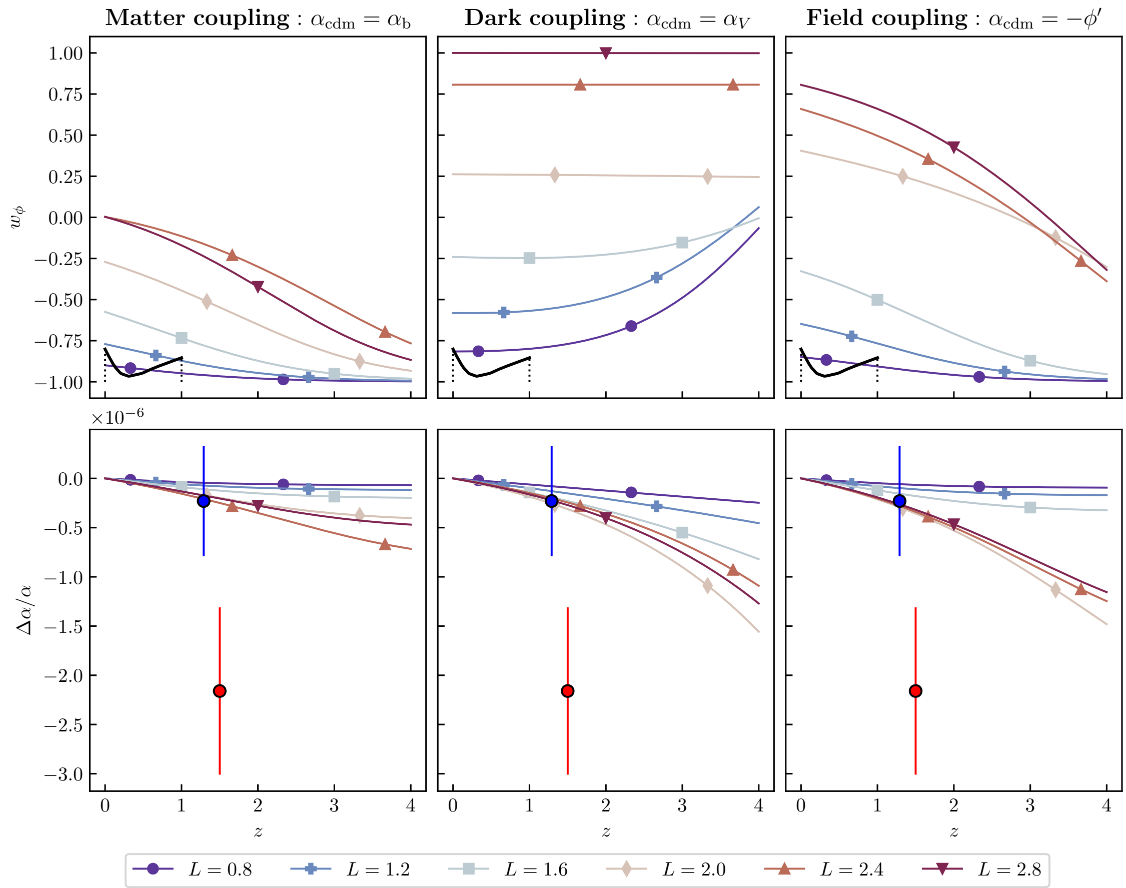

Figure 5.5: **[RaDS, exp]** Dark energy equation of state, w_ϕ, and variations of fine-structure constant, $\Delta\alpha/\alpha$, in high L regime. For the corresponding phase space plots, see Fig. 5.4.

5.1.3 BSBM extension

5.1.3.1 L dependence

The results of direct integration of the BSBM model (Eq. 3.41) in the "high" L regime which we considered for quintessence and the runaway dilaton scenario are shown in Fig. 5.8.

The first detail to note is the fact that the field is being displaced back, i.e. rolling up the exponential potential. This effect is due to the rather low value of the field speed in the present, $\psi'_0 = 0.007 \times 10^{-6}$, which requires the field to be travelling back in a decelerated fashion and switching direction very recently (see top panels).

On the middle panels, we have plotted the energy densities relative to critical of the field, Ω_ψ, and matter, $\Omega_{\rm m}$, on the right one, and the kinetic, Ω_T, and potential, Ω_V, components of the field on the left. We can see that for all values of L the universe tends to have been dominated by the kinetic energy at some point in the past. This is, of course, problematic,

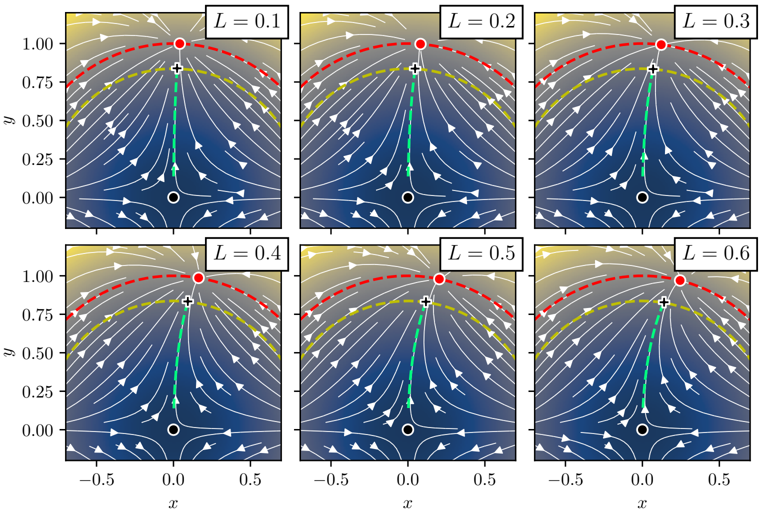

(A) Matter coupling: $\alpha_{\mathrm{cdm}} = \alpha_{\mathrm{b}}$

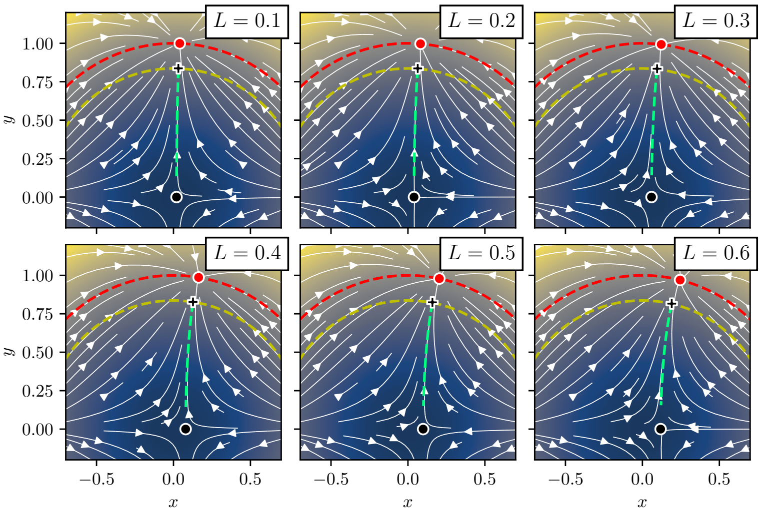

(B) Dark coupling: $\alpha_{\mathrm{cdm}} = \alpha_V$

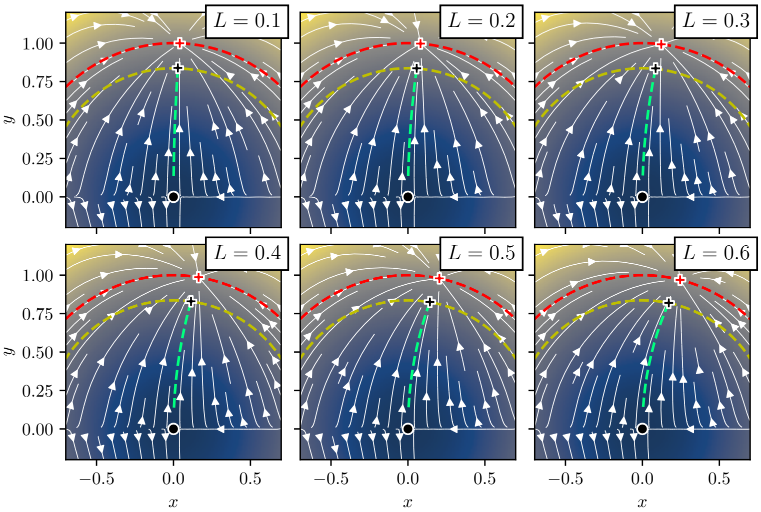

(C) Field coupling: $\alpha_{\mathrm{cdm}} = -\phi'$

FIGURE 5.6: **[RaDS, exp]** Phase space plots in the low L regime.

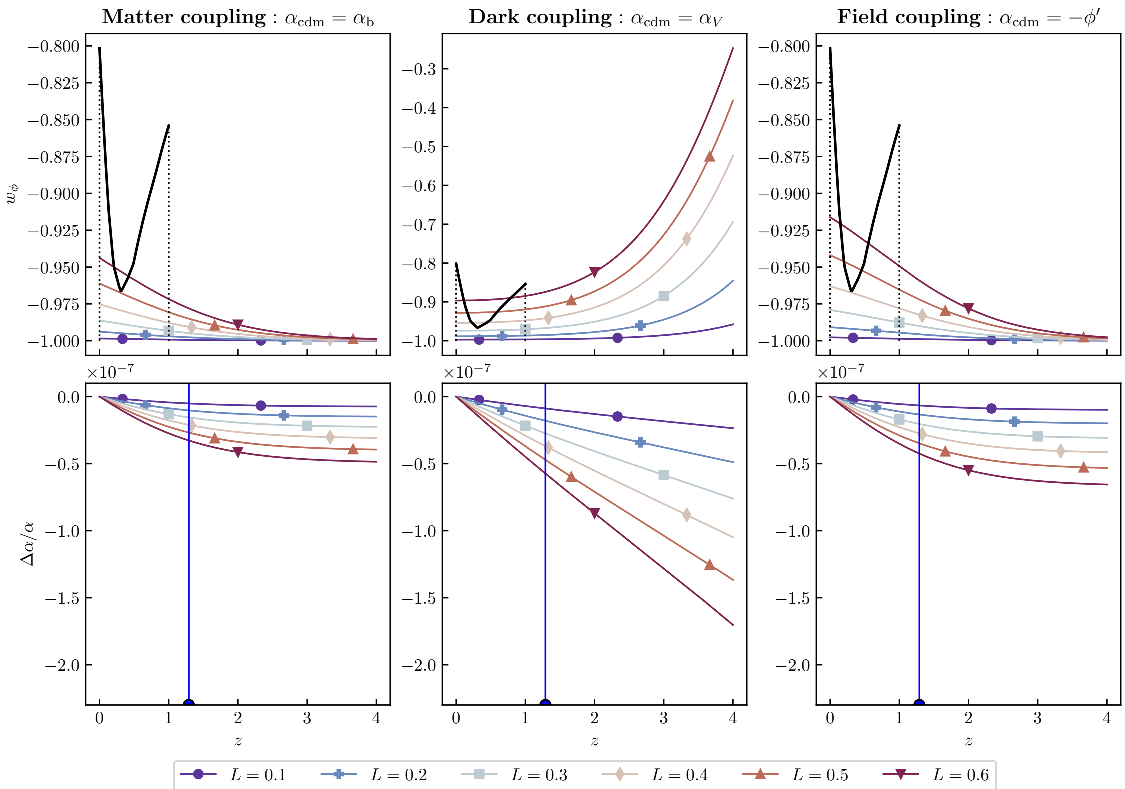

Figure 5.7: **[RaDS, exp]** Dark energy equation of state, w_ϕ, and variations of fine-structure constant, $\Delta\alpha/\alpha$, in low L regime. For the corresponding phase space plots, see Fig. 5.6.

because it leads to excessive acceleration and disruption of large scale structure formation. This is exactly the problem which the phase space analysis has solved in the other models.

It is clear that constraints on the dark energy equation of state are violated in all but one case, where $L = 0.1$.

Moreover, this model produces absurdly high variations of α. Although it is not easily seen, at redshift $z = 1$, we have obtained $\Delta\alpha/\alpha \sim \mathcal{O}(1)$, which is roughly six orders of magnitude higher than current bounds. Moreover, the bounds are positive, as opposed to what we have found in the previous models and in the data.

The key to understanding this strange behaviour is to look at the plot containing the relative energy densities of [46] (bottom panel of Fig. 1). The field, which in the original model has no potential energy*, is clearly subdominant throughout the universe's evolution, $\Omega_\psi \ll 1$. The fact that the field is not being forced to evolve due to some potential allows it to not be displaced by large amounts, nor gather significant speed.

*We can also think of it having a constant potential energy, namely the cosmological constant.

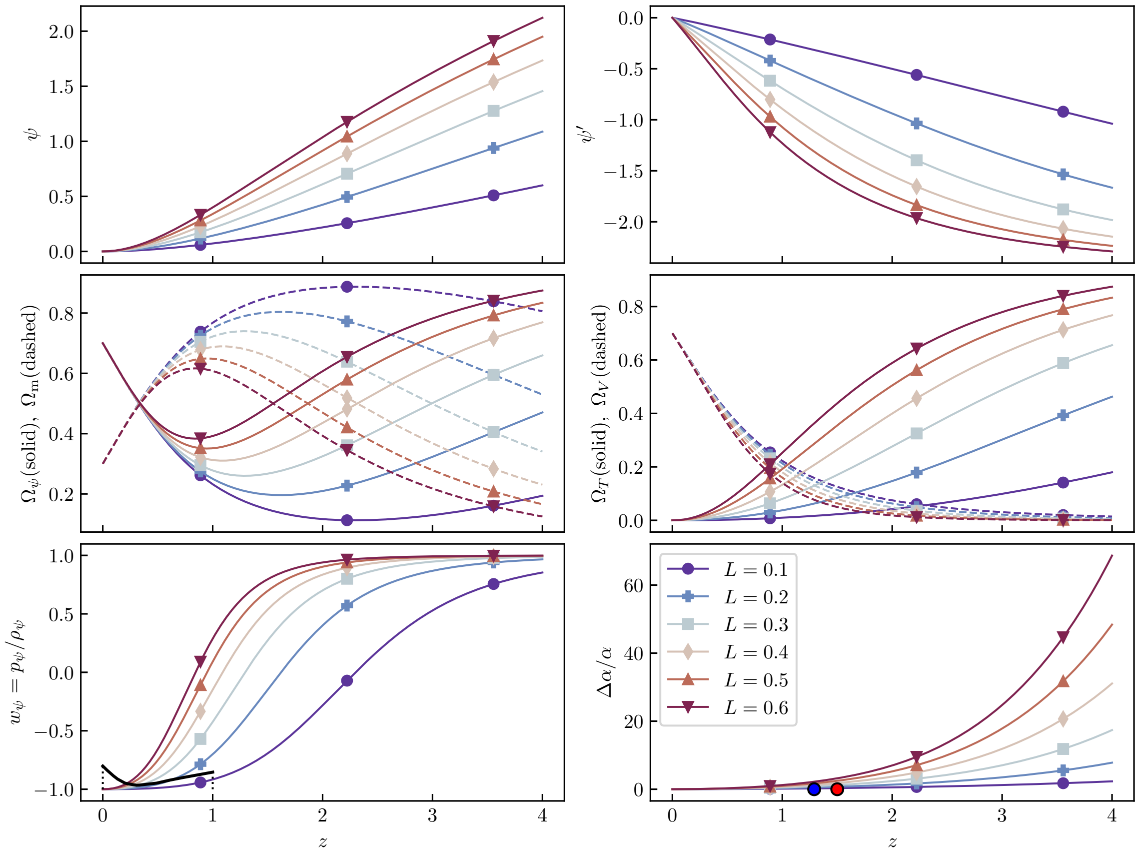

FIGURE 5.8: **[BSBM, exp]** Field value and speed, ψ and ψ', relative energy densities, $\Omega_i = \rho_i/\rho_{\rm c}$, dark energy equation of state, w_ψ, and variations of α, $\Delta\alpha/\alpha$, in low L regime, with present day field speed $\psi_0' = 0.007 \times 10^{-6}$.

This is not the case in our model – which is a modification of the original BSBM to have the dilaton provide all of the dark energy. The field is forced to roll and the bigger the slope, the farther it will travel. For order ppm variations of α, we need:

$$\left|\frac{\Delta\alpha}{\alpha}\right| = \left|e^{2(\psi-\psi_0)} - 1\right| \lesssim 10^{-6} \quad \Leftrightarrow \quad \psi - \psi_0 \lesssim \frac{1}{2}\log\left(1 \pm 10^{-6}\right) \simeq \pm 0.5 \times 10^{-6} \quad . \tag{5.1}$$

The required displacement is seven orders of magnitude smaller than what is attainable with $L \sim \mathcal{O}(1)$.

Clearly, our modification to the BSBM model is in some conflict with observations, although flatter potentials could alleviate some of the issues. More importantly, this is a clear indication of the strong tension between our model and the Swampland conjectures, because for $L \sim \mathcal{O}(1)$ we find $\Delta\psi \gtrsim \mathcal{O}(1)$, already at $z = 4$, and growing. Hence, either the distance (Eq. 2.1) or the de Sitter conjecture (Eq. 2.3) is satisfied, but not both.

5.1.3.2 ψ'_0 dependence

The other interesting parameter to track the model over is the present day field speed. Results for $\psi'_0 \in [0.001, 0.01, 0.1, 1.0]$ with $L = 1$ can be seen in Fig. 5.9. Below $\psi'_0 \sim \mathcal{O}(0.01)$, the evolution is very similar, the most notable difference being the variations of α, which, as before, are too high to agree with experimental results.

The present day field speed that gives the lowest variations of the fine-structure constant is $\psi'_0 = 1.0$, i.e. the highest. This happens because, for such a high speed, the field would not have reached its turning point within the considered redshift range. Because the field is moving forward, its displacement is $\psi(z) - \psi_0 \leq 0$, so $e^{2(\psi - \psi_0)} \leq 1$. In the limit of large field displacements, α variations have the asymptotic limit $\Delta\alpha/\alpha \to -1$. If we went far enough back in time, eventually we would find the field's turning point and, beyond that, $\Delta\alpha/\alpha$ would explode as well. It seems this model is doomed to always have an infinite electron charge at some limit.

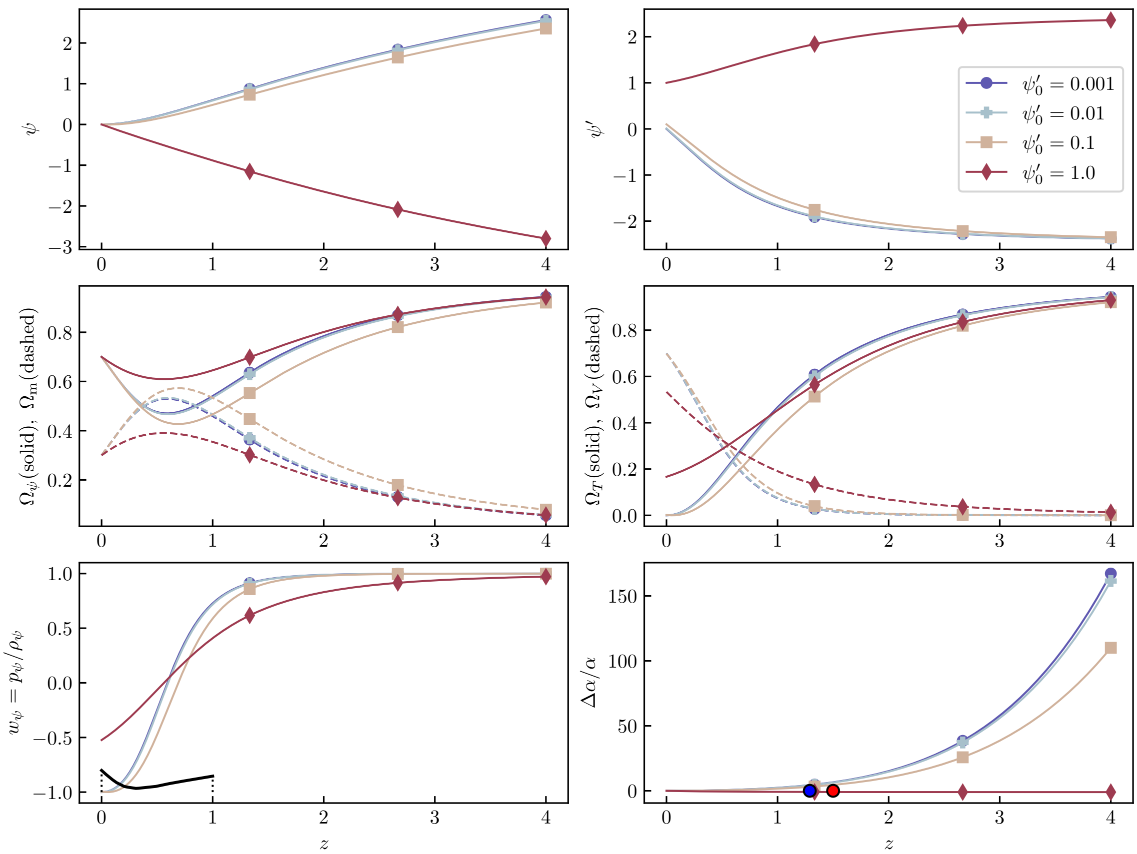

FIGURE 5.9: **[BSBM, exp]** Field value and speed, ψ and ψ', relative energy densities, $\Omega_i = \rho_i/\rho_c$, dark energy equation of state, w_ψ, and variations of α, $\Delta\alpha/\alpha$, over range of present day field speeds, ψ'_0, with $L = 1$.

All of the values considered are in clear conflict with w_ψ data. Though the α data cannot be easily compared with in the image due to scale differences, we can show that it does not overlap with any of the plotted lines. As a short back-of-envelope calculation, if we assume $\psi - \psi_0 \simeq -1$ at $z = 1.5$, we get $\left[\Delta\alpha/\alpha\right]_{z=1.5} \simeq e^{-3} - 1 \simeq -0.95$, which is a lot higher in magnitude than the archival data predict.

5.2 Cosine potential

5.2.1 Quintessence

5.2.1.1 c dependence

In Fig. 5.10, we find similar plots to those of Fig. 5.8, but now for the quintessence field with a cosine potential. To analyse the dependence of this model on the parameter c, we have chosen $\phi_0 = 0$, i.e. we assume that we are on top of the cosine potential. Although improbable, it serves an illustrative purpose.

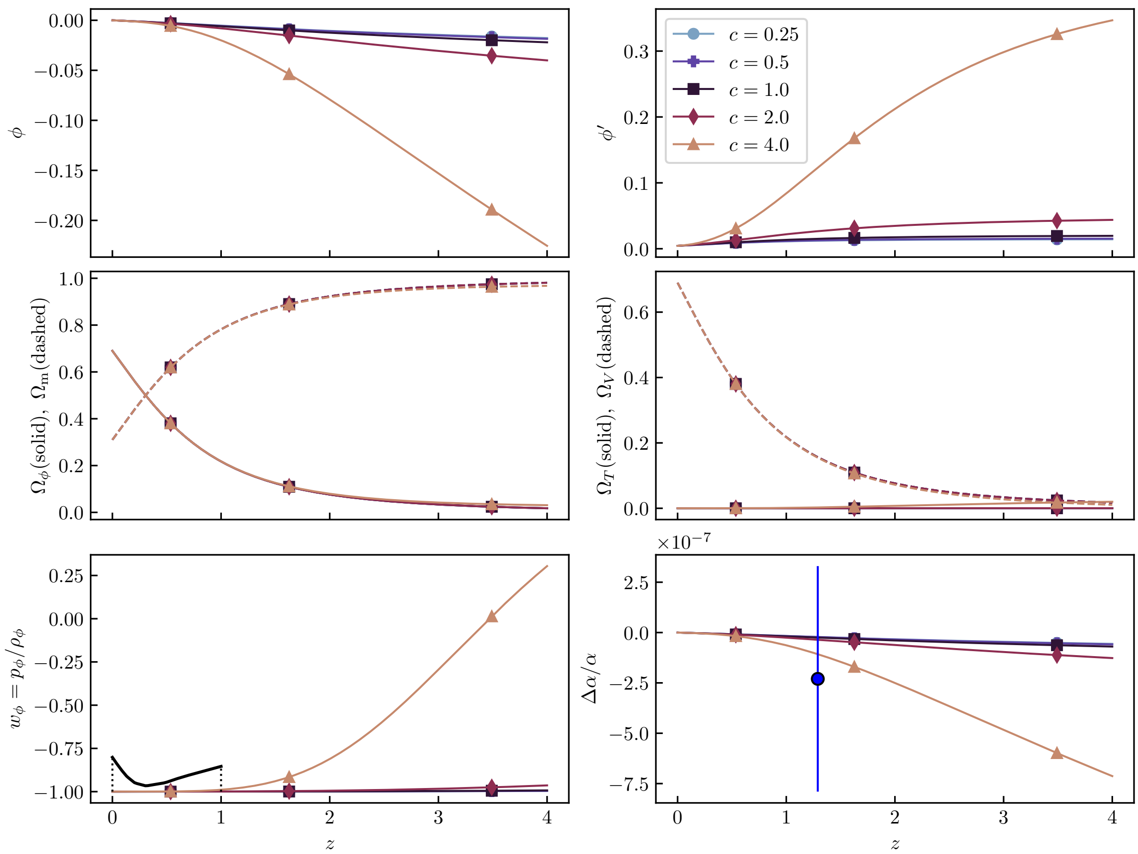

FIGURE 5.10: **[Q, cos]** Field value and speed, ϕ and ϕ', relative energy densities, $\Omega_i = \rho_i/\rho_\mathrm{c}$, dark energy equation of state, w_ϕ, and variations of α, $\Delta\alpha/\alpha$, over a range of c, with $\phi_0 = 0$ and $\phi_0' = 4.43 \times 10^{-3}$.

We find, in this case, that there is not much of a difference in relative energy densities between the considered values of c. We see that matter tends dominate the past, which is a good sign for the model.

The irrelevance of the field's kinetic energy is expected. As opposed to what we saw in the BSBM with an exponential potential, which required the field to be moving very fast in the past, in this model the field is able to maintain relatively low speeds which eventually decrease due to Hubble drag. Of course, if we went to high enough redshifts the speed would have to increase for the field to have sufficient kinetic energy to counteract Hubble drag. This is not a problem if we bare in mind the fact that quintessence is supposed to model late-time cosmology.

Both dark energy equation of state and variations of α predicted in this model seem to be in agreement with current observations, i.e. Scolnic *et al.* (2018) [33] data and dedicated α measurements. However, at redshifts $z \leq 1$, we see a stronger correlation of c with α than with w_ϕ.

For the higher values of c, the field has to cross many more peaks of the potential, loosing energy along the way, so it travels with greater velocity.

5.2.1.2 ϕ_0' dependence

In Fig. 5.11, we plot the evolution of the recent universe for range of present day field speeds, ϕ_0', with $\phi_0 = 0$ and $c = 1$. This means once again the assumption that we find ourselves at a maximum of the potential.

The field displacement is only $\mathcal{O}(1)$ when $\phi_0' \gtrsim \mathcal{O}\left(10^{-1}\right)$, so the distance and de Sitter conjectures can be simultaneously satisfied if $\phi_0' \lesssim 10^{-1}$.

Field speeds $\phi_0' \lesssim 0.1$ are within the 1σ range of the dedicated data, while no plotted lines fall within 1σ of the archival data, though a certain range where $0.1 < \phi_0' < 1$ should be in agreement with this dataset. For the dark energy equation of state data, $\phi_0' = 0.1$ seems to be very close to the limiting case which satisfies the data.

5.2.1.3 ϕ_0 dependence

This is our first encounter with the dependence of the model on ϕ_0, in other words, the question of where we are on the potential. The results of the evolution for $c\phi_0 \in \left\{0, \pm\frac{\pi}{6}, \pm\frac{\pi}{3}\right\}$, with $c = 1$ and $\phi_0' = 4.43 \times 10^{-3}$ are plotted in Fig. 5.12. First note that, in the Ω_i and

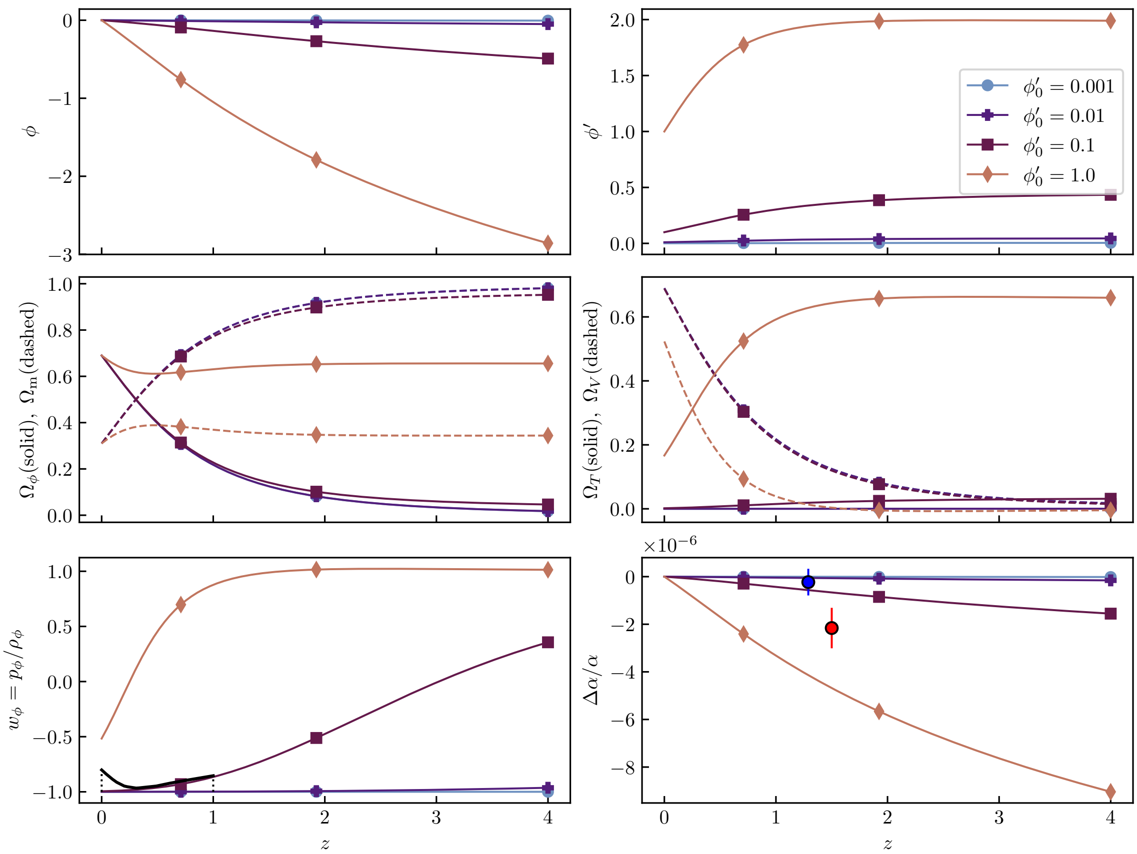

FIGURE 5.11: **[Q, cos]** Field value and speed, ϕ and ϕ', relative energy densities, $\Omega_i = \rho_i/\rho_c$, dark energy equation of state, w_ϕ, and variations of α, $\Delta\alpha/\alpha$, over a range of ϕ'_0, with $\phi_0 = 0$ and $c = 1$.

w_ϕ plots, the lines corresponding to the same absolute value of $c\phi_0$ more or less overlap, because ϕ' is roughly symmetric and Ω_ϕ and w_ϕ depend on ϕ'^2.

Recall (Eq. 4.12) that the closer we are to $\phi_0 = \frac{n\pi}{2c}$, the bigger the potential's amplitude and its slope at ϕ_0*. The requirement that ϕ'_0 be so low, implies that the field be coming from the nearby minima of the potential, where it is negative (see Ω_V on the right panel of the middle row of Fig. 5.12). To counteract the rather big slope, the kinetic energy must be high (see ϕ' on the left panel of the first row).

For the represented values, w_ϕ constraints are only met by the $\phi_0 = 0$ case, although some range close to it is probably viable, too.

With close attention, one can see the error bars just poking out of the blue dot, so the $\phi_0 = 0$ case clearly satisfies the dedicated data. Meanwhile, the archival data is satisfied by some interval close to $c\phi = -\pi/6$, so it would select for universes where we would currently be climbing towards the top of the potential.

*The slope is $\left.\frac{dV}{d\phi}\right|_{\phi=\phi_0} = -V_0 c \tan(c\phi_0)$.

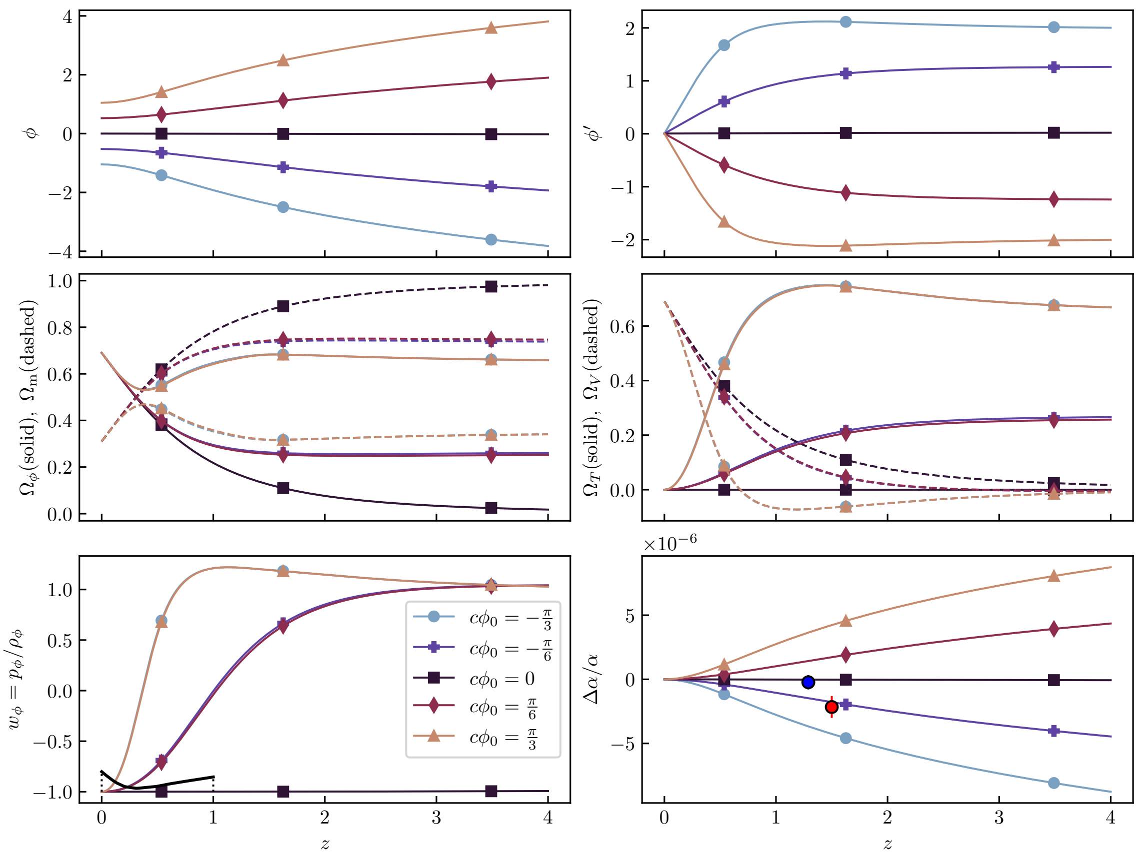

FIGURE 5.12: **[Q, cos]** Field value and speed, ϕ and ϕ', relative energy densities, $\Omega_i = \rho_i/\rho_{\rm c}$, dark energy equation of state, w_ϕ, and variations of α, $\Delta\alpha/\alpha$, over a range of ϕ_0, with $\phi_0' = 4.43 \times 10^{-3}$ and $c = 1$.

5.2.2 Runaway dilaton scenario

As we will see below, there are some numerical problems arising in the dark coupling scenario, because the forcing on the field equation gets very large for extremal values of ϕ_0, ϕ_0' and c, so the solution is very sensitive to the integration step. These problems have not gone away by integrating the equations in time, t, number of e-folds, N, and redshift, z. The numerical issues simply manifest themselves in different parts of the integration range, which is not surprising. Suppose we create an equally spaced array of values of N and see a significant accumulation of numerical errors by the 12$^{\text{th}}$ value (black encircled orange dot in Fig. 5.13). It would correspond to some redshift value.

On the other hand, if the original array is of equally spaced z values, after the same number of steps, we will be further in the redshift range (black encircled blue dot of Fig. 5.13). However, this comes at the expense of precision at the beginning of the integration, so further analysis would be required to see if one is better than the other.

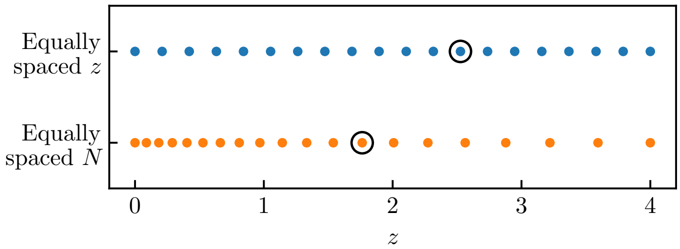

FIGURE 5.13: Example of grid spacing difference.

In many instances, the error is such that we get $H^2 < 0$, so the cosmic time integration, which cannot be expressed without factors of $H(t) = \sqrt{H^2(t)}$, gives the worst results. For this reason, we have stuck with an integration in N. We will not focus on these numerical matters, because that is not the point we are trying to make. Away from the more extreme cases, Eq. 3.23 is relatively well behaved.

5.2.2.1 c dependence

In Fig. 5.14, we find the results for the runaway dilaton scenario under our three simplifying assumptions with regards to the coupling to dark matter. Not surprisingly, we find the matter and field coupling cases to be very similar. For the small value of $\alpha_{\text{had0}} \ll 1$ the contribution of the coupling to matter in the last term of Eq. 3.23 is negligible in comparison to the $\mathcal{O}(c)$ coupling to the potential (dark energy). When $\alpha_{\text{cdm}} = -\phi'$, the contribution of the dark matter fluid to the equation of motion is only through ρ_c (see Eq. 3.32).

A bit more curious is the fact that in the matter and field coupling scenarios we do not get a strong dependence on c for any of the plotted quantities.

As discussed above, the dark coupling case suffers from some numerical stability issues, and we can get some insight about their origin by noting that the singular point in the ϕ' panel of Fig. 5.14 is very close to the point where Ω_V crosses the origin (black dashed lines in the second to fourth rows). At that redshift, the field is transitioning from being in the negative part of the cosine potential to having postitive potential energy. For some reason the other components of the universe, which contribute to ρ as defined in Eq. 3.28, have small energy densities, $\rho \ll 1$ and the forcing terms of Eq. 3.23 become huge. This leads to high acceleration and, consequently, the singular behaviour of ϕ'.

Apart from these peculiarities, all cases produce $w_\phi(z < 1)$ and $\Delta\alpha/\alpha$ which agree with current bounds.

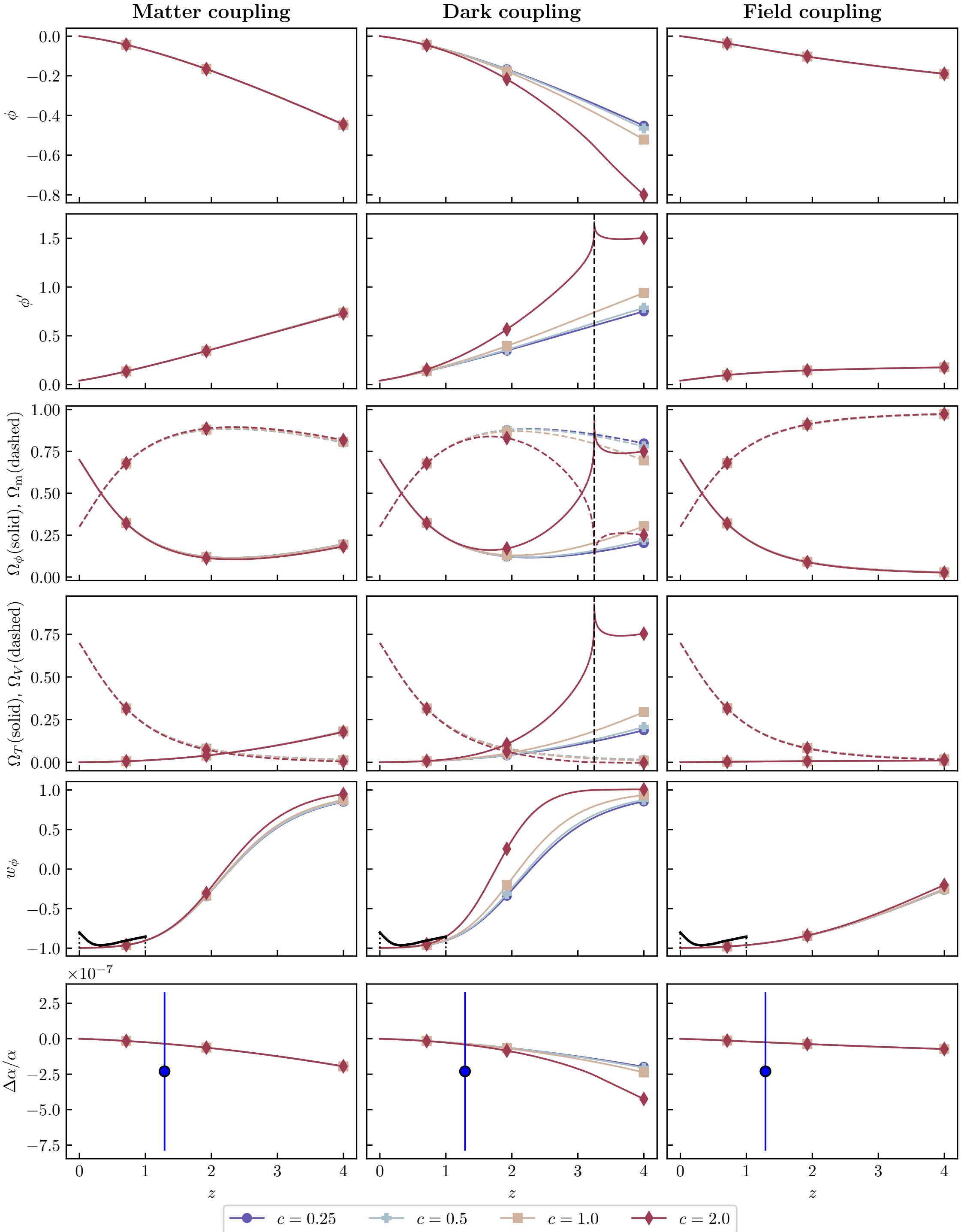

Figure 5.14: **[RaDS, cos]** Field value and speed, ϕ and ϕ', relative energy densities, $\Omega_i = \rho_i/\rho_c$, dark energy equation of state, w_ϕ, and variations of α, $\Delta\alpha/\alpha$, over a range of c, with $\phi_0 = 0$ and $\phi'_0 = 4.038 \times 10^{-2}$.

5.2.2.2 ϕ'_0 dependence

The evolution of the runaway dilaton for several values of ϕ'_0 is plotted in Fig. 5.15.

Note that, in this model, we have not chosen the top value ϕ'_0 to be 1, because of the different definition of the field, compared to quintessence. We chose the maximum value to represent based on the kinetic energy density relative to critical. Since in this model we have $\Omega_T = \phi'^2/3$ (rather than $\Omega_T = \phi'^2/6M_{\rm Pl}^2$), to get the same value, we use $\phi'^2_{0,\rm max}/3 = 1/6M_{\rm Pl}^2$, which corresponds to $\phi'_{0,\rm max} = 1/\sqrt{2}M_{\rm Pl} \simeq 0.707$, after setting $M_{\rm Pl} = 1$.

Again, in the dark coupling scenario we see some discontinuities due to the numerical instabilities caused by $V(\phi)$ crossing the origin at some value of z (black dashed lines).

In all three coupling scenarios, we see a higher sensitivity to the scale of ϕ'_0 than we saw on the value of c in the previous section.

In terms of general features of the plotted quantities, the field coupling case seems to be the outlier. The difference in field dynamics due to this coupling effectively reduces the field speed, because it lessens the force term of Eq. 3.23. As a consequence, we get lower kinetic energy density, Ω_T, lower field displacement, ϕ, lower variations of α and a dark energy equation of state which remains close to $w_\phi = -1$ for longer.

Predicted values of $\Delta\alpha/\alpha$ are of order ppm or smaller for all considered field speeds, ϕ'_0. However, due to the way in which the variations evolve, at the effective redshifts of each dataset, they only satisfy the dedicated data. Dark energy equation of state constraints can only be satisfied for $\phi'_0 \lesssim 0.01$.

5.2.2.3 ϕ_0 dependence

In Fig. 5.16, we plot the results for various values of ϕ_0. Here, too, we have reduced the values shown by one half (cf. Fig. 5.12), because huge numerical errors appear at $c|\phi_0| \gtrsim \frac{\pi}{4}$, which render the plots useless. The redshifts at which the potential energy crosses $V(\phi) = 0$ are, once more, the black dashed lines in the ϕ' and Ω_i panels. This time we have two extreme cases suffering from the numerical issues described above, namely $c\phi_0 = -\frac{\pi}{6}, -\frac{\pi}{12}$. Because the field is moving forward in all but the $c\phi_0 = \frac{\pi}{6}$ case, only the aforementioned cases have had to cross the origin in the plotted redshift interval.

We point out the insensitivity of the results to the value ϕ_0 in the matter and field coupling cases. All scenarios are in agreement with constraints on varying-α from the dedicated data. The $w_{\rm DE}$ data seems to exclude the negative values of $c\phi_0$ we have considered

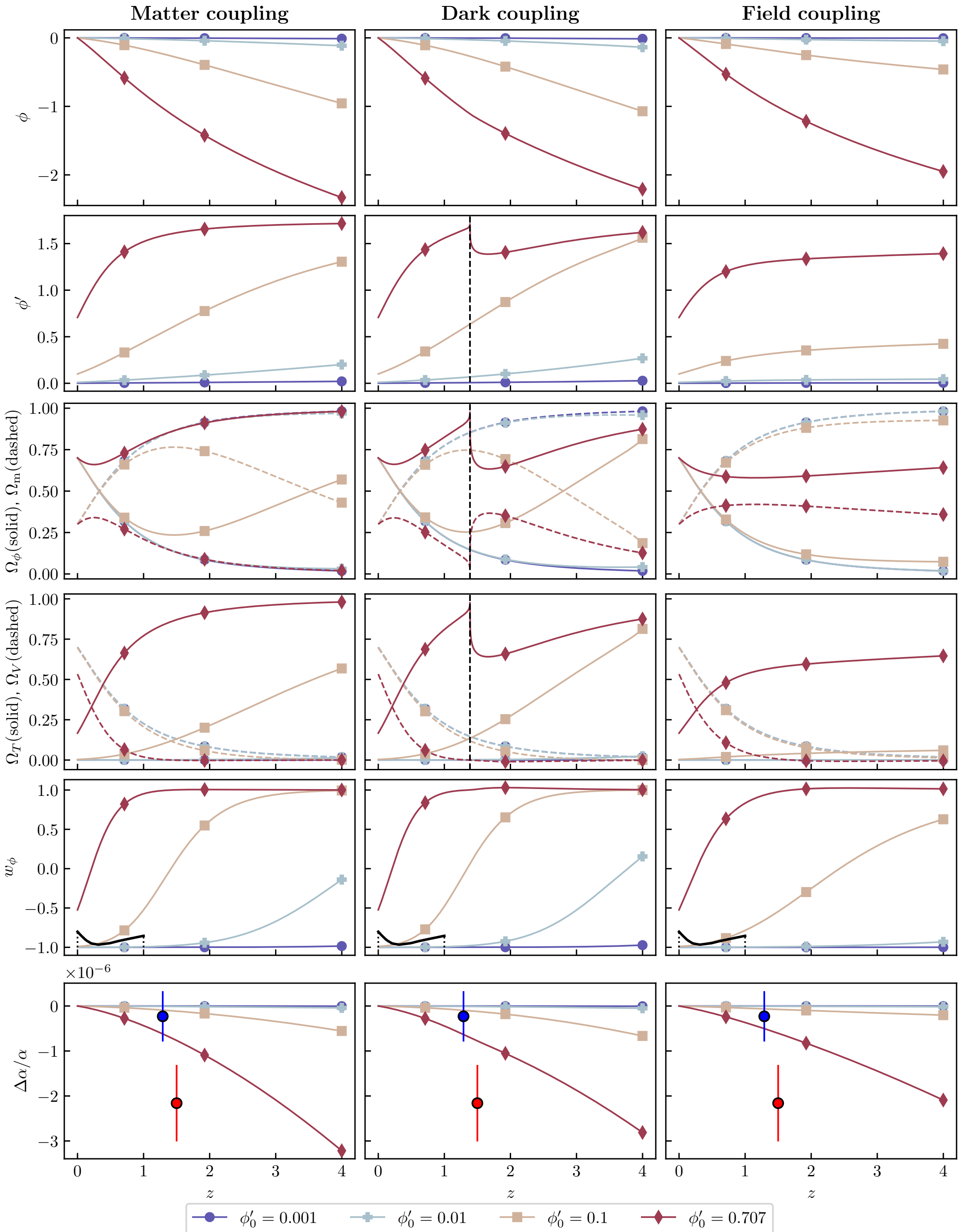

Figure 5.15: **[RaDS, cos]** Field value and speed, ϕ and ϕ', relative energy densities, $\Omega_i = \rho_i/\rho_c$, dark energy equation of state, w_ϕ, and variations of α, $\Delta\alpha/\alpha$, over a range of ϕ'_0, with $\phi_0 = 0$ and $c = 1$.

in the dark coupling scenario, but to account for all values in the matter and field coupling scenarios.

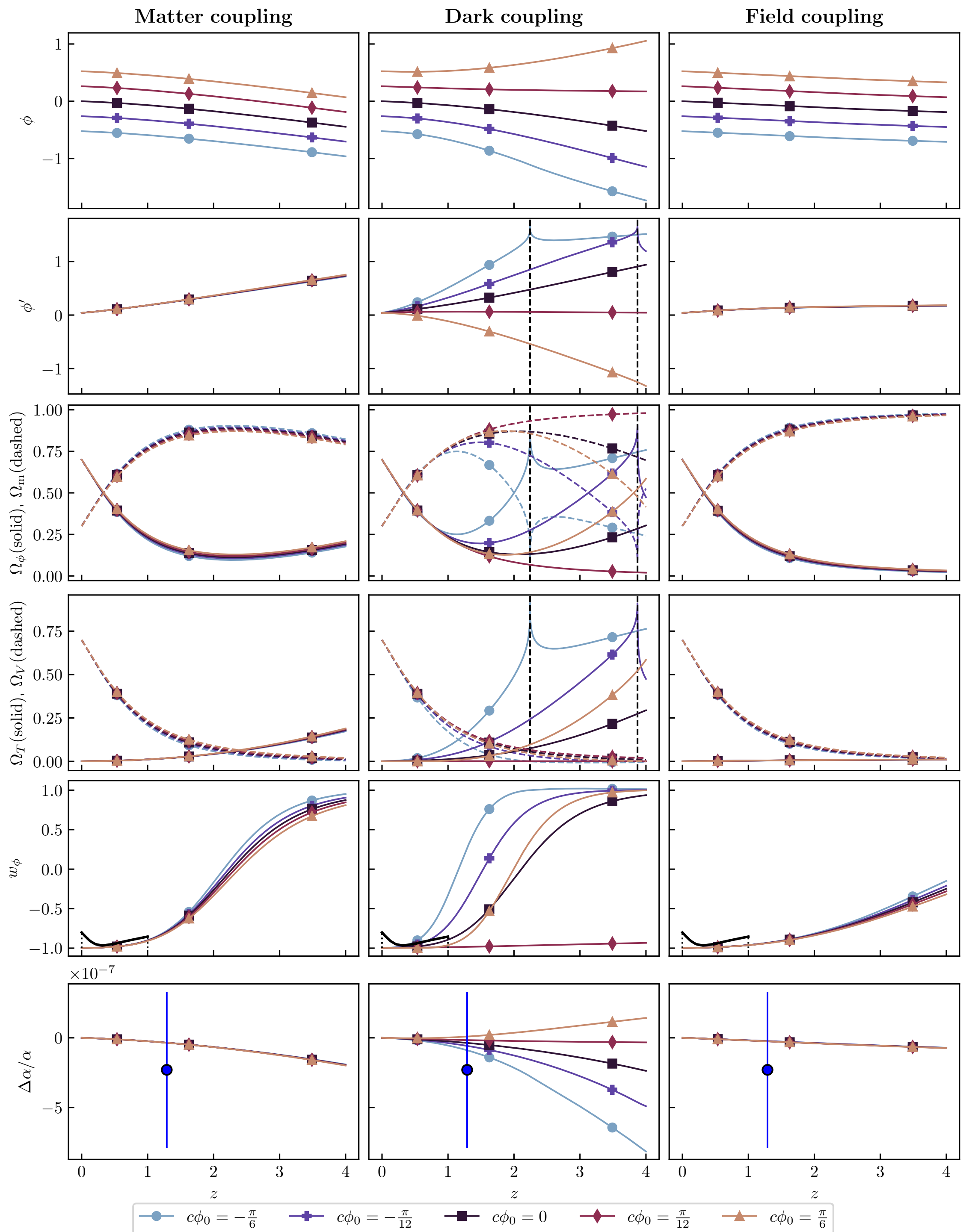

FIGURE 5.16: **[RaDS, cos]** Field value and speed, ϕ and ϕ', relative energy densities, $\Omega_i = \rho_i/\rho_c$, dark energy equation of state, w_ϕ, and variations of α, $\Delta\alpha/\alpha$, over a range of ϕ_0, with $\phi'_0 = 4.038 \times 10^{-2}$ and $c = 1$.

5.2.3 BSBM extension

Most of the comments we have made on the quintessence model apply here, so we will focus on pointing out the differences.

5.2.3.1 c dependence

The results of this model can be seen in Fig. 5.17. Although the ψ and ψ' curves are somewhat similar in shape to those of ϕ and ϕ' of Fig. 5.10, respectively, we note the difference in scale of both, which is higher in quintessence than in the BSBM extension. This has to do with our atomic clock "prior" on the present day field speed (see Sec. 4.3.2), which sets a scale for field speeds given the similarity between the equations of motion (cf. Eqs. 3.6 and 3.41). The difference in shape of the curves is caused by both the forcing term in the BSBM equation and the fact that ψ is only able to explore a $\mathcal{O}\left(10^{-4}\right)$ neighbourhood of the top of the potential, compared to the $\mathcal{O}\left(10^{-1}\right)$ neighbourhood that quintessence is able to explore.

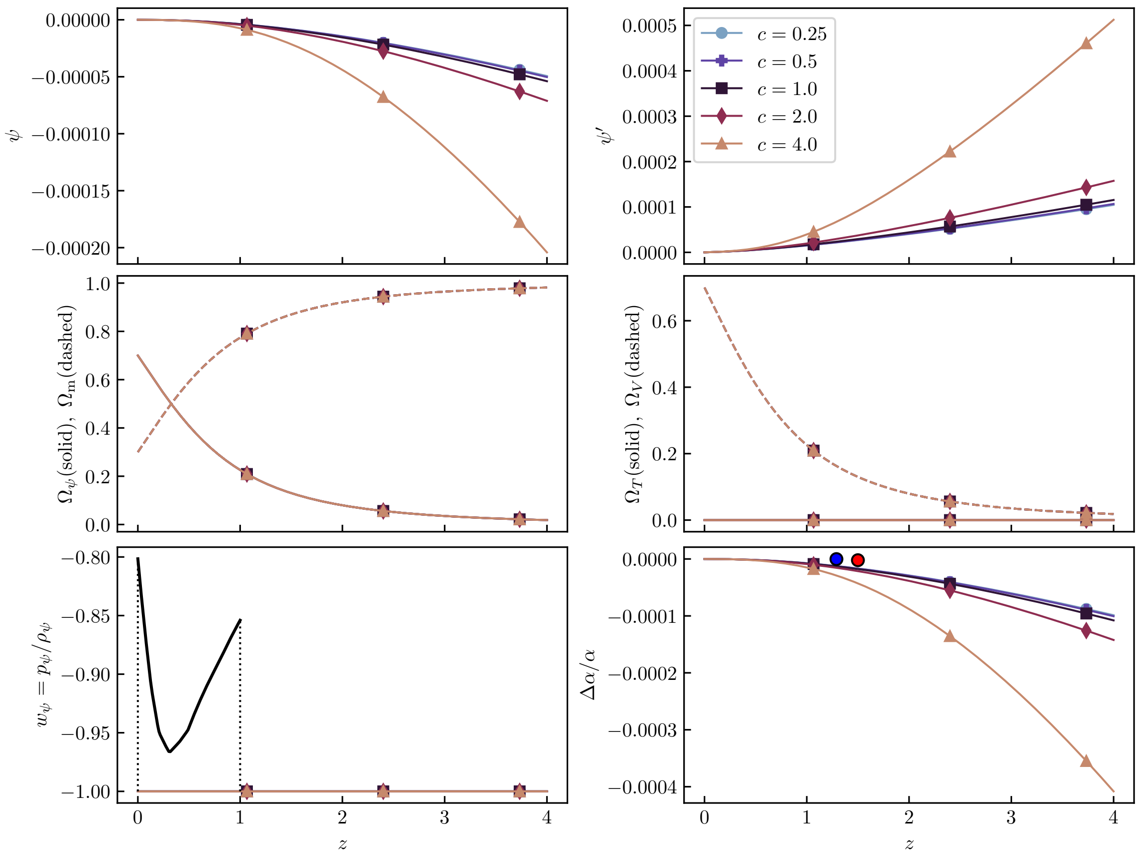

Figure 5.17: **[BSBM, cos]** Field value and speed, ψ and ψ', relative energy densities, $\Omega_i = \rho_i/\rho_c$, dark energy equation of state, w_ψ, and variations of α, $\Delta\alpha/\alpha$, over a range of c, with $\psi_0 = 0$ and $\psi'_0 = 0.007 \times 10^{-6}$.

The referred prior also implies field speeds which yield "natural" values of $\Delta\alpha/\alpha$. As had been the problem for this model with an exponential potential (cf. Sec. 5.1.3), the large variations of α are caused by the fact that the field is forced to move down some potential, which does not bode well with the phenomenology of the model, where the field was originally intended to be slowly rolling on a flat potential (a cosmological constant).

Due to the extremely low field speeds – and hence kinetic energies – selected by the atomic clocks data yield an equation of state which very easily satisfies the constraints we are using.

5.2.3.2 ψ_0' dependence

The ψ_0' dependence of this model is portrayed in Fig. 5.18. Again, comparing with quintessence (Fig. 5.11), for the higher values of ψ_0' we do not get as much of a difference in magnitude between the two models in terms of field displacement and speed. We

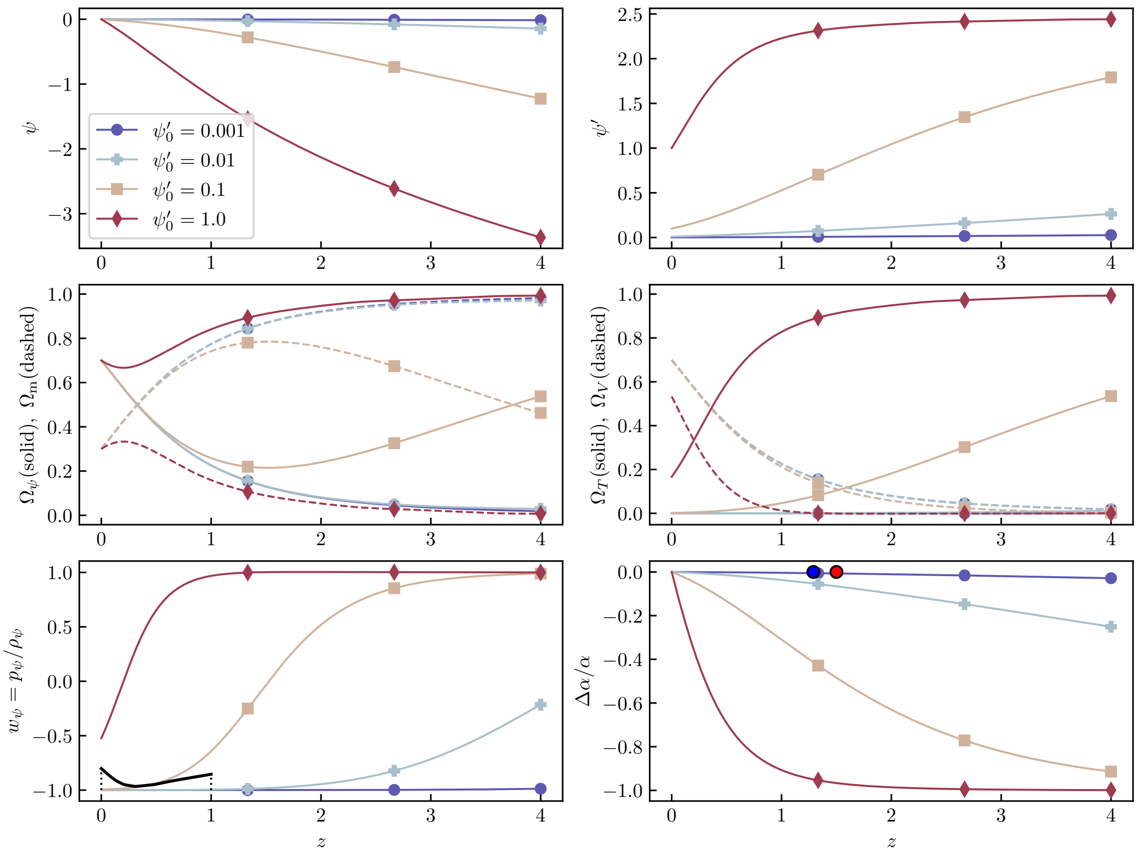

FIGURE 5.18: **[BSBM, cos]** Field value and speed, ψ and ψ', relative energy densities, $\Omega_i = \rho_i/\rho_c$, dark energy equation of state, w_ψ, and variations of α, $\Delta\alpha/\alpha$, over a range of ψ_0', with $\psi_0 = 0$ and $c = 1$.

conclude that for $\psi_0' \gtrsim 0.1$, the force term on the R.H.S. of Eq. 3.41 has a negligible effect on the field dynamics. However, for smaller values, the counteracting force provided by this term must be overcome if the field is to have the same present day position and speed. We thus get the noticeably higher speeds, kinetic energies and equations of state of the field when $\psi_0' \lesssim 0.1$, compared to quintessence.

Constraints on w_ϕ are satisfied by $\phi_0' \lesssim 0.01$, but none of the considered values give $\Delta\alpha/\alpha \lesssim 10^{-6}$.

5.2.3.3 ψ_0 dependence

Apart from variations of α all the plots of Figs. 5.19 and 5.12 look fairly similar. The other noticeable difference is the fact that the field's kinetic energy is already dominant with the $|c\phi_0| = \frac{\pi}{6}$. Of course, this is expected, because of the higher field speed needed to combat the decelerating term. As we have seen before, even in the cases where the field

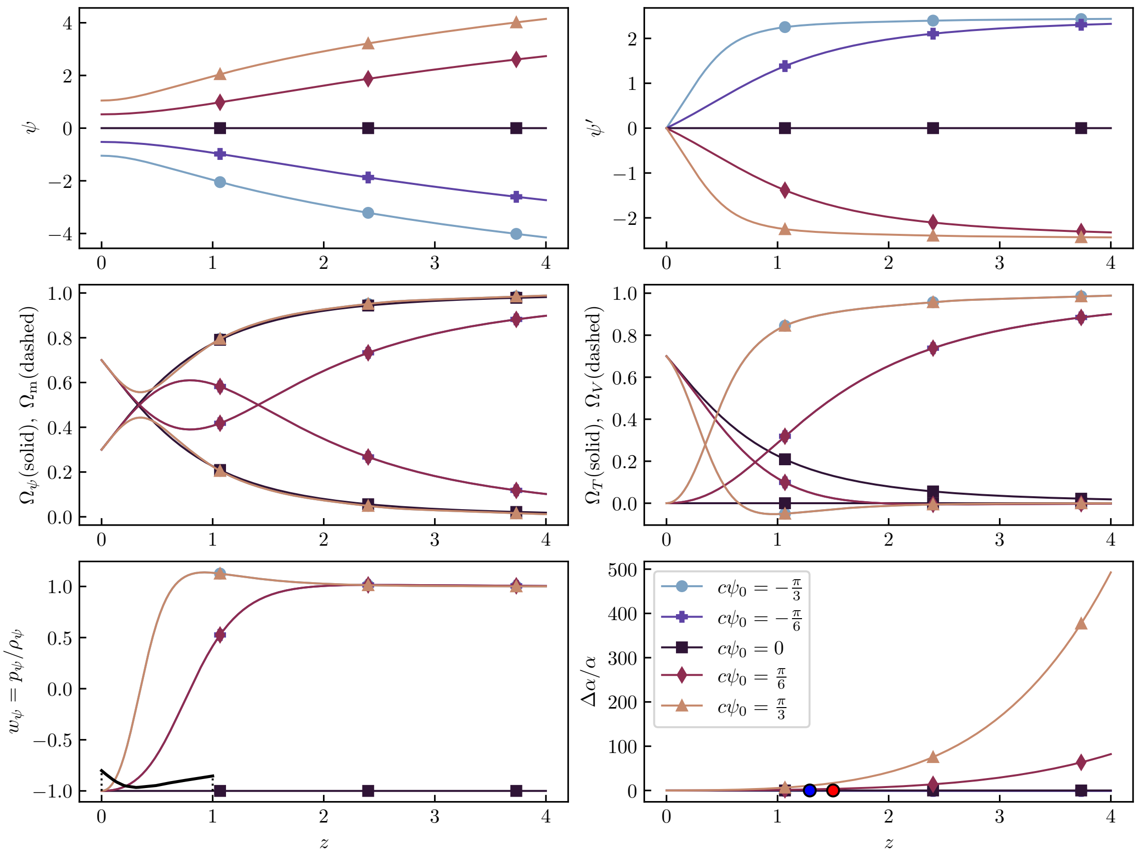

Figure 5.19: **[BSBM, cos]** Field value and speed, ψ and ψ', relative energy densities, $\Omega_i = \rho_i/\rho_c$, dark energy equation of state, w_ψ, and variations of α, $\Delta\alpha/\alpha$, over a range of ψ_0, with $\psi_0' = 0.007 \times 10^{-6}$ and $c = 1$.

is growing, such that we get negative variations of α, we get variations which are several orders of magnitude higher than experiments indicate. Again we find that only values of $c\phi_0$ near the top of the potential are able to satisfy w_{DE} constraints.

Chapter 6

Conclusion

After analyzing the cosmological predictions of quintessence, the runaway dilaton scenario and the Sandvik-Barrow-Magueijo extension of Bekenstein's model, in particular for the dark energy equation of state, w_{DE}, and the variation of the fine-structure constant with redshift, $\Delta\alpha/\alpha$, we come to several conclusions.

First and more qualitatively, the models indeed behave very differently in spite of their similar low energy (low coupling) limits. The fact that the phenomenological couplings, however small, lead to big dynamical differences between the runaway dilaton and the quintessence fields – the latter of which is not influenced by this coupling – is quite astounding. The difference between both of these and the BSBM extension could be foreseen to a certain extent, due to the changes that the redefinition of the electromagnetic sector imply for the energy distribution in a BSBM universe.

One surprising result, comes from our change to the original BSBM extension, where we have promoted the cosmological constant, Λ, to a variable potential energy, $V(\psi)$, which helps drive the scalar field's evolution. Though the model is still comparable to a quintessence type model, the implications for variations of the fine-structure constant are stark. This highlights the obvious (but for the inattentive physicist/cosmologist not so obvious) fact that in Bekenstein's model for varying α, the phenomenology lies in the definition of the field itself, rather than in the definition of the coupling of said field to the EM-sector. In quintessence, we *already* have a field and introduce the coupling ζ. In Bekenstein's original model and the BSBM extension, we have ΛCDM cosmology and introduce a field, ψ.

This implies that, given the results we have obtained, the BSBM extension can only be made compatible with Class I models – where DE is entirely attributed to the dynamics of the scalar fields – through hardcore fine-tuning. Moreover, though this is not strictly forbidden, it definitely places the BSBM model in the Swampland. In terms of how the variations of α are generated, it turns out that this model is actually much more similar to a rolling tachyon, where $B_F(\phi) = V(\phi)/V(\phi_0)$ (see [8]), and the O&P extension, where $B_F(\phi) \simeq 1 + \zeta_F(\phi - \phi_0) + \xi_F(\phi - \phi_0) + ...$, is more akin to a quintessence type field.

Model	$w_{\rm DE}$	$\Delta\alpha/\alpha$ (archival)	$\Delta\alpha/\alpha$ (dedicated)
Quintessence	$L \lesssim 0.5$	$L \gtrsim 1.6$	$L \lesssim 1.2$
RaDS - matter	$L \lesssim 0.5$	Ruled Out	Unconstrained
RaDS - dark	$L \lesssim 0.3$	Ruled Out	Unconstrained
RaDS - field	$L \lesssim 0.4$	Ruled Out	Unconstrained
BSBM extension	$L \lesssim 0.1$	Ruled Out	Ruled Out

TABLE 6.1: Summary of bounds for the exponential potential, $V(\phi) \propto e^{-L\phi}$, assuming $\Omega_{\rm b0} = 0.05$, $\Omega_{\rm cdm0} = 0.25$, $\Omega_{\rm r0} \simeq 0$, $\Omega_{\phi 0} = 0.7$ and with present day field speeds calculated from atomic clock bounds [49].

Using a simple and merely representative approach, we were able to see the level of constraints we can obtain using, spectroscopic, atomic clocks and cosmological data. The results of this analysis for the exponential potential is summarized in Table 6.1.

The caveat here is that we have used the maximal values of ζ, $\alpha_{\rm had0}$ and $\zeta_{\rm m}$ allowed by the MICROSCOPE data and used the atomic clocks data to determine the present day field speed, ϕ_0', essentially placing very stringent priors on the allowed field displacements. For more general values of the couplings – unconstrained by η data – α data is expected to place tighter constraints on $\Delta\phi$, and consequently on L, than $w_{\rm DE}$. Another possibility is to use α data, in tandem with the cosmological data, to place constraints on the couplings instead.

We were also able to describe the characteristics of the runaway dilaton scenario's phase space in some detail. This has helped us determine the phase space trajectories which do not disrupt large scale structure formation, through qualitative arguments.

A robust statistical analysis (similar to the one done in [9]) of the runaway dilaton scenario and the BSBM extension with exponential and cosine potentials is left for future work. It would also be interesting to include the O&P extension and other potentials in such an endeavour to see if such models play well with the Swampland conjectures. Critical to obtaining actual constraints – not just representative ones – would be to use more data, in particular, from other late-time cosmological parameters and from the early universe.

Appendix A

Fixed points

A.1 Quintessence

As we have seen, the phase space equations for quintessence are:

$$\begin{aligned} x' &= \sqrt{\frac{3}{2}}Ly^2 - \frac{3}{2}x\left[(1-w_m)\left(1-x^2\right) + (1+w_{\mathrm{m}})y^2\right] \\ y' &= -\sqrt{\frac{3}{2}}Lxy + \frac{3}{2}y\left[(1-w_m)x^2 + (1+w_{\mathrm{m}})\left(1-y^2\right)\right] \quad . \end{aligned} \tag{A.1}$$

If we add $0 = 2-(1-w_m)-(1+w_m)$ inside the brackets of the expression for x', it is easy to see that it yields the same expression in the brackets of y', with an extra term outside:

$$x' = \sqrt{\frac{3}{2}}Ly^2 - 3x + \frac{3}{2}x\left[(1-w_m)x^2 + (1+w_{\mathrm{m}})\left(1-y^2\right)\right] \quad . \tag{A.2}$$

Now we calculate $x'/x - y'/y = 0$, assuming $x \neq 0$, $y \neq 0$ and imposing $x' = y' = 0$ to get rid of the terms in brackets:

$$\sqrt{\frac{3}{2}}L\frac{y^2}{x} - 3 + \sqrt{\frac{3}{2}}Lx = 0 \quad \Leftrightarrow \quad y^2 = \frac{\sqrt{6}}{L}x - x^2 \quad . \tag{A.3}$$

Substituting y^2 into $x' = 0$, we have:

$$3x - \sqrt{\frac{3}{2}}Lx^2 - 3x + \frac{3}{2}x\left[(1-w_m)x^2 + (1+w_m)\left(1 - \frac{\sqrt{6}}{L}x + x^2\right)\right] = 0 \quad . \tag{A.4}$$

After a bit of algebra, the solutions of this quadratic equation are:

$$x = \sqrt{\frac{3}{2}}\frac{1+w_m}{L} \quad \vee \quad x = \frac{L}{\sqrt{6}} \quad . \tag{A.5}$$

Plugging these values into the expression for y^2, we have:

$$y^2 = \frac{3}{2}\frac{1-w_m^2}{L^2} \quad \vee \quad y^2 = 1 - \frac{L^2}{6} \quad , \tag{A.6}$$

so, finally, the non-trivial fixed points are:

$$(x^*, y^*) = \begin{cases} \left(\frac{L}{\sqrt{6}} \ , \ \sqrt{1-\frac{L^2}{6}}\right) \\ \left(\sqrt{\frac{3}{2}}\frac{1+w_m}{L} \ , \ \sqrt{\frac{3}{2}}\frac{\sqrt{1-w_m^2}}{L}\right) \end{cases} \quad . \tag{A.7}$$

A.2 Runaway dilaton scenario

Starting with the field Eq. 3.32 and substituting x and y as defined in Eq. 3.34 one obtains:

$$\begin{aligned}
x' = \frac{\phi''}{\sqrt{3}} &= -\frac{3}{2\sqrt{3}}\left[(\phi' + \alpha_{\rm b})\Omega_{\rm b} + (\phi' + \alpha_{\rm cdm})\Omega_{\rm cdm} + 2(\phi' + 2\alpha_V)\Omega_V\right] \\
&= -\frac{3}{2}\left[\left(x + \frac{\alpha_{\rm b}}{\sqrt{3}}\right)\frac{H_0^2}{H^2}\Omega_{\rm b0}(1+z)^3 + \left(x + \frac{\alpha_{\rm cdm}}{\sqrt{3}}\right)\frac{H_0^2}{H^2}\Omega_{\rm cdm0}(1+z)^3 + 2\left(x + \frac{2}{\sqrt{3}}\alpha_V\right)y^2\right] \\
&= -\frac{3}{2}\left[\left(x + \frac{\alpha_{\rm b}\Omega_{\rm b0} + \alpha_{\rm cdm}\Omega_{\rm cdm0}}{\sqrt{3}\Omega_{\rm m0}}\right)\left(1 - x^2 - y^2\right) + 2\left(x + \frac{2}{\sqrt{3}}\alpha_V\right)y^2\right] \\
&= -\frac{3}{2}\left[\left(x - x_{\rm fp}\right)\left(1 - x^2 - y^2\right) + 2\left(x + \frac{2}{\sqrt{3}}\alpha_V\right)y^2\right] \\
&= \left(\sqrt{\frac{3}{2}}L - 3x\right)y^2 - \frac{3}{2}(x - x_{\rm fp})\left(1 - x^2 - y^2\right) \\
&= \sqrt{\frac{3}{2}}Ly^2 - 3x + \frac{3}{2}x\left[2\left(1-y^2\right) - \frac{x - x_{\rm fp}}{x}\left(1 - x^2 - y^2\right)\right] \\
&= \sqrt{\frac{3}{2}}Ly^2 - 3x + \frac{3}{2}x\left[\left(1 - \frac{x_{\rm fp}}{x}\right)x^2 + \left(1 + \frac{x_{\rm fp}}{x}\right)\left(1 - y^2\right)\right] \quad ,
\end{aligned} \tag{A.8}$$

where in the second line we have used Eq. 3.33, in the third we used:

$$\Omega_{\rm m} = \Omega_{\rm m0}(1+z)^3\frac{H_0^2}{H^2} = 1 - x^2 - y^2 \quad . \tag{A.9}$$

and in the fourth we have introduced the definition:

$$x_{\rm fp} = -\frac{(\alpha_{\rm b}\Omega_{\rm b0} + \alpha_{\rm cdm}\Omega_{\rm cdm0})}{\sqrt{3}\Omega_{\rm m0}} \quad . \tag{A.10}$$

Note that $H^2 = \Omega_{\rm m0}(1+z)^3 H_0^2/\big(1-x^2-y^2\big)$ and differentiating this expression with respect to N, we get:

$$2HH' = \frac{\Omega_{\rm m0}H_0^2(1+z)^3}{1-x^2-y^2}\left(\frac{3z'}{1+z}+\frac{2\big(xx'+yy'\big)}{1-x^2-y^2}\right) \quad \Leftrightarrow \quad \frac{H'}{H} = \frac{xx'+yy'}{1-x^2-y^2}-\frac{3}{2} \ , \tag{A.11}$$

where we have used $dz/dN = -(1+z)$. As we have done for the quintessence field, taking the derivative of y^2 with respect to N, we get:

$$\begin{aligned}\Big(y^2\Big)' = 2yy' &= \frac{V'}{3M_{\rm Pl}^2H^2} - 2\frac{VH'}{3M_{\rm Pl}^2H^2} = \frac{V}{3M_{\rm Pl}^2H^2}\left(\frac{\partial_\phi V}{V}\phi' - 2\frac{H'}{H}\right) \\ &= -y^2\left[-\sqrt{3}x\frac{\partial_\phi V}{V} + 2\frac{H'}{H}\right] = -y^2\left[\sqrt{6}Lx + 2\frac{H'}{H}\right] \ .\end{aligned} \tag{A.12}$$

Isolating y' and substituting H'/H, we have:

$$\begin{aligned} y' &= y\left(-\sqrt{\frac{3}{2}}Lx + \frac{3}{2} - \frac{xx'+yy'}{1-x^2-y^2}\right) \\ &= y\frac{1-x^2-y^2}{1-x^2}\left(-\sqrt{\frac{3}{2}}Lx + \frac{3}{2} - \frac{xx'}{1-x^2-y^2}\right) \\ &= \frac{y}{1-x^2}\left[\left(-\sqrt{\frac{3}{2}}Lx + \frac{3}{2}\right)\Big(1-x^2-y^2\Big) - xx'\right] \\ &= \frac{y}{1-x^2}\left\{\left[-\sqrt{\frac{3}{2}}Lx + \frac{3}{2}\Big(1+x\big(x-x_{\rm fp}\big)\Big)\right]\Big(1-x^2-y^2\Big) + \left(3x - \sqrt{\frac{3}{2}}L\right)xy^2\right\} \\ &= y\left\{-\sqrt{\frac{3}{2}}Lx + \frac{3}{2}\Big[1+x\big(x-x_{\rm fp}\big)\Big]\frac{1-x^2-y^2}{1-x^2} + \frac{3x^2y^2}{1-x^2}\right\} \\ &= y\left\{-\sqrt{\frac{3}{2}}Lx + \frac{3}{2}\frac{\Big[1+x\big(x-x_{\rm fp}\big)\Big]\big(1-x^2-y^2\big) + 2x^2y^2}{1-x^2}\right\} \\ &= y\left[-\sqrt{\frac{3}{2}}Lx + \frac{3}{2}\frac{\big(1-x^2\big)\big(1+x^2-y^2\big) - xx_{\rm fp}\big(1-x^2-y^2\big)}{1-x^2}\right] \\ &= -\sqrt{\frac{3}{2}}Lxy + \frac{3}{2}y\left[\left(1+\frac{xx_{\rm fp}}{1-x^2}\right)x^2 + \left(1-\frac{xx_{\rm fp}}{1-x^2}\right)\Big(1-y^2\Big)\right] \ . \end{aligned} \tag{A.13}$$

A.2.1 Matter- and dark-coupling

Since in the matter- and dark-coupling scenarios $x_{\rm fp}$ is independent of x and y, the fixed points and their stability depend only on L and $x_{\rm fp}$. Once again there are three trivial fixed points with $y = 0$:

$$(x^*, y^*) = \big(x_{\rm fp}, 0\big), (\pm 1, 0) \ , \tag{A.14}$$

and it can be easily checked that $(x^*, y^*) = \left(\frac{L}{\sqrt{6}}, \sqrt{1-\frac{L^2}{6}}\right)$ is still a fixed point. The other non-trivial fixed point is obtained by choosing $-\sqrt{3/2}Lx + 3/2 = 0$ to cancel the first two terms inside the parenthesis in the first line of Eq. A.13. Plugging the resulting x value into Eq. A.8 and solving for y, we get:

$$x^* = \frac{\sqrt{6}}{2L} \quad , \quad y^* = \sqrt{\frac{\left(\frac{3}{2} - \sqrt{\frac{3}{2}}x_{\rm fp}L\right)\left(1-\frac{3}{2L^2}\right)}{L^2 - \sqrt{\frac{3}{2}}x_{\rm fp}L - \frac{3}{2}}} \quad . \tag{A.15}$$

Note that this non-trivial fixed point has two singularities; the one at $L = 0$ as in the quintessence case, but also one at:

$$L = \frac{\sqrt{\frac{3}{2}}x_{\rm fp} \pm \sqrt{\frac{3}{2}x_{\rm fp}^2 + 6}}{2} \quad , \tag{A.16}$$

due to the denominator of y^* in Eq. A.15. For $0 < L < \left(\sqrt{\frac{3}{2}}x_{\rm fp} + \sqrt{\frac{3}{2}x_{\rm fp}^2 + 6}\right)/2$, the denominator is negative and the solution only exists as long as the numerator is negative as well, leading to a non-existence of the fixed point in the interval $\min\left[\sqrt{\frac{3}{2}}, \frac{\sqrt{6}}{2x_{\rm fp}}\right] < L < \left(\sqrt{\frac{3}{2}}x_{\rm fp} + \sqrt{\frac{3}{2}x_{\rm fp}^2 + 6}\right)/2$, as can be seen in Fig. A.1.

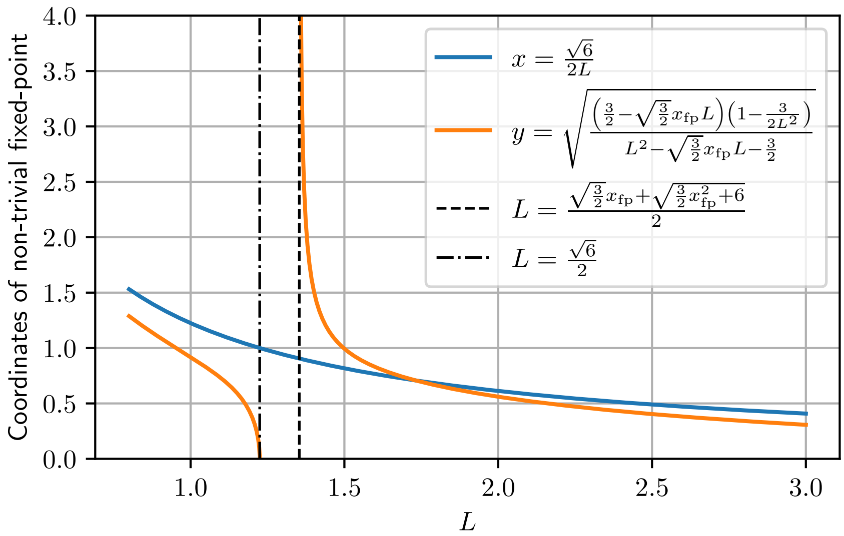

FIGURE A.1: Coordinates of the non-trivial fixed point with peculiar existence conditions of the runaway dilaton model, with $x_{\rm fp} = 0.2$.

For $|x_{\rm fp}| < 1$, which we are interested in, there is an upper limit (not depicted in Fig. A.1) of $L < \frac{\sqrt{6}}{2x_{\rm fp}}$; for the expected low values of $x_{\rm fp} \sim \mathcal{O}\left(10^{(-n)}\right)$ this limit is $L \lesssim \mathcal{O}(10^n)$, where n represents the order of magnitude of the strongest coupling of the dilaton to the matter fields, i.e. $\max\left[\alpha_{\rm b}, \alpha_{\rm cdm}\right]$.

A.2.2 Field-coupling

The coupling of the dilaton to dark matter in this scenario is $\alpha_{\mathrm{cdm}} = -\phi' = -\sqrt{3}x$. Let $s = \Omega_{\mathrm{b0}}/\Omega_{\mathrm{m0}}$ and $t = \Omega_{\mathrm{cdm0}}/\Omega_{\mathrm{m0}}$ be the ratios of baryons and cold dark matter to all matter, respectively, so we can write:

$$x_{\mathrm{fp}} = -\frac{\alpha_{\mathrm{had}}}{\sqrt{3}} s + tx \quad . \tag{A.17}$$

Eqs. A.8 and A.13 can then be rewritten:

$$x' = \sqrt{\frac{3}{2}} L y^2 - 3x + \frac{3}{2} x \left[\left(1 - t + \frac{\alpha_{\mathrm{had}} s}{\sqrt{3} x} \right) x^2 + \left(1 + t - \frac{\alpha_{\mathrm{had}} s}{\sqrt{3} x} \right) \left(1 - y^2 \right) \right] \tag{A.18}$$

$$\begin{aligned} y' = -\sqrt{\frac{3}{2}} L x y + \frac{3}{2} y \Bigg[& \left(1 - \frac{\frac{\alpha_{\mathrm{had}}}{\sqrt{3}} s x - t x^2}{1 - x^2} \right) x^2 \\ & + \left(1 + \frac{\frac{\alpha_{\mathrm{had}}}{\sqrt{3}} s x - t x^2}{1 - x^2} \right) \left(1 - y^2 \right) \Bigg] \end{aligned} \tag{A.19}$$

This system of equations also has three fixed points with $y = 0$ and two with $y \neq 0$. When using a symbolic solver, the latter two have very complicated expressions, but, as can be seen in Fig. 5.6c, one of them seems to match $(x, y) = \left(L/\sqrt{6}, \sqrt{1 - L^2/6} \right)$, which can be proven by plugging this fixed point into the equations. The other one is indeed too complicated, so we will not bother writing it down. The trivial fixed points and the saddle-point solution which can again represent dark energy or matter dominated past are given by:

$$\begin{aligned} (x^*, y^*) &= (\pm 1, 0) \\ (x^*, y^*) &= \left(-\frac{\alpha_{\mathrm{had}}}{\sqrt{3}}, 0 \right) \quad , \end{aligned} \tag{A.20}$$

where we have used the fact that $s + t = 1$. For practical purposes, these are the most important ones. We use $(x^*, y^*) = (\pm 1, 0)$ to guarantee that the only point capable of representing the past is the saddle-point, and use the saddle-point as the starting point of our trajectory through phase space. Whichever the future fixed point is, we will find out by just performing the integration.

Appendix B

Linear stability analysis

Linear stability analysis (LSA) allows us to find the stability of a fixed point, i.e. whether it is a saddle point, a stable or unstable node, a spiral, etc. (see Chapter 2 of [47]). In the simplest approach, we need to calculate the Jacobian of the vector field:

$$J(x,y) = \begin{bmatrix} \frac{\partial x'}{\partial x} & \frac{\partial x'}{\partial y} \\ \frac{\partial y'}{\partial x} & \frac{\partial y'}{\partial y} \end{bmatrix} \tag{B.1}$$

its trace, $\tau(x,y)$, and determinant, $\Delta(x,y)$, and evaluate them at each fixed point. We leave an explicit dependence of the matrix on x and y, since it will be easier to plug the fixed points into it and then calculate τ and Δ.

B.1 Quintessence

Each element of the Jacobian can be calculated explicitly:

$$\frac{\partial x'}{\partial x} = -\frac{3}{2}\left[(1-w_m)\left(1-3x^2\right)+(1+w_{\rm m})y^2\right] \tag{B.2}$$

$$\frac{\partial x'}{\partial y} = \sqrt{6}Ly - 3(1+w_m)xy \tag{B.3}$$

$$\frac{\partial y'}{\partial x} = -\sqrt{\frac{3}{2}}Ly + 3(1-w_m)xy \tag{B.4}$$

$$\frac{\partial y'}{\partial y} = -\sqrt{\frac{3}{2}}Lx + \frac{3}{2}\left[(1-w_m)x^2+(1+w_{\rm m})\left(1-3y^2\right)\right] \tag{B.5}$$

	Fixed point, trace and determinant	Type
(a)	$(x^*, y^*) = (0,0)$ $\tau = 3w_m$ $\Delta = -\frac{9}{4}\left(1 - w_m^2\right)$	Saddle-point: $\forall L$
$(b_\pm)$	$(x^*, y^*) = (\pm 1, 0)$ $\tau = 3\left(2 - w_m \mp \frac{L}{\sqrt{6}}\right)$ $\Delta = 9(1 - w_m)\left(1 \mp \frac{L}{\sqrt{6}}\right)$	Both unstable nodes: $L^2 < 6$ Saddle-point $(+1,0)$: $L^2 > 6$ Unstable node $(-1,0)$: $L^2 > 6$
(c)	$(x^*, y^*) = \left(\frac{L}{\sqrt{6}}, \sqrt{1 - \frac{L^2}{6}}\right)$ $\tau = -3\left(2 + w_m - \frac{L^2}{2}\right)$ $\Delta = 9\left[1 + w_m - (3 + w_m)\frac{L^2}{6} + \frac{L^4}{18}\right]$	Stable node: $L^2 < 3(1 + w_m)$ Saddle-point: $3(1 + w_m) < L^2 < 6$ Non-existent: $L^2 > 6$
(d)	$(x^*, y^*) = \left(\sqrt{\frac{3}{2}}\frac{1 + w_m}{L}, \sqrt{\frac{3}{2}}\frac{\sqrt{1 - w_m^2}}{L}\right)$ $\tau = -\frac{3}{2}(1 - w_m)$ $\Delta = \frac{9}{2}\left[\left(1 - w_m^2\right) - 3\frac{1 - w_m + w_m^2 + w_m^3}{L^2}\right]$	Saddle-point: $L^2 < 3(1 + w_m)$ Stable node: $3(1 + w_m) < L^2$

TABLE B.1: Summary of fixed points in phase space of quintessence and their stability in terms of L and w_m.

B.2 Runaway dilaton scenario

The stability conditions (Table B.2) ascertained from the traces and determinants (see Fig. B.1) of the Jacobian of the runaway dilaton's phase space Eqs. 3.35 and 3.36 assume small couplings of the dilaton to other fluids, i.e. $|\alpha_i| \ll 1$. The highest value of x_{fp} obtained in the considered scenarios is when there is no baryonic matter and the dilaton couples to the dark sector in a universal way $\alpha_{\text{cdm}} = \alpha_V = -L/2\sqrt{2}$:

$$x_{\text{fp}} < \frac{L}{2\sqrt{6}} \sim 0.204L \quad . \tag{B.6}$$

	Fixed point, trace and determinant	Type
(a)	$(x^*, y^*) = (x_{\rm fp}, 0)$ $\tau = -\frac{x_{\rm fp}}{2}\left(\sqrt{6}L - 3x_{\rm fp}\right)$ $\Delta = -\frac{3}{4}(1-x_{\rm fp})(1+x_{\rm fp})\left(3-\sqrt{6}Lx_{\rm fp}\right)$	Saddle-point: $L < \frac{\sqrt{6}}{2x_{\rm fp}}$, $\lvert x_{\rm fp}\rvert < 1$
$(b_\pm)$	$(x^*, y^*) = (\pm 1, 0)$ $\tau = \frac{12 \mp \left(\sqrt{6}L + 9x_{\rm fp}\right)}{2}$ $\Delta = \frac{3}{2}(1 \mp x_{\rm fp})\left[6 \mp \left(\sqrt{6}L + 3x_{\rm fp}\right)\right]$	Both unstable nodes: $L < \sqrt{6}\left(1 - \frac{x_{\rm fp}}{2}\right)$ Saddle-point $(+1, 0)$: $L > \sqrt{6}\left(1 - \frac{x_{\rm fp}}{2}\right)$ Unstable node $(-1, 0)$: $L > \sqrt{6}\left(1 - \frac{x_{\rm fp}}{2}\right)$
(c)	$(x^*, y^*) = \left(\frac{L}{\sqrt{6}}, \sqrt{1 - \frac{L^2}{6}}\right)$ $\tau = \frac{3}{2}(L-2)(L+2)$ $\Delta = \frac{(L^2-6)(L^2-3)}{2}$	Stable node: $L^2 < 3$ Saddle-point: $3 < L^2 < 6$ Non-existent: $L^2 > 6$
(e)	$(x^*, y^*) = \left(\frac{\sqrt{6}}{2L}, \sqrt{\frac{\left(\frac{3}{2} - \sqrt{\frac{3}{2}}x_{\rm fp}L\right)\left(1 - \frac{3}{2L^2}\right)}{L^2 - \sqrt{\frac{3}{2}}x_{\rm fp}L - \frac{3}{2}}}\right)$ $\tau = -\frac{3\left(L - \sqrt{6}x_{\rm fp}\right)\left(L^2 - \frac{3}{2}\right)}{2L\left(L^2 - \sqrt{\frac{3}{2}}x_{\rm fp}L - \frac{3}{2}\right)}$ $\Delta = -\frac{3(L^2-3)\left(L^2 - \frac{3}{2}\right)\left(\sqrt{6}Lx_{\rm fp} - 3\right)}{2L^2\left(L^2 - \sqrt{\frac{3}{2}}x_{\rm fp}L - \frac{3}{2}\right)}$	Saddle-point: $L < \sqrt{\frac{3}{2}}$ Non-existent: $\sqrt{\frac{3}{2}} < L < \sqrt{\frac{3}{8}}x_{\rm fp} + \sqrt{\frac{3}{8}x_{\rm fp}^2 + \frac{3}{2}}$ Saddle-point: $\sqrt{\frac{3}{8}}x_{\rm fp} + \sqrt{\frac{3}{8}x_{\rm fp}^2 + \frac{3}{2}} < L < \sqrt{3}$ Stable node: $\sqrt{3} < L < \frac{\sqrt{6}}{2x_{\rm fp}}$

Table B.2: Summary of fixed points in phase space of a runaway dilaton and their stability in terms of L and $\lvert x_{\rm fp}\rvert \ll 1$. These are only valid in matter and dark coupling scenarios, where $x_{\rm fp}$ does not depend on (x, y) (see Sec. A.2.2). For a visual summary of these conditions, see Fig. B.1.

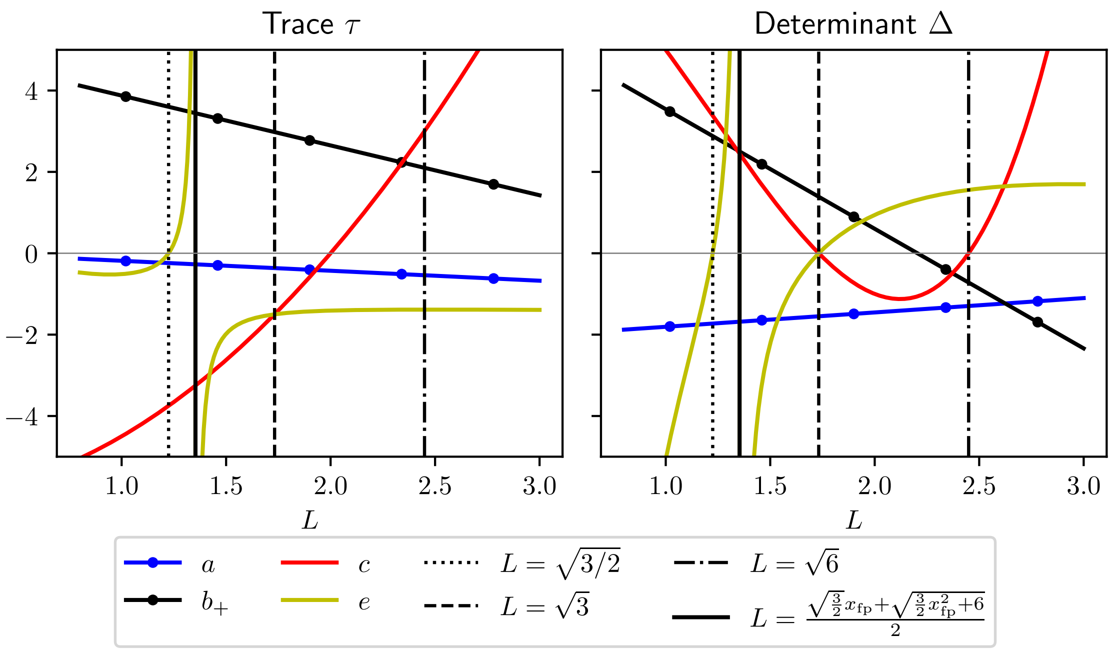

FIGURE B.1: Traces and determinants of fixed points in phase space of the runaway dilaton with $x_{\mathrm{fp}} = 0.2$. The labels a, b_+, c and e represent the fixed points by the order in which they appear in Table B.2.

Bibliography

[1] C. Vafa, "The String Landscape and the Swampland," Oct 2005. [Online]. Available: https://arxiv.org/abs/hep-th/0509212 [Cited on pages 1 and 8.]

[2] E. Palti, "The Swampland: Introduction and Review," *Fortschritte der Physik*, vol. 67, no. 6, p. 1900037, Apr 2019. [Online]. Available: https://doi.org/10.1002%2Fprop.201900037 [Cited on pages 1, 4, 8, and 9.]

[3] C. M. Will, "The Confrontation between General Relativity and Experiment," *Living Rev. Rel.*, vol. 17, p. 4, 2014. [Cited on page 2.]

[4] P. Touboul *et al.*, "MICROSCOPE Mission: Final Results of the Test of the Equivalence Principle," *Phys. Rev. Lett.*, vol. 129, no. 12, p. 121102, 2022. [Cited on pages 3, 28, 35, and 38.]

[5] J. De Vuyst, "A Natural Introduction to Fine-Tuning," *arXiv e-prints*, p. arXiv:2012.05617, Dec. 2020. [Cited on page 3.]

[6] M. T. Murphy, A. L. Malec, and J. X. Prochaska, "Precise limits on cosmological variability of the fine-structure constant with zinc and chromium quasar absorption lines," *Monthly Notices of the Royal Astronomical Society*, vol. 461, no. 3, pp. 2461–2479, 06 2016. [Online]. Available: https://doi.org/10.1093/mnras/stw1482 [Cited on pages 3 and 37.]

[7] M. T. Murphy and K. L. Cooksey, "Subaru Telescope limits on cosmological variations in the fine-structure constant," *Monthly Notices of the Royal Astronomical Society*, vol. 471, no. 4, pp. 4930–4945, 07 2017. [Online]. Available: https://doi.org/10.1093/mnras/stx1949 [Cited on pages 3, 34, and 37.]

[8] C. J. A. P. Martins, "The status of varying constants: a review of the physics, searches and implications," *Reports on Progress in Physics*, vol. 80, no. 12, p. 126902, Dec. 2017. [Cited on pages 4, 17, 21, 33, 37, and 60.]

[9] N. Schöneberg, L. Vacher, J. D. F. Dias, M. M. C. D. Carvalho, and C. J. A. P. Martins, "News from the Swampland – Constraining string theory with astrophysics and cosmology," 2023. [Cited on pages ix, 5, 18, 19, 20, 21, and 60.]

[10] S. Mukhi, "String theory: a perspective over the last 25 years," *Classical and Quantum Gravity*, vol. 28, no. 15, p. 153001, Jun 2011. [Online]. Available: https://dx.doi.org/10.1088/0264-9381/28/15/153001 [Cited on page 7.]

[11] T. Taylor and G. Veneziano, "Dilaton couplings at large distances," *Physics Letters B*, vol. 213, no. 4, pp. 450–454, 1988. [Online]. Available: https://www.sciencedirect.com/science/article/pii/0370269388912907 [Cited on page 8.]

[12] M. R. Douglas and S. Kachru, "Flux compactification," *Rev. Mod. Phys.*, vol. 79, pp. 733–796, May 2007. [Online]. Available: https://link.aps.org/doi/10.1103/RevModPhys.79.733 [Cited on page 8.]

[13] M. Raveri, W. Hu, and S. Sethi, "Swampland Conjectures and Late-Time Cosmology," *Phys. Rev. D*, vol. 99, no. 8, p. 083518, 2019. [Cited on pages 8, 10, and 13.]

[14] P. Agrawal, G. Obied, P. J. Steinhardt, and C. Vafa, "On the Cosmological Implications of the String Swampland," *Phys. Lett. B*, vol. 784, pp. 271–276, 2018. [Cited on pages ix, 8, 10, 12, 13, 28, 32, 37, and 38.]

[15] P. Agrawal, G. Obied, and C. Vafa, "H_0 tension, swampland conjectures, and the epoch of fading dark matter," *Phys. Rev. D*, vol. 103, no. 4, p. 043523, 2021. [Cited on pages 8 and 13.]

[16] H. Ooguri and C. Vafa, "On the geometry of the string landscape and the swampland," *Nuclear Physics B*, vol. 766, no. 1, pp. 21–33, 2007. [Online]. Available: https://www.sciencedirect.com/science/article/pii/S0550321306008455 [Cited on page 9.]

[17] M. van Beest, J. Calderón-Infante, D. Mirfendereski, and I. Valenzuela, "Lectures on the Swampland Program in String Compactifications," *Physics Reports*, vol. 989, pp. 1–50, 2022, lectures on the Swampland Program in String

Compactifications. [Online]. Available: https://www.sciencedirect.com/science/article/pii/S0370157322003295 [Cited on page 9.]

[18] G. Obied, H. Ooguri, L. Spodyneiko, and C. Vafa, "De Sitter Space and the Swampland," 2018. [Cited on pages 9 and 10.]

[19] F. Denef, A. Hebecker, and T. Wrase, "de Sitter swampland conjecture and the Higgs potential," *Phys. Rev. D*, vol. 98, p. 086004, Oct 2018. [Online]. Available: https://link.aps.org/doi/10.1103/PhysRevD.98.086004 [Cited on page 10.]

[20] H. Ooguri, E. Palti, G. Shiu, and C. Vafa, "Distance and de Sitter conjectures on the Swampland," *Physics Letters B*, vol. 788, pp. 180–184, 2019. [Online]. Available: https://www.sciencedirect.com/science/article/pii/S037026931830858X [Cited on page 10.]

[21] R. Bousso, "A covariant entropy conjecture," *Journal of High Energy Physics*, vol. 1999, no. 07, pp. 004–004, Jul 1999. [Online]. Available: https://iopscience.iop.org/article/10.1088/1126-6708/1999/07/004 [Cited on page 10.]

[22] A. G. Riess, A. V. Filippenko, P. Challis, A. Clocchiatti, A. Diercks, P. M. Garnavich, R. L. Gilliland, C. J. Hogan, S. Jha, R. P. Kirshner, B. Leibundgut, M. M. Phillips, D. Reiss, B. P. Schmidt, R. A. Schommer, R. C. Smith, J. Spyromilio, C. Stubbs, N. B. Suntzeff, and J. Tonry, "Observational Evidence from Supernovae for an Accelerating Universe and a Cosmological Constant," *The Astronomical Journal*, vol. 116, no. 3, p. 1009, Sep 1998. [Online]. Available: https://dx.doi.org/10.1086/300499 [Cited on page 10.]

[23] S. Perlmutter, G. Aldering, G. Goldhaber, R. A. Knop, P. Nugent, P. G. Castro, S. Deustua, S. Fabbro, A. Goobar, D. E. Groom, I. M. Hook, A. G. Kim, M. Y. Kim, J. C. Lee, N. J. Nunes, R. Pain, C. R. Pennypacker, R. Quimby, C. Lidman, R. S. Ellis, M. Irwin, R. G. McMahon, P. Ruiz-Lapuente, N. Walton, B. Schaefer, B. J. Boyle, A. V. Filippenko, T. Matheson, A. S. Fruchter, N. Panagia, H. J. M. Newberg, W. J. Couch, and T. S. C. Project, "Measurements of Ω and Λ from 42 High-Redshift Supernovae," *The Astrophysical Journal*, vol. 517, no. 2, p. 565, Jun 1999. [Online]. Available: https://dx.doi.org/10.1086/307221 [Cited on page 10.]

[24] Planck Collaboration, N. Aghanim, Y. Akrami, M. Ashdown, J. Aumont, C. Baccigalupi, M. Ballardini, A. J. Banday, R. B. Barreiro, N. Bartolo, S. Basak, R. Battye,

K. Benabed, J. P. Bernard, M. Bersanelli, P. Bielewicz, J. J. Bock, J. R. Bond, J. Borrill, F. R. Bouchet, F. Boulanger, M. Bucher, C. Burigana, R. C. Butler, E. Calabrese, J. F. Cardoso, J. Carron, A. Challinor, H. C. Chiang, J. Chluba, L. P. L. Colombo, C. Combet, D. Contreras, B. P. Crill, F. Cuttaia, P. de Bernardis, G. de Zotti, J. Delabrouille, J. M. Delouis, E. Di Valentino, J. M. Diego, O. Doré, M. Douspis, A. Ducout, X. Dupac, S. Dusini, G. Efstathiou, F. Elsner, T. A. Enßlin, H. K. Eriksen, Y. Fantaye, M. Farhang, J. Fergusson, R. Fernandez-Cobos, F. Finelli, F. Forastieri, M. Frailis, A. A. Fraisse, E. Franceschi, A. Frolov, S. Galeotta, S. Galli, K. Ganga, R. T. Génova-Santos, M. Gerbino, T. Ghosh, J. González-Nuevo, K. M. Górski, S. Gratton, A. Gruppuso, J. E. Gudmundsson, J. Hamann, W. Handley, F. K. Hansen, D. Herranz, S. R. Hildebrandt, E. Hivon, Z. Huang, A. H. Jaffe, W. C. Jones, A. Karakci, E. Keihänen, R. Keskitalo, K. Kiiveri, J. Kim, T. S. Kisner, L. Knox, N. Krachmalnicoff, M. Kunz, H. Kurki-Suonio, G. Lagache, J. M. Lamarre, A. Lasenby, M. Lattanzi, C. R. Lawrence, M. Le Jeune, P. Lemos, J. Lesgourgues, F. Levrier, A. Lewis, M. Liguori, P. B. Lilje, M. Lilley, V. Lindholm, M. López-Caniego, P. M. Lubin, Y. Z. Ma, J. F. Macías-Pérez, G. Maggio, D. Maino, N. Mandolesi, A. Mangilli, A. Marcos-Caballero, M. Maris, P. G. Martin, M. Martinelli, E. Martínez-González, S. Matarrese, N. Mauri, J. D. McEwen, P. R. Meinhold, A. Melchiorri, A. Mennella, M. Migliaccio, M. Millea, S. Mitra, M. A. Miville-Deschênes, D. Molinari, L. Montier, G. Morgante, A. Moss, P. Natoli, H. U. Nørgaard-Nielsen, L. Pagano, D. Paoletti, B. Partridge, G. Patanchon, H. V. Peiris, F. Perrotta, V. Pettorino, F. Piacentini, L. Polastri, G. Polenta, J. L. Puget, J. P. Rachen, M. Reinecke, M. Remazeilles, A. Renzi, G. Rocha, C. Rosset, G. Roudier, J. A. Rubiño-Martín, B. Ruiz-Granados, L. Salvati, M. Sandri, M. Savelainen, D. Scott, E. P. S. Shellard, C. Sirignano, G. Sirri, L. D. Spencer, R. Sunyaev, A. S. Suur-Uski, J. A. Tauber, D. Tavagnacco, M. Tenti, L. Toffolatti, M. Tomasi, T. Trombetti, L. Valenziano, J. Valiviita, B. Van Tent, L. Vibert, P. Vielva, F. Villa, N. Vittorio, B. D. Wandelt, I. K. Wehus, M. White, S. D. M. White, A. Zacchei, and A. Zonca, "Planck 2018 results. VI. Cosmological parameters," *A&A*, vol. 641, p. A6, Sep. 2020. [Cited on page 10.]

[25] S. Weinberg, "The cosmological constant problem," *Rev. Mod. Phys.*, vol. 61, pp. 1–23, Jan 1989. [Online]. Available: https://link.aps.org/doi/10.1103/RevModPhys.61.1 [Cited on page 11.]

[26] E. D. Valentino, O. Mena, S. Pan, L. Visinelli, W. Yang, A. Melchiorri, D. F. Mota, A. G. Riess, and J. Silk, "In the realm of the Hubble tension – a review of solutions*," *Classical and Quantum Gravity*, vol. 38, no. 15, p. 153001, Jul 2021. [Online]. Available: https://dx.doi.org/10.1088/1361-6382/ac086d [Cited on page 11.]

[27] A. H. Guth, "Inflationary universe: A possible solution to the horizon and flatness problems," *Phys. Rev. D*, vol. 23, pp. 347–356, Jan 1981. [Online]. Available: https://link.aps.org/doi/10.1103/PhysRevD.23.347 [Cited on page 11.]

[28] A. D. Linde, "A New Inflationary Universe Scenario: A Possible Solution of the Horizon, Flatness, Homogeneity, Isotropy and Primordial Monopole Problems," *Phys. Lett. B*, vol. 108, pp. 389–393, 1982. [Cited on page 11.]

[29] ——, "Chaotic Inflation," *Phys. Lett. B*, vol. 129, pp. 177–181, 1983. [Cited on page 11.]

[30] E. W. Kolb and M. S. Turner, *The Early Universe*. CRC Press, 1990. [Cited on page 11.]

[31] M. Cicoli, J. P. Conlon, A. Maharana, S. Parameswaran, F. Quevedo, and I. Zavala, "String Cosmology: from the Early Universe to Today," 2023. [Online]. Available: https://arxiv.org/abs/2303.04819 [Cited on page 12.]

[32] A. Achúcarro and G. A. Palma, "The string swampland constraints require multi-field inflation," *Journal of Cosmology and Astroparticle Physics*, vol. 2019, no. 02, p. 041, Feb 2019. [Online]. Available: https://dx.doi.org/10.1088/1475-7516/2019/02/041 [Cited on page 12.]

[33] D. M. Scolnic, D. O. Jones, A. Rest, Y. C. Pan, R. Chornock, R. J. Foley, M. E. Huber, R. Kessler, G. Narayan, A. G. Riess, S. Rodney, E. Berger, D. J. Brout, P. J. Challis, M. Drout, D. Finkbeiner, R. Lunnan, R. P. Kirshner, N. E. Sanders, E. Schlafly, S. Smartt, C. W. Stubbs, J. Tonry, W. M. Wood-Vasey, M. Foley, J. Hand, E. Johnson, W. S. Burgett, K. C. Chambers, P. W. Draper, K. W. Hodapp, N. Kaiser, R. P. Kudritzki, E. A. Magnier, N. Metcalfe, F. Bresolin, E. Gall, R. Kotak, M. McCrum, and K. W. Smith, "The complete light-curve sample of spectroscopically confirmed sne ia from pan-starrs1 and cosmological constraints from the combined pantheon sample," *The Astrophysical Journal*, vol. 859, no. 2,

p. 101, May 2018. [Online]. Available: https://dx.doi.org/10.3847/1538-4357/aab9bb [Cited on pages 12, 32, 35, and 47.]

[34] M. Chevallier and D. Polarski, "Accelerating Universes with Scaling Dark Matter," *International Journal of Modern Physics D*, vol. 10, no. 02, pp. 213–223, Apr 2001. [Online]. Available: https://doi.org/10.1142/s0218271801000822 [Cited on page 12.]

[35] E. V. Linder, "Exploring the Expansion History of the Universe," *Phys. Rev. Lett.*, vol. 90, p. 091301, Mar 2003. [Online]. Available: https://link.aps.org/doi/10.1103/PhysRevLett.90.091301 [Cited on page 12.]

[36] S. Tsujikawa, "Quintessence: a review," *Classical and Quantum Gravity*, vol. 30, no. 21, p. 214003, Oct 2013. [Online]. Available: https://dx.doi.org/10.1088/0264-9381/30/21/214003 [Cited on page 17.]

[37] T. Damour and A. Polyakov, "The string dilaton and a least coupling principle," *Nuclear Physics B*, vol. 423, no. 2, pp. 532–558, 1994. [Online]. Available: https://www.sciencedirect.com/science/article/pii/0550321394901430 [Cited on page 20.]

[38] T. Damour, F. Piazza, and G. Veneziano, "Violations of the equivalence principle in a dilaton-runaway scenario," *Phys. Rev. D*, vol. 66, p. 046007, Aug 2002. [Online]. Available: https://link.aps.org/doi/10.1103/PhysRevD.66.046007 [Cited on pages 20, 21, and 22.]

[39] ——, "Runaway Dilaton and Equivalence Principle Violations," *Phys. Rev. Lett.*, vol. 89, p. 081601, Aug 2002. [Online]. Available: https://link.aps.org/doi/10.1103/PhysRevLett.89.081601 [Cited on page 20.]

[40] L. Vacher, N. Schöneberg, J. D. F. Dias, C. J. A. P. Martins, and F. Pimenta, "Runaway dilaton models: Improved constraints from the full cosmological evolution," *Phys. Rev. D*, vol. 107, p. 104002, May 2023. [Online]. Available: https://link.aps.org/doi/10.1103/PhysRevD.107.104002 [Cited on page 21.]

[41] C. J. A. P. Martins and L. Vacher, "Astrophysical and local constraints on string theory: Runaway dilaton models," *Phys. Rev. D*, vol. 100, no. 12, p. 123514, 2019. [Cited on page 21.]

[42] J. D. Bekenstein, "Fine-structure constant: Is it really a constant?" *Phys. Rev. D*, vol. 25, pp. 1527–1539, Mar 1982. [Online]. Available: https://link.aps.org/doi/10.1103/PhysRevD.25.1527 [Cited on page 24.]

[43] K. A. Olive and M. Pospelov, "Evolution of the fine structure constant driven by dark matter and the cosmological constant," *Phys. Rev. D*, vol. 65, p. 085044, Apr 2002. [Online]. Available: https://link.aps.org/doi/10.1103/PhysRevD.65.085044 [Cited on page 24.]

[44] C. S. Alves, A. C. O. Leite, C. J. A. P. Martins, T. A. Silva, S. A. Berge, and B. S. A. Silva, "Current and future constraints on extended Bekenstein-type models for a varying fine-structure constant," *Phys. Rev. D*, vol. 97, no. 2, p. 023522, 2018. [Cited on page 24.]

[45] L. Vacher, J. D. F. Dias, N. Schöneberg, C. J. A. P. Martins, S. Vinzl, S. Nesseris, G. Cañas Herrera, and M. Martinelli, "Constraints on extended Bekenstein models from cosmological, astrophysical, and local data," *Phys. Rev. D*, vol. 106, p. 083522, Oct 2022. [Online]. Available: https://link.aps.org/doi/10.1103/PhysRevD.106.083522 [Cited on pages 24 and 29.]

[46] H. B. Sandvik, J. D. Barrow, and J. a. Magueijo, "A Simple Cosmology with a Varying Fine Structure Constant," *Phys. Rev. Lett.*, vol. 88, p. 031302, Jan 2002. [Online]. Available: https://link.aps.org/doi/10.1103/PhysRevLett.88.031302 [Cited on pages 24, 25, and 43.]

[47] S. H. Strogatz, *Nonlinear Dynamics and Chaos: With Applications to Physics, Biology, Chemistry and Engineering*, 2nd ed. CRC Press., 2000. [Cited on pages 27 and 67.]

[48] Y. Akrami, R. Kallosh, A. Linde, and V. Vardanyan, "The Landscape, the Swampland and the Era of Precision Cosmology," *Fortschritte der Physik*, vol. 67, no. 1-2, Nov 2018. [Online]. Available: https://doi.org/10.1002/prop.201800075 [Cited on page 32.]

[49] R. Lange, N. Huntemann, J. M. Rahm, C. Sanner, H. Shao, B. Lipphardt, C. Tamm, S. Weyers, and E. Peik, "Improved Limits for Violations of Local Position Invariance from Atomic Clock Comparisons," *Phys. Rev. Lett.*, vol. 126, p. 011102, Jan

2021. [Online]. Available: https://link.aps.org/doi/10.1103/PhysRevLett.126.011102 [Cited on pages 32 and 60.]

[50] C. Martins, F. Ferreira, and P. Marto, "Varying fine-structure constant cosmography," *Physics Letters B*, vol. 827, p. 137002, 2022. [Online]. Available: https://www.sciencedirect.com/science/article/pii/S0370269322001368 [Cited on pages 33 and 34.]

[51] J. K. Webb, J. A. King, M. T. Murphy, V. V. Flambaum, R. F. Carswell, and M. B. Bainbridge, "Indications of a Spatial Variation of the Fine Structure Constant," *Phys. Rev. Lett.*, vol. 107, p. 191101, Oct 2011. [Online]. Available: https://link.aps.org/doi/10.1103/PhysRevLett.107.191101 [Cited on page 33.]

[52] C. J. A. P. Martins and A. M. M. Pinho, "Fine-structure constant constraints on dark energy," *Phys. Rev. D*, vol. 91, p. 103501, May 2015. [Online]. Available: https://link.aps.org/doi/10.1103/PhysRevD.91.103501 [Cited on page 37.]